

SPATIALLY- AND DIRECTIONALLY-VARYING
REFLECTANCE OF MILLI-SCALE FEATHER
MORPHOLOGY

A Dissertation

Presented to the Faculty of the Graduate School

of Cornell University

in Partial Fulfillment of the Requirements for the Degree of

Doctor of Philosophy

by

Todd Alan Harvey

August 2012

© 2012 Todd Alan Harvey
ALL RIGHTS RESERVED

SPATIALLY- AND DIRECTIONALLY-VARYING REFLECTANCE OF
MILLI-SCALE FEATHER MORPHOLOGY

Todd Alan Harvey, Ph.D.

Cornell University 2012

Birds have evolved diverse plumage through sophisticated morphological modifications. The interaction of light with these modifications alters the reflectance from feathers, producing complex and directionally-variable visual signals. I hypothesize that structural modifications of the feather produce anisotropic reflectance, the direction of which is determined by the orientation of the structure of the vane.

Variation in reflectance originates from the interplay of light with two classes of feather structure: its surface and subsurface volume. Different structural scales within the two structural classes influence light scattering within the UV-visible spectrum. The overall shape and surface of the feather vane (the macro-scale) and of its component members (the milli-scale) scatter light according to principles of geometric optics. Subsurface nano-scale structure in many feathers generate so-called “structural coloration,” which is a purely physical optics phenomenon and can differ drastically from ordinary coloration mechanisms such as pigmentation. Iridescence, from which many feathers derive their vivid, eye-catching changeable color, is one type of structural color that varies as a function of viewing angle.

This thesis presents investigations into a previously understudied aspect of avian visual signaling: directional reflectance and its relationship to milli-scale structure. Having observed that the stratified nano-scale morphology of structurally-colored plumage contours the milli-scale cortex of the vane, I determined that measurements of the milli-scale could be substituted for a more complex study of

directional reflectance from the nano-scale. I thereby hypothesize that the direction of the reflectance from a vaned feather can be predicted from the orientation of its milli-scale morphology—its barbs and barbules. In collaboration with my colleagues at Cornell University, I developed non-destructive tools and methods to investigate the signaling potential of the feather. I correlate measurements of directional light scattering to the milli-scale morphology of select samples of structurally-colored bird plumage. The results of these analyses lead to a more thorough understanding of the relationships between directional reflectance and the structure of the feather itself. Having found the reflectance to be anisotropic, I demonstrate that the change in the direction of the reflectance over the surface of the vane can in fact be predicted from the orientation of the different branches of the barb. The improved understanding of the variation in directional reflectance over the surface of the feather, a phenotypic component, should allow for better comprehension of avian behavior, evolution of morphological adaptations, and the synthesis of more accurate predictive models.

BIOGRAPHICAL SKETCH

Todd Harvey was born in Tucson, Arizona and raised in various parts of the United States while his father pursued his PhD and career in Optical Science and Engineering. As an undergraduate at Brigham Young University, Todd began studying Applied Physics with Computer Applications. But after two years of coursework and two years of internships in optical fabrication and surface scattering (culminating in work on NASA's Chandra Observatory), he attempted to forge a new path by completing instead a degree in Visual Art and Design with an emphasis in photography and computer-aided rendering.

Following graduation he spent a decade in the film industry producing computer-generated creatures and digital effects. Inspired by the academic papers that he read for his work on *Lord of the Rings* and *King Kong*, Todd decided to pursue graduate studies. He entered the Master's program in Computer Graphics at Cornell University in the Fall of 2006. With the encouragement of his advisors to investigate feather appearance, he found that the fundamental ties between feather morphology and optical scattering had not been sufficiently explored by the disciplines to which computer graphics generally turns in order to build predictive models.

By the fall of 2010 it seemed obvious that he and his research were more appropriately hosted by the field of Zoology, where he became a PhD candidate under the interdisciplinary committee of Dr. Susan Suarez (Biomedical Sciences), Dr. Ellis Loew (Physiology), Dr. Steve Marschner (Computer Science), Dr. Kimberley Bostwick (Ecology and Evolutionary Biology and Curator, Birds and Mammals, Cornell University Museum of Vertebrates) and Dr. John Hermanson (Zoology). In fall of 2010, he also began a position as Visiting Assistant in Research to Dr. Richard O. Prum, Professor of Ornithology, Ecology and Evolutionary Biology, at

Yale University and Head Curator of Vertebrate Zoology at The Peabody Museum
of Natural History.

Dedicated to my father

ACKNOWLEDGEMENTS

A veritable army of people has provided counsel and support to bring to pass the completion of this thesis.

First, I must thank my committee for their cooperative efforts, detailed readings of papers, counsel, guidance and encouragement. I am grateful to Dr. Kim Bostwick and Dr. Steve Marschner for encouraging and facilitating the porting of my research and academic life from one field to another, as well as for their intellectual generosity and collaboration. I thank Dr. Susan Suarez for graciously taking on the position of chair when no one else could, for her “whip-cracking” (always in the nicest possible way), as well as her organizational and editorial gifts. Thanks to Dr. Ellis Loew for his enthusiasm and catalytic role and to Dr. John Hermanson for his thoughtful support. I must particularly thank Dr. Robert Gilmour for expanding my possibilities and Dr. Ellen Gainor for giving her blessing. I am grateful to Dr. Donald Greenberg for taking me into the Computer Graphics program, for his support while his student, for his interdisciplinary vision for the field, and for suggesting birds. Dr. James Harvey, CREOL, University of Florida, provided suggestions and a sounding board for my understanding of optical scattering theory, as well as careful reading of manuscripts – not to mention hours of fatherly and academic advice.

For assistance in the world of CT scans, I am grateful for the work and advice of Mark Riccio, Cornell Micro-CT Facility, Cornell University; Dr. Joshua Van Houten, MicroCT Facility, Yale Core Center for Musculoskeletal Disorders, Yale University; Dr. Matthew Colbert, High-resolution X-ray CT Facility, University of Texas, Austin; and Teresa Feo, Yale University. Kalliope Stournaras, University Freiburg, was instrumental for her translation from German of a critical Durrer and Villiger paper. Thanks to Edwin Scholes at the Macaulay Library, Cornell

Lab of Ornithology; and Charles M. Dardia, Cornell Museum of Vertebrates, for introducing me to *C. cupreus*.

Thanks to my many colleagues in Computer Graphics at Cornell University who contributed to this work over several years. First, I thank the other two of the “three amigos” that began our journey in the program together, for your camaraderie, advice and collaboration: Brendan Holt who finished first; David Kaplan who also reminded us there was life out of the lab...in the mountains somewhere. Dr. Jon Moon taught me how to use the Cornell Spherical gantry; Wenzel Jakob contributed programming expertise in Java and OpenGL and a commensurate interest in fine food; Dr. Jaroslav Křivánek reworked the demosaicing pipeline and implemented a plane fitting function to our framework and offered an example of social ease for all computer scientists; Edgar Velázquez-Armendáriz offered his Java and MATLAB implementations of OpenEXR for our use and a winning smile to go with it; Jeff Wang showed me the ropes (even if I ignored them at times); Dr. Piti Irawan could teach me without leaving me to feel like an idiot; Dr. Miloš Hašan gave those midnight MATLAB consults; Dr. Adam Arbree; and Konstantin Shkurko offered his skill with applied mathematics. If I have missed anyone, I apologize profusely. Thanks to Dr. Anil Nerode for bringing matrix algebra from the abstract to the concrete for me (finally!!).

At Yale University, I would like to thank everyone who welcomed me and became my surrogate Zoology/EEB family for the past 18 months in the lab of Dr. Richard Prum, including Jacob Berv, Jacob Musser, Dr. Vinodkumar Saranathan, and Dr. Chris Clark. Also thank you to the many friendly people at the Peabody Museum of Natural History, including Dr. Kristof Zyskowski and Dr. Stefan Nicolescu for your intellectual and practical contributions. Thank you also to my

collaborators in Computer Science at Yale University, Dr. Min Kim, Dr. Holly Rushmeier and Patrick Paczkowski.

Numerous people at Cornell University have provided tangible, friendly (and patient!) support: Hurf Sheldon, Linda Stephenson, Peggy Andersen in the Program of Computer Graphics; Janna Lamey and Arla Hourigan in the College of Veterinary Medicine; Diane Whitmore in the School of Architecture; and Shirley Weaver in the Cornell Graduate School. At Yale University, Karen Broderick smoothed the way. Thank you to the staff of the Library at the Lab of Ornithology, Cornell University, for your assistance.

Special thanks to Dr. Richard Prum, Department of Ecology and Evolutionary Biology, Yale University, for his enthusiasm for interdisciplinary work and his financial and intellectual support over the past year.

Thanks to my wife, Jennifer Helvey, for her tireless critical editing, humor, and all-around saintliness. I am grateful for a mother who always encouraged a curious mind. Thank you to my in parents-in-law, Lou and Barbara Helvey, for their support during these lean years.

Finally, thanks to Joe Letteri of Weta Digital, who unknowingly started me on this journey years ago. Sorry I'm late for work.

This research was supported by funding from the National Science Foundation (NSF CAREER award CCF-0347303 and NSF grant CCF-0541105).

CONTENTS

Biographical Sketch	iii
Dedication	v
Acknowledgements	vi
Contents	ix
List of Tables	xi
List of Figures	xii
Preface	1
1 Introduction	2
2 Review of Technical Principles	5
2.1 Feather Morphology and Appearance	5
2.2 Exterior Factors Impacting Feather Appearance	13
2.3 Directional Scattering and Measurement	15
2.3.1 Radiometry	15
2.3.2 Specular and Diffuse Reflection	17
2.3.3 Plumage Studies	19
2.4 Anisotropy from Fibers	23
2.5 Mechanisms of Color Reflectance in Feathers	26
2.5.1 Spectrally Unselective Specular Surface Reflection	26
2.5.2 Pigmentation	27
2.5.3 Incoherent Scattering	28
2.5.4 Coherent Scattering	29
2.5.4.1 Coherent Scatterers	29
2.5.4.2 Thin-films	30
2.5.4.3 Ordered Photonic Matrix	32
2.5.4.4 Quasi-ordered Photonic Matrix	34
2.6 Summary	36
Appendix A Feather Vane Appearance Diversity	37
3 Methods for Measuring Spatially- and Directionally-varying Light Scattering from Biological Material	42
3.1 Abstract (Short)	42
3.2 Abstract (Long)	42
3.3 Protocol	44
3.4 Representative Results	57
3.5 Disclosures	64
3.6 Discussion	64
3.7 Acknowledgements	66

4	Directional Reflectance and Milli-scale Feather Morphology of the African Emerald Cuckoo, <i>Chrysococcyx cupreus</i>	67
4.1	Introduction	68
4.2	Background	71
4.3	Geometric Framework	77
4.4	Methods	80
4.4.1	Directional Reflectance Measurements	80
4.4.2	Reflectance Metrics	83
4.4.3	MicroCT Measurements and Morphometrics	86
4.5	Results	86
4.5.1	Barb Axes Predict the Orientation of the Reflectance Cones	87
4.5.2	Directionally and Spatially-integrated Reflectance of Discrete Structures	94
4.5.3	Emerging Properties of the Vane in the Far-field	95
4.5.4	Grazing Angle Reflectance of the Rami	98
4.6	Discussion	100
5	The Blue Jay, <i>Cyanocitta cristata</i>: Diffuse Scattering Case Study	106
5.1	Relationship Between Structure and Diffuse Reflection	107
5.2	Local Area Averages	107
5.3	Variation in the Diffuse and Specular Reflectance of Barbs	110
5.4	Global Area Average	111
5.5	Integration of Non-Diffuse Components	112
5.6	Summary	112
	Appendix B Directional Scattering Plots	114
B.1	Normalized Radius	114
B.2	Displaced Radius	115
B.3	Color Schemes	118
B.4	Naming Conventions	119
B.5	Coordinate Systems	121
6	Conclusion	123
	Bibliography	125

LIST OF TABLES

2.1	Sample measurements densely, sparsely, or not at all	16
4.1	Reflectance and morphology statistics of <i>C. cupreus</i>	93

LIST OF FIGURES

2.1	Pennaceous feather vane structure	6
2.2	Cross-section of rachis and its attached rami and barbules	7
2.3	Cross-section of barb along with distal and proximal barbules	7
2.4	Feather Spatial and Directional Variation	9
2.5	Vane asymmetry, rotation, bend, and concavity	10
2.6	Iridescent barbule modifications	11
2.7	Feather barb damaged by keratinolytic bacterium	12
2.8	Geometric bases for variation in directional reflectance.	18
2.9	Hair fiber schematic	24
2.10	Surface and subsurface refraction directions from finished wood	24
2.11	Refraction cones from wood fibers	25
2.12	Traverse cross-section of a Chrysococcyx barbule	33
2.13	Blue Jay: nano-structure, PSD, and predicted reflectance spectra	35
A.1	Diverse appearance characteristics of contour feather vanes	39
3.1	Protocol schematic overview	59
3.2	Gantry configuration with flattened feather	60
3.3	Aggregate directional scattering from different shaped regions	60
3.4	Directional plotting functions and color reflectance schemes	61
3.5	Directional reflectance from seven camera directions	62
3.6	Reflectance color as a function of θ on USC diagram	63
3.7	Reflected color (Hue, Chroma, Luminance) as function of θ	63
3.8	Spatially-varying directional reflectance of <i>C. cupreus</i>	64
3.9	Feather image rectification	64
4.1	Photo of <i>C. cupreus</i> and its tertial feather	70
4.2	Pennaceous feather vane and barb structure	72
4.3	Micro-scale roughness on directional reflectance.	74
4.4	Cross-sectional shape on directional reflectance.	76
4.5	Cone of reflectance from a cylinder	76
4.6	Geometry of fiber reflection and cone-hemisphere intersection	78
4.7	Geometry of direction cosine space	78
4.8	Gantry schematic and directional reflectance map	81
4.9	Gantry configuration with a freeform feather	81
4.10	Directional sampling and mapping on the hemisphere	82
4.11	Directional reflectance between adjacent barbs of <i>C. cupreus</i>	88
4.12	MicroCT reconstructions and schematics of the vane of <i>C. cupreus</i>	89
4.13	Directional reflectance from different barb components of <i>C. cupreus</i>	90
4.14	Directional reflectance from a region of the medial vane of <i>C. cupreus</i>	96
4.15	Directional reflectance from regions of both vanes of <i>C. cupreus</i>	96
4.16	Directional reflectance from a ramus of <i>C. cupreus</i>	99

5.1	Traverse cross-section of a blue-colored <i>C. cristata</i> feather barb . .	108
5.2	Directional scattering from 3 differently colored regions of <i>C. cristata</i>	109
5.3	Directional scattering from 3 differently colored rami of <i>C. cristata</i>	110
5.4	Directional scattering from a large region of <i>C. cristata</i> vane	111
5.5	Directional scattering from <i>C. cristata</i> barbules	113
B.1	Example of directional scattering plotting functions and color schemes.	116
B.2	Three directions from which to view directional scattering plots . .	117

PREFACE

To pursue interdisciplinary study is to work at the intersection of fields, to find commonality between disciplines that may at first seem disparate. When I began my own academic journey, I did so thinking that the common thread in my long-term interests was light and its interaction with the physical world. I have come to find that this is only partially true. For nearly a decade I was employed in the lighting and rendering of computer-generated animation and visual effects for big-budget Hollywood movies. Every story has its main character; over the years, I rendered many pivotal vertebrate and invertebrate organismal characters with a variety of integuments. On every project, as an artist and engineer, I worked from reference material—sometimes photographic, but whenever possible from physical specimens of the organisms themselves. We employed physically-based algorithms to render final performances life-like and photorealistic. When established algorithms failed, we used a little “pixel dust” to make up the difference. But in every case, a physically-based approach provided the most efficient and effective result. At the start of my graduate research, Dr. Kim Bostwick, Curator of Mammals and Ornithology at the Cornell Museum of Vertebrates, introduced me to the bird skins in the collection. The best reference collection with which I had had the privilege of working, these birds proved a tool for new discovery, both scientific and self. At the core, I have found my interests are ultimately organism-centered. Light is the means by which an organism is revealed and performs in its world—natural or cinematic. To understand the organism, we must study its underlying morphology and light’s interaction with it.

CHAPTER 1

INTRODUCTION

Birds have evolved feathers of astounding diversity. Feathers are fundamental to how birds interact with their world; they assist in movement and flight, are a determining factor in an organism's overall visual identity, and often play a role in its social interaction. Past and current research delves into the signaling function of feathers. One branch of research investigates how signals are generated, with particular attention to the nano-scale adaptation known as structural color¹. Other biologists have and continue to study the behavioral function of plumage, from crypsis to communication².

An aspect of feather morphology that has not yet received the attention it deserves with regard to signaling function is the geometry of the feather vane at the millimeter-scale (i.e. $10\mu m - 1mm$). Numerous previous case studies have established the vast morphological modifications of the milli-scale structure of the vane³, specifically with regard to the evolution of the feather itself⁴, its method of development, and its unique structural qualities enabling flight [Videler, 2006], etc. While a cursory glance might suggest that a feather is a flat plane, every feather has "texture," a complex, milli-scale topography generated by the shape and orientation of the feather sub-structures—the barbs and barbules. The topography determines the angles at which incoming light will scatter from the organism, revealing and

¹Studies regarding structural coloration are numerous. A few examples of such research are [Gadow, 1882, Mason, 1923a,b, Auber, 1957, Huxley, 1968, Land, 1972, Dyck, 1974, Prum et al., 1998, Prum, 1999, Hill and McGraw, 2006a, Kinoshita, 2008]

²See, for example, [Butcher and Rohwer, 1989, Dugatkin and Reeve, 2000, Hill and McGraw, 2006b, Gomez, 2007]

³For studies focused on the morphology of the vane, see [Mascha, 1905, Sick, 1937, Lucas and Stettenheim, 1972, Rutschke, 1974, Stettenheim, 1974, 2000, Shawkey and Hill, 2004]

⁴For references on the evolution and development of the feather, see [Dyck, 1985, Prum and Williamson, 2001, Prum and Brush, 2002, Prum and Dyck, 2003, Prum, 2005]

defining it. A change in the form and orientation of feather barb and barbule structures in turn changes its interaction with light, and thus alters appearance. The angle at which light strikes the feather can change because of the movement of the light source (sun/shade), the movement of the bird from one place to another, the bird's movement of its feathers in various ways or a change in the position of the viewer. Birds move and their environment changes around them; feather appearance is therefore dynamic. I suspected that the milli-scale structure of a feather has an important role in the changeable appearance of birds.

Previous research has established that birds exhibit high levels of modified barb and barbule structure. But do these modifications enhance or suppress a directional component of their signal? I began my investigations by asking: for every specific component of the modified milli-scale structure, is there a corresponding signal function and can I identify and measure the signal? If so, how do the modified morphological arrangements determine the overall directional reflectance of the vane? In other words, how do the milli-scale adaptations influence the signal of the feather as the angle of illumination or viewing changes? And finally, based on the principles of geometric optics, can I predict the directionality of the signal based on the geometry of the milli-scale structure?

To support this line of inquiry and the accompanying hypotheses, I developed in collaboration with my colleagues at Cornell University a novel, non-destructive protocol to measure and analyze the morphology and the directional reflectance from the milli-scale structure of feathers. Following the protocol, I analyzed the directional reflectance of short sections of individual milli-scale structures—rami, and the base and pennulum of the distal and proximal barbule—of the vane. I found that each short section of each milli-scale structure of the vane produced

a signature signal, the specular reflectance of which was highly directional and anisotropic. I sought to explain the direction of the specular reflectance from each structure as a cone of emerging light, the base of which is centered on each structure's longitudinal axis. Borrowing a technique from the field of Computer Graphics appearance modeling—the plane-fitting method of Marschner et al [Marschner et al., 2005]—I found the orientation of an implied plane (which contains the base of the cone) from the directional reflectance data. Using a micro-CT scanner, I measured and reconstructed the milli-scale structure of the vane. When I compared the orientation of the fit plane to the orientation of the milli-scale structure, I found that the orientation is identical. In this way I have shown that the direction of the specular reflectance of the vane can be precisely predicted from the geometry of its barbs. The exciting implications of my predictive model are that perhaps all the directional effects in feathers can be understood in the same way and, furthermore, that I may have identified a previously unrecognized adaptive significance of milli-scale feather morphology.

This dissertation first presents a background chapter which reviews feather morphology, radiometry, and relevant computer graphics concepts and models. Next, a methods chapter delineates our protocol in detail and presents representative results. [Note its final intended form will have a video component produced by the Journal of Visualized Experiments.] Finally, it contains two case study chapters: *Chrysococcyx cupreus* (African Emerald Cuckoo) offers a dramatic case of highly directional or glossy specular reflectance; and *Cyanocitta cristata* (Blue Jay) provides a look at relatively “matte” or directionally diffuse reflectance.

CHAPTER 2

REVIEW OF TECHNICAL PRINCIPLES

I anticipate readers from diverse fields and make little assumption for the readers' familiarity with the background principles of feather morphology and appearance, directional scattering, anisotropy from fibers, and classes of color production in feathers. Sections 2.1, 2.2, 2.3, 2.4 and 2.5 review fundamentals of these disciplines with application to this thesis. Those familiar with basic principles may not need to read the full explanations; a scan of the subject headings will familiarize the informed researcher with the range of phenomena involved.

2.1 Feather Morphology and Appearance

Feathers consist primarily of beta-keratin¹, a fibrous protein polymer forming microscopic filaments that have strong mechanical properties [Gill, 2007]. Various other compounds as well as keratin—significantly melanin and air—enrich the mechanical and color properties of feathers. Variation in the organization of the structure of the feather comprised of keratin, melanin, and air leads to a wide array of coloration in bird plumage.

There are several classes of feathers, each with a distinct structure. The vaned feather—a class including the flight and contour feathers which cover the outer surface of the body—is the most conspicuous; a bird's appearance is directly related to the peculiar properties of these feathers. Flight feathers of the wing, called remiges, and flight feathers of the tail, called rectrices, are pennaceous structures. A pennaceous feather vane is characterized by a firmly textured, tightly inter-

¹Beta-keratins are unique to birds and reptiles and form other hard structures such as the beak and claws.

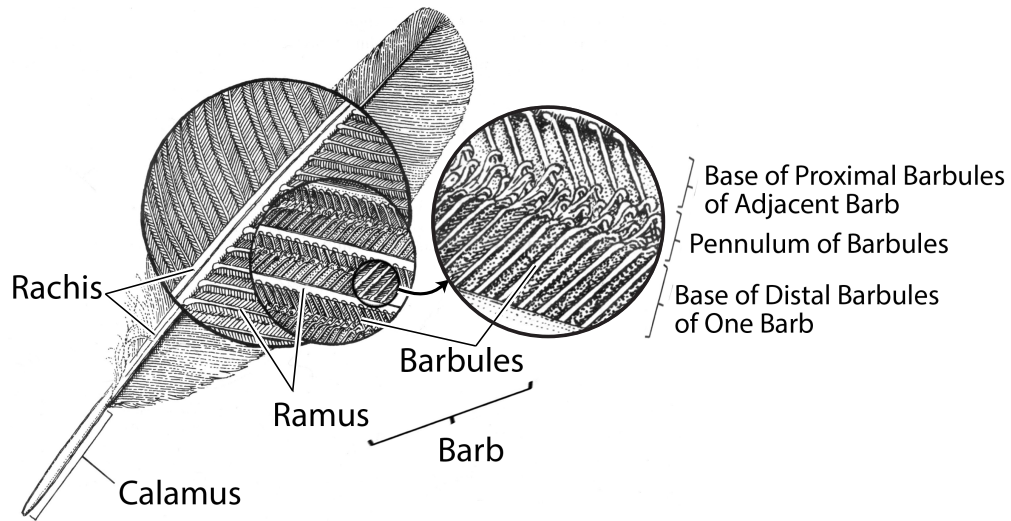
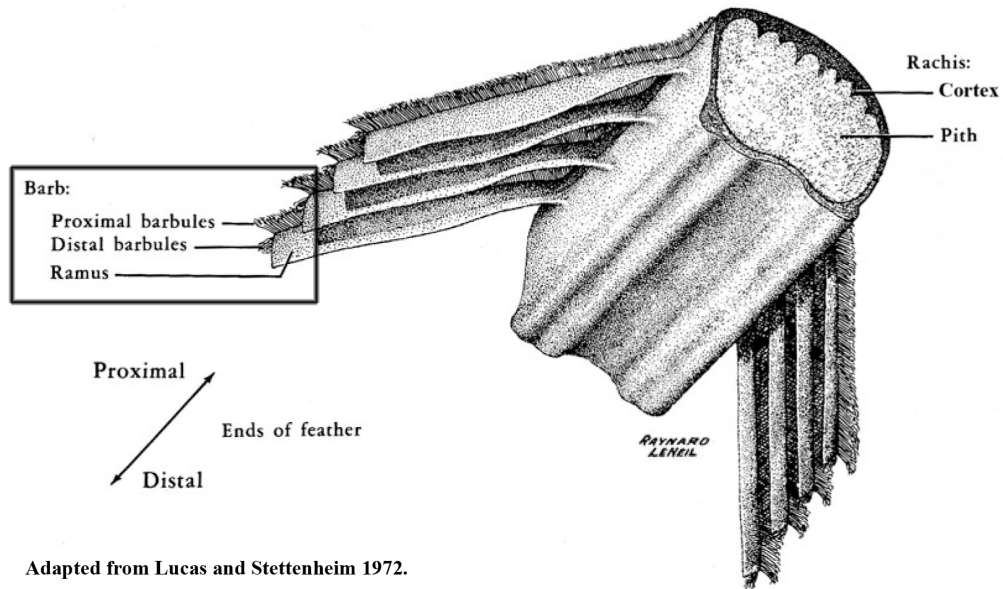


Figure 2.1: Pennaceous feather vane structure. Adapted from [Clark Jr., 2004].

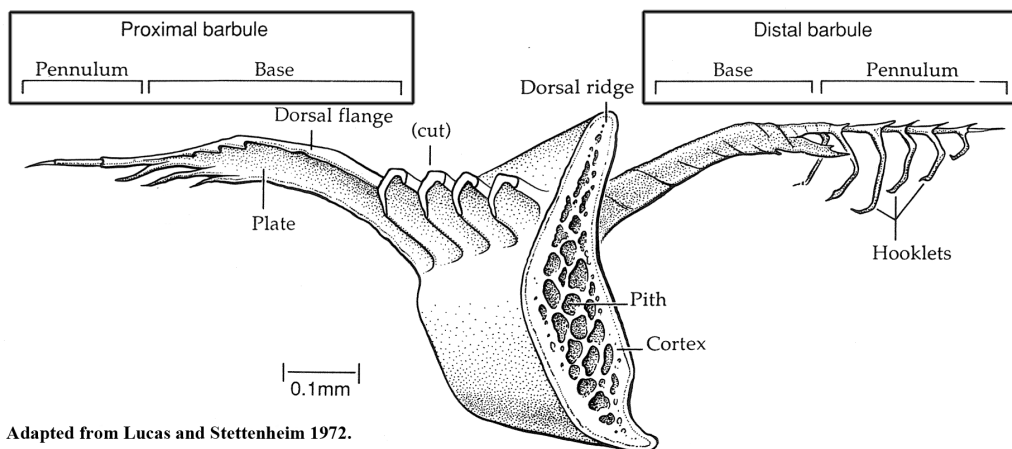
locking structure. This formation is important for creating lift for flight. Most important for this thesis, the periodic structure of the pennaceous vane also affects appearance and signaling; the more organized the feather structure, the more coherent the aggregate reflection.

The surface topography of the vaned feather is three-dimensional and complex. The vaned feather is constructed of two opposing vanes flanking the main shaft, or rachis (Figure 2.1). Along the length of the rachis, barbs branch off at regular intervals (Figures 2.1 and 2.2). Each barb consists of a long thin shaft, or ramus, from which branch two rows of barbules, one set proximally, and the other distally (Figure 2.3). Each barbule consists of two main parts, a basal shaft and pennulum. Hooklets interlock the distal barbule of one ramus to the proximal barbule of the adjacent ramus. The regularly branched network of specialized fibrous structure, as described, creates a periodic milli-scale surface topography interleaving four types of structure: ramus, base of the proximal barbule, base of the distal barbule, and pennulum of the distal barbule .



Adapted from Lucas and Stettenheim 1972.

Figure 2.2: Close-up of a section of rachis is shown in cross-section. Barbs—comprised of a ramus and barbules—branches from the rachis. Adapted from [Lucas and Stettenheim, 1972].



Adapted from Lucas and Stettenheim 1972.

Figure 2.3: A barb ramus in cross-section along with its attached distal and proximal barbules. The structure of the barbules, including the hooklets, are typical of a regime or rectrices. Adapted from [Lucas and Stettenheim, 1972].

For the purposes of this study, I divide the structure of the feather into four classifications ordered by size: macro-scale, milli-scale, micro-scale, and nano-scale (Figure 2.4). The macro-scale constitutes the largest structural formations, those which may be resolved by the naked eye (order of $1mm$ and larger). The milli-scale consists of formations that can be readily observed with the assistance of an optical microscope or CT-scan ($10\mu m-1mm$); barbs and barbules are critical components of the milli-scale category. The micro-scale relates to small surface and subsurface formations pertaining to the barbs and barbules which are large with respect to the wavelength of light and are small with respect to the scale of the surface or volume to which they belong ($700nm-10\mu m$). The nano-scale refers to structures the size of which is in the wavelength range of the visible and UV spectrum ($300nm-700nm$). Micro-scale and nano-scale structures can be observed using an electron microscope.

The variation within each classification leads to differences in visual appearance between bird species. The remarkable range of combinations, vast and consequently difficult to quantify, can be observed in the specimens contained in the collection at the Cornell Museum of Vertebrates. Initial observations lead to the assignment of phenomenological descriptors such as velvety, hairy, dusty, woven, waxy, glossy, specular, iridescent, anisotropic, etc. (Figure A.1). Further study leads to greater understanding of the attributes which contribute to these sensory observations. A few representative cases of more frequently observed attributes illuminate the variety of factors involved in the construction of a feather's appearance at each of the four classification scales.

The macro-scale structure—that which can be observed with the naked eye—of a feather, encompasses its overall length, width, and (a)symmetry. The two

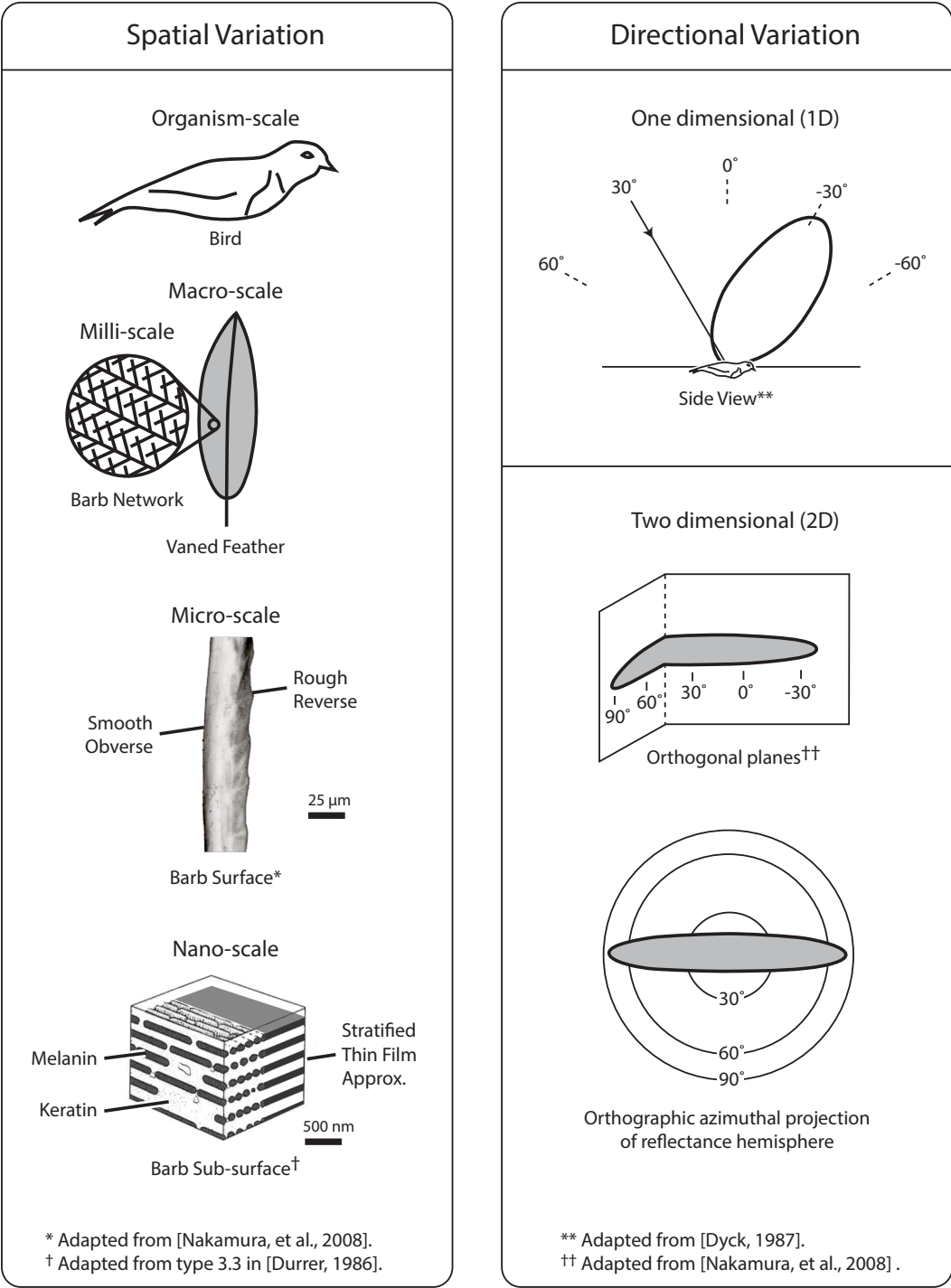


Figure 2.4: Feather spatial and directional variation.



Figure 2.5: This large primary flight feather belonging to a substantial bird (e.g. vulture) is an exaggerated example of vane asymmetry, axial rotation, proximal-distal bend, medial-lateral bend, and ventrally oriented concavity in both proximal-distal and medial-lateral orientations. (Unidentified feather from the teaching collection of the Cornell University Museum of Vertebrates)

opposing vanes of a feather may be similar in form, but in other cases the shape of the two vanes may differ due to functional requirements. Since vanes share the same central axis, the difference in vane shape is largely dependent on its outside profile. A primary flight feather may be asymmetrical, with opposing wide and narrow vanes. Occasionally a notch may be observed in either vane. The feather may bend gently along the proximal-distal axis, which usually produces a concavity in the ventral direction. The degree of bend is variable; many feathers are relatively flat (absence of bend). Some feathers have an axial rotation, most dramatically displayed in primary flight feathers, but less so in secondary flight feathers, while tertiary flight feathers are the flattest of the remiges. A pennaceous feather vane consists of a firm, inter-locked, fabric-like construction, which may ripple, undulate, or wave; the frequency of the waves is a function of the milli-scale structure (Figure 2.5).

For many feathers the milli-scale structure of the vane defines their appearance. Although every pennaceous feather consists of rachis and barbs—with the barbs in turn consisting of rami and distal and proximal barbules—the individ-

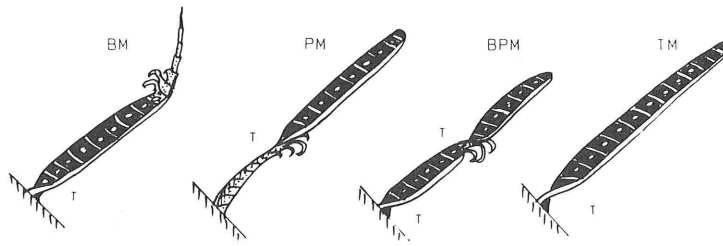


Figure 2.6: Modification of iridescent barbules. *T* site of torsion; *BM* basal part modified; *PM* pennulum modified; *BPM* basal part and pennulum modified (e.g. *Chrysococcyx cupreus*); *TM* total barbule modified [Durrer, 1986]. © 1986, Springer/Kluwer Academic Publishers. Reprinted with kind permission from Springer Science and Business Media.

ual attributes and the interaction of these major components define the milli-scale structure. As the primary axis of the feather, the rachis determines the orientation of the vane. The angles at which the barbs emerge from the rachis, and the angles at which the distal and proximal barbules emerge from the barb’s ramus, affect feather appearance; barbule rotation and twist provide spatial variation. Barbule cross-sectional shape and overlap with neighboring barbules may limit exposed surface area, significantly impacting directional reflectance [Nakamura et al., 2008]. Barbule length also plays an important role: longer distal barbules may cover the neighboring barb, essentially removing the barbs from the reflection function; shorter barbules instead ensure the ramus contributes to the aggregate reflection. The modified pennulum of an iridescent barbule may include a broad flattened surface for reflecting light [Durrer, 1986]. In his writings on modifications to iridescent barbules, Durrer classifies *Chrysococcyx* as “basal part and pennulum modified” or type *BPM* (Figure 2.6). Finally, each barb structure—ramus, proximal barbule and distal barbule—may display different color characteristics which add visual complexity to the textured surface.

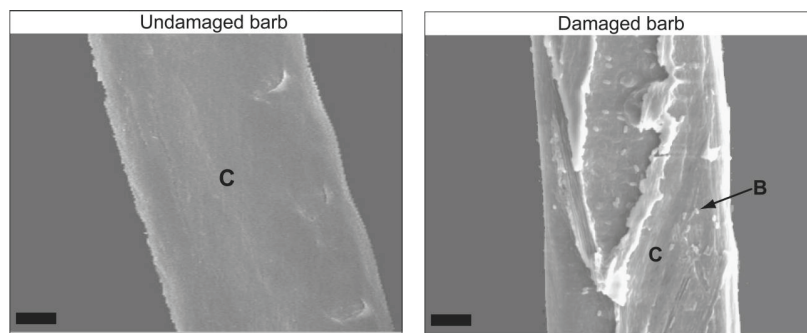


Figure 2.7: Scanning electron micrograph ($500\times$) of the outer surface of a feather barb experimentally damaged by the keratinolytic bacterium, *Bacillus pumilus*, and an undamaged feather barb. C = cortex, B = bacterial cells [Shawkey et al., 2007]. Reproduced with permission.

The characteristics of the micro-scale structure of the feather also lead to variation in appearance. There is presently little ornithological research in this area. In the *Columba Livia* (Rock Dove) iridescent neck plumage, for example, the smooth obverse surface of the distal barbules (Figure 2.4) may increase the glossiness of the specular reflection [Nakamura et al., 2008]. The surface of *Goura Victoria* (Victoria Crowned Pigeon), on the other hand, is peppered with small “lubricating” particles which may contribute to a diffuse-like reflection (Figure A.1). Preening oils generated by some birds and applied to feathers during preening are known to add gloss and shift the light absorption characteristics [Surmacki and Nowakowski, 2007]. Keratinolytic bacteria can refigure feather surfaces differentiating the light reflectance in birds of the same species. [Shawkey et al., 2007] (Figure 2.7).

Beneath the surface of the barb and barbule at the nano-scale are color producing structures formed by keratin, melanin and air. Keratin forms the cortex of the barb or barbule. At the core of the barb, air vacuoles frequently form. Melanin, a brown or black pigment, may be deposited in the medulla or scattered within the cortex. Melanin granules can take the form of spheres, ellipsoids, rods, and sticks (See Section 2.5.4.1) [Durrer, 1977, 1986]. The melanin deposits may be randomly

distributed or highly ordered, e.g. forming near solid layers or boundaries (See Figure 2.4 and Section 2.5.4.2). Iridescent color can be produced from interference between light waves reflected from the upper and lower boundaries of single thin-film-like layer of melanin. Light reflected from stratified layers of melanin separated by keratin can constructively interfere, producing brighter, more saturated specular reflection than that of a single layer [Prum, 1999]. Another important case of structural coloration involves air distributed in a quasi-organized matrix within a keratin layer—the formation is often referred to as “spongy keratin” (See Section 2.5.4.4).

2.2 Exterior Factors Impacting Feather Appearance

In addition to a feather’s natural structure and pigmentation, feather reflectance studies must also account for the impact of exterior factors.

Somewhat like human hair and nails, feathers are dead structures (hair and nails continue to grow at their root; feathers, once fully grown, remain unchanged until they are replaced). Feather replacement (known as a molt) occurs regularly with age and season, except in the case of accidental loss which leads to immediate regrowth. [Gill, 2007]. Exterior forces such as light, abrasion and destructive organisms can cause damage, particularly to an aging feather, and change its appearance over time. Bacteria, fungi, and arthropod ectoparasites [Proctor and Owens, 2000, Proctor, 2003, Clayton et al., 2003] break down the smallest of feather structures, most commonly, the barbule. Feather-degrading bacteria may alter feather coloration after the feather is fully formed (between molt and the breeding season) [Shawkey et al., 2009a]. The unpredictability of the effect of feather-

degrading bacteria is illustrated by *Sialia sialis* (Eastern Bluebird). Researchers have shown that feather degradation actually *increases* color expression of *S. sialis*. The degraded feather is significantly brighter and has greater spectral saturation than feathers not degraded by keratinolytic bacteria. The anatomical explanation for these differences probably lies in reduced thickness of the light absorbing cortex and subsequently increased exposure of the spongy layer (Figure 2.7).

When referencing specimens in museum collections to create analytical feather models, researchers must bear in mind that individual specimens differ according to their life cycle: gender, maturity, and season each play their role in feather appearance. Museum collections attempt to minimize environmental factors that adversely affect bird specimen plumage. Despite great care, however, specimen preparation can affect plumage coloration. Different mechanisms of coloration will vary in their susceptibility to different sources of degradation. Protective waxes and oils may be stripped causing either immediate change in gloss, shift in spectral reflectance, and long-term susceptibility to deterioration [Surmacki and Nowakowski, 2007]. Overhandling can lead to breakage and mishandling can lead to soiling which can change reflectance spectral distribution. Few studies have been conducted comparing museum collections to live birds. Doucet compared spectral reflectance measurements of live birds and museum specimens, including melanin and spongy keratin structures and concluded that, in general, museum specimens reliably represent the coloration of wild, live birds [Doucet and Hill, 2009].

2.3 Directional Scattering and Measurement

2.3.1 Radiometry

Radiometric terms describe physical quantities and can be measured with laboratory equipment. Strictly speaking, radiometry is a function of wavelength, time, position, direction, and polarization. Definitions of radiometric terms are outlined by Nicodemus [Nicodemus et al., 1977]. Since polarization is not known to play a role in avian vision, we are primarily interested in position, direction, and wavelength, along with the specialized morphology of each feather we measure. By relating the radiance exiting a small region on the surface of a feather to the radiance incident upon the material, we may quantify the effect of the material. To express the radiant exitance from a particular position, a sample surface is broken into small regions (pixels). The direction is specified as a point on a unit sphere centered on the sample position. The unit sphere may be divided into two hemispheres; the reflected hemisphere is the set of all directions over a surface; the transmitted hemisphere is the set of all directions under a surface. For any illuminated surface, a finite amount of incident energy of a given direction is redirected into both hemispheres about the surface.

Although each parameter in the light scattering equation – morphology, position, direction, and wavelength – critically influences feather appearance, in practical terms, the ability of any scientific instrument to sample all 4 components may be limited. An instrument may sample a component densely, sparsely, or not at all (Table 2.1).

	None	Sparse	Dense
Wave			
Direction			
Position			
Morphology			

Table 2.1: The ability of any scientific instrument to sample all components of reflectance and accompanying structure may be limited. An instrument may sample a component densely, sparsely, or not at all.

When reflectance is measured for the purpose of studying a specific organism, the instrumentation needs to be calibrated to the spectral response of that organism’s visual system. The human visual system contains three color cones. A naive representation of human chromaticity space is the isosceles triangle, with each corner representing the maximum stimulus of a cone. Perceptual studies extend our understanding of human color perception beyond the physiology of the human eye. Photometric terms describe how a human observer responds to light; the human visual system has a non-linear response to light of different frequencies and the International Commission on Illumination (CIE) has established standard chromaticity diagrams adapted to account for human color perception. In the human visual system, perceptual response to color stimulus has been extensively studied, but our understanding of the avian visual system is largely limited to the physiology of the avian eye. The avian eye has 4 color cones, one more than the human 3-cone system. While a human can see wavelengths in the visible spectrum, the addition of a violet or UV opsin in birds, extends avian vision into the near ultraviolet (NUV). Without a clear understanding of perceptual response, bird color space is commonly represented as a regular tetrahedron.

2.3.2 Specular and Diffuse Reflection

The reflection is *specular* when only one reflected direction exists for each incident direction (Figure 2.8). A purely specular reflecting material is smooth (i.e. irregularities are small compared with a wavelength of light). On the contrary, when a material is rough (i.e. irregularities are large compared with a wavelength of light), reflection from collimated incident light scatters over a broad range of directions. Reflection from rough surfaces is called *diffuse* (Figure 2.8). The two cases are the extremes of a continuum. When light strikes most real world surfaces, the directional behavior of the reflected light falls into one of two intermediate ranges, often categorized as *glossy specular* and *directional diffuse* reflectance (glossy specular reflectance shown in Figure 2.8).

Feathers exhibit a vast range of directional scattering behavior, the exact directional distribution depends on the nature of the material itself. Analytical modeling of directional reflectance from feathers should consider the surface geometry at the microscopic level. Directional reflectance from rough surfaces can be accounted for using micro-facet surface modeling. Micro-facet modeling statistically predicts the direction of reflected light by modeling the micro-scale roughness of the surface as an orientation-distribution of micro-facets. Using this geometric model, we can predict the probability of a ray reflecting in any given direction over a hemisphere. In computer graphics, this probabilistic treatment is an important feature of many physically-based illumination models. For the purposes of this thesis, it is useful to recognize that prior work established a correlation between an increase in surface roughness and an increase in directional distribution of the reflectance in a wide range of materials.

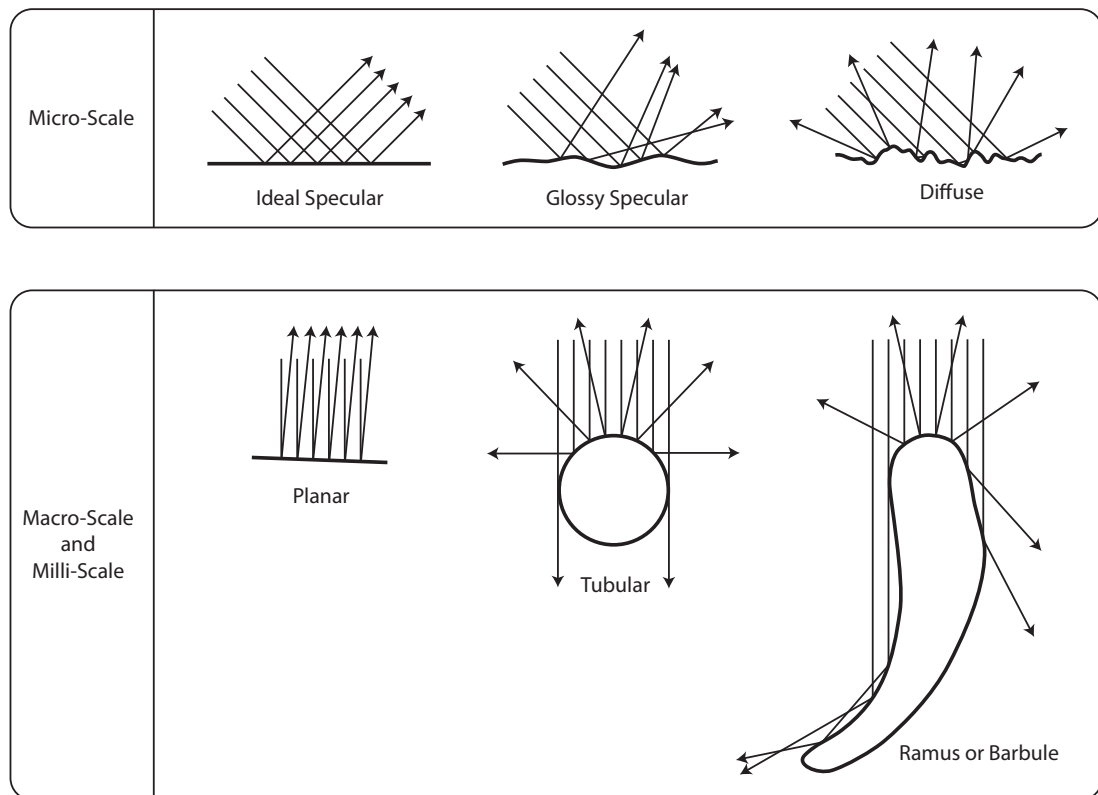


Figure 2.8: Geometric bases for variation in the distribution of directional reflectance.

2.3.3 Plumage Studies

Irradiance from feathers, like most heterogeneous real world materials, varies with position and direction. The feather of each bird species is composed of a unique organization of nano-, milli-, micro-, and macro-scale bio-optical structures which in aggregate exhibits distinctive directional scattering (Figure 2.4). Directional scattering investigations of bird plumage have been nearly absent in scientific studies. Bird reflectance research is still in an early stage, presently amounting to a patchwork of approaches with minimal overlap in technique, in part due to the different disciplines which have attacked the problem and their corresponding goals.

The earliest study I have found was conducted by Jan Dyck [Dyck, 1987], in which three one-dimensional photometric reflectance measurements (Figure 2.4) of the intact green plumage on the back of *Ptilinopus spp.* (Fruit Dove) were contrasted to that of an *Ducula concinna* (Imperial Pigeon). From his work we learn how innovations in the structure of the distal barbules of *Ptilinopus spp.* modify the direction of reflected light to produce a directionally diffuse appearance more common among birds with color producing rami. Atypical of feathers that produce color through interference, the feathers of some species of *Ptilinopus* are not specularly reflecting (e.g. *Pt. Rivoli*). The innovation, a row of tiny convex reflectors along the length of each distal barbule, reflects light with greater angular distribution and isotropy than the unmodified barbule. Dyck investigated the development of the innovation within multiple taxa in the genus to consider its phylogenetic origins. Though the color production is brilliant green, his photometric measurements captured only the luminance of the reflectance.

More recently, Osorio and Ham conducted a suite of directional measurements on fifteen structurally colored bird species [Osorio and Ham, 2002]. They captured

one-dimensional spectral directional reflectance from individual feathers averaged over a one-millimeter diameter spot of the intact, flattened vane. Directional reflectance was measured around two orthogonal axes—distal–proximal and medial–lateral—in the plane of the feather. They observed a range of diffusely and directionally reflecting plumage, including iridescence. Their results demonstrate a color change with either an alteration in the direction of the incident light or view. When illuminated from a point source, they found that the peak wavelength λ_{max} of the reflectance was linearly related to the angle between the incident lighting and viewing direction and independent of the surface direction. But outside the controlled lighting of their experimental setup, they observed that feathers could change in colour (hue) as a bird moves (with rotation of the surface direction). They explain that although λ_{max} is independent of surface direction under a point source, when illuminated diffusely the effective direction of the light source (e.g. the part of the sky reflected by the feather) varies with its surface direction. In other words, a change in the surface direction of a specularly reflecting feather invokes a change in the angle between its incident and viewing directions. The spectral component of Osorio and Ham’s goniometric measurements enabled inquiry in color change as a function of direction, but they conducted their experiments within the limitations of one dimension of reflected light.

Yoshioka and Kinoshita reported spectral directional reflectance measurements of peacock feathers [Yoshioka and Kinoshita, 2002]. Unlike the intact vane measurements of Osorio and Ham, they measured a single dissected barbule as well as a region of several dissected barbs containing many barbules. They too measured reflectance in one-dimension, but they explicitly measured around the barbule axis and correlated their reflectance measurements to the morphology of the barbule. They explain that although a simple lattice of nano-scale structure can suggest

the presence of optical interference, it cannot explain the widely spread angular reflectance from the feather. To reconcile the discrepancy, they introduce a statistical model for the smoothly curved surface of the barbule. The crescent shape of the transverse cross-section of the barbule tilts the nano-scale lattice with respect to incident light spreading the reflection in the plane perpendicular to the barbule axis.

In a subsequent study, Nakamura, Yoshioka and Kinoshita investigated the one-dimensional spectral directional reflectance of the structural color of the neck feather of the *C. livia* [Nakamura et al., 2008]. In a continuation of their prior work, they further investigate how milli-scale structures of the feather control the angular range of the reflectance. When a single barbule is dissected and measured in isolation, its complete transverse cross-sectional curvature primarily determines the angular range of its reflectance. But when a barb with its rows of barbules is dissected and measured, a portion of the curved cross-section of each barbule is covered by its adjacent barbule. The lateral overlap of adjacent barbules lessens the surface's degree of curvature, effectively limiting the angular range of the reflection. In addition to the one-dimensional spectral methodology established in their prior work on the Peacock, they measured the RGB reflectance of dissected components in two directional dimensions (Figure 2.4). Once dissected, the barb reveals both the distal and proximal barbules branching in opposite directions from either side of the barb. The authors note, almost in passing that the reflection pattern from the dissected barb forms a cross in two dimensions, consistent with the angle between the barbules. However, only the distal barbules are visible on an obverse intact vane, so their results are not useful for determining the signaling potential of that organism. The main body of their work focuses on the two-color reflectance of the exposed distal barbules. Their results, mapped in human perceptual color

space, demonstrate the color change from green to purple, passing through the achromatic point.

It is perhaps not surprising that these directional scattering studies are focused almost entirely on iridescent specimens. The two exceptions of two non-iridescent structural coloration, European Jay [Osorio and Ham, 2002] and *Ptilinopus rivoli* (White-bibbed Fruit Dove) [Dyck, 1987]), are still studied within the context of iridescence. Osorio and Ham use the European Jay as a foil; Dyck selects the White-bibbed Fruit Dove for its non-iridescent color specialization in contrast with the iridescence typical of other less specialized species in its genus.

Comprehensive directional scattering data is essential to fully understand the evolution and signaling function of specialized plumage morphology. All published measurements to date insufficiently characterize spatially-varying directional and hemispherical reflectance, and directional transmittance of any degree not at all. Furthermore, data gathered from non-structural samples is completely absent from the literature. As we have seen, excellent work has been conducted in one directional dimension, but two-dimensional studies will allow fuller account. Imaging and optical scattering instrumentation have evolved and matured and there are real opportunities to integrate existing and emerging techniques to measure reflectance and feather morphology. The overarching objective should be to more densely sample each component of the light scattering function and relate reflectance to specific morphology.

2.4 Anisotropy from Fibers

Many materials of the natural world exhibit anisotropy. Anisotropic Reflection models have long been a topic of research in computer graphics. Metal and dielectric materials with micro-facets oriented in a characteristic direction exhibit anisotropy, i.e. light scatters narrowly in the direction of elongation and widely in the direction orthogonal to the elongation [Kajiya, 1985]. Kajiya approaches the problem of rendering anisotropic surfaces as a problem of hierarchy of scale. The largest scale is the geometric model. The smallest scale simulates the finest detail; this is the realm of lighting models. Kajiya and Kay address the limits of rendering fine geometric detail such as fur and hair by treating fine geometry as a texture rather than geometry [Kajiya and Kay, 1989]. They present a new type of texture map, a “texel”, intended to represent a complex collection of surfaces contained within a volume. A texel is essentially a three-dimensional array of parameters that approximate visual properties of a collection of micro-surfaces and are replace detailed geometry. The texel supplies “the *painter’s illusion*, a suggestion that there is detail in the scene far beyond the resolution of the image. When one examines a painting closely the painter’s illusion falls apart: zooming in on a finely detailed object in a painting reveals only meaningless blotches of color” [Kajiya and Kay, 1989]. As with a painting, a texel approximates the texture of (for example) a feather viewed from normal distance, the appearance of which is generated by fine-scale geometry (barbs and barbules) that the eye cannot resolve.

Marschner, et. al. in 2003 conduct scattering measurements from individual hair fibers [Marschner et al., 2003] that illustrate visually significant effects not predicted by Kajiya and Kay’s classic phenomenological model which models the hair fiber as an opaque cylinder. While Kajiya and Kay account for light scat-

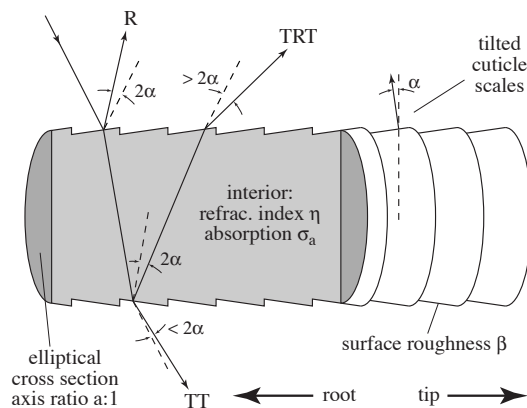


Figure 2.9: Hair fiber schematic [Marschner et al., 2003]. © 2003 Association for Computing Machinery, Inc. Reprinted by permission.

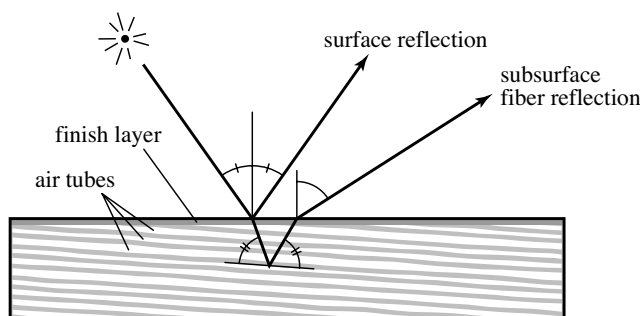


Figure 2.10: Surface and subsurface reflection directions from wood surface and wood subsurface fibers [Marschner et al., 2005]. © 2005 Association for Computing Machinery, Inc. Reprinted by permission.

tering with a diffuse term and a single specular term, Marschner et al. measure and model three specular highlights: one reflected from the cuticle surface, a secondary highlight due to internal reflection off the back side of the fiber, and a tertiary highlight due to transmission through the fiber (Figure 2.9). Marschner’s measurements of translucent hair fibers examine in-plane and out-of-plane scattering, scattering with rotation about the fiber axis, and hemispherical scattering.

Marschner, et. al. in 2005 measure and model the appearance of finished wood. Wood doesn’t conform to the “usual notion of anisotropic surface reflection.” Species specific wood grain pattern leads to spectacular spatially varying

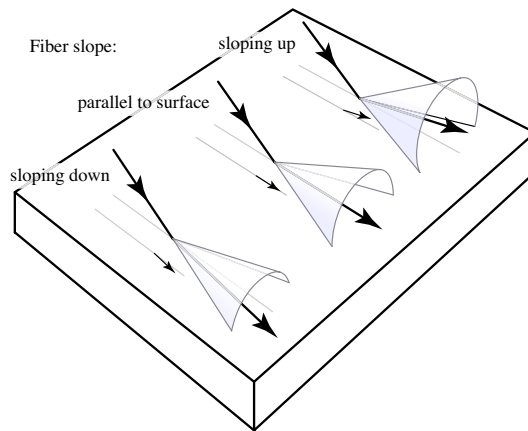


Figure 2.11: Reflection cones from fibers [Marschner et al., 2005]. © 2005 Association for Computing Machinery, Inc. Reprinted by permission.

directional scattering. Anisotropy from wood is due to the wood fibers below the surface (Figure 2.10). “Wood...is very much like hair turned inside out: instead of a bundle of near-parallel dielectric fibers in air, we have a solid block of dielectric filled with near-parallel air tubes.”

The characteristic highlight in wood, like the anisotropic surface highlight modeled by Kajiya-Kay [Kajiya and Kay, 1989], emerges on a cone. The axis of the cone—the fiber of the wood grain—varies in three dimensions and is not constrained to lie in the plane of the surface. The axis may vary its orientation tangentially within the plane of the surface or it may point into or out of the surface (Figures 2.11). They fit their reflection model for wood independently at each pixel by estimating the fiber axis and applying a fixed highlight width. The model relates the fiber direction to the incident and exitant directions of the directional scattering data and assumes the brightest samples are near the subsurface specular cone.

We predict the fibrous structure of the barb to scatter light in a similar manner to the materials discussed above. If the cross-sectional shape of the canonical rami

and canonical barbule approximates that of a cylinder, then the same reflection cone which is the basis of all aforementioned prediction models, could apply to the feather (Figure 2.8).

2.5 Mechanisms of Color Reflectance in Feathers

Diverse mechanisms of coloration are manifest in bird plumage. There are a number of useful overviews that cover the range of issues pertinent to feather color and function [Durrer, 1986, Dyck, 1974, Rutschke, 1974, Stettenheim, 1974, Prum, 1999]. Rick Prum most recently produced a comprehensive review of structural coloration in bird plumage [Prum, 2006]. The general organization and technical approach of this section is influenced by his publications. The ornithological literature is replete with morphology case studies; I have included below at least one example for each major mechanism.

2.5.1 Spectrally Unselective Specular Surface Reflection

Many feathers exhibit a white specular highlight, a form of surface reflection. The surface highlight color forms independent of the medullary color mechanisms. Surface highlights form on plumage of all colors, but are most visible when contrasted against saturated medullary reflection (Section 5.2). The *Xiphorhynchus* feathers in figure A.1, inset F1–F3, reflect a diffuse red pigmented color from the medulla and a contrasting white highlight from the cortex surface; the total appearance resembles a red glass fiber.

The micro-surface roughness and macro-shape of the cortex (a component of the milli-surface) modulates highlight appearance. Minimal micro-surface roughness creates narrow highlights (Figure 2.8). Increased roughness broadens highlights by distributing the reflected energy over a wider range of angles. Extreme roughness distributes the energy so widely that the local appearance of a distinct highlight is eliminated.

A flattened macro-surface reflects light at all points on the surface in similar direction (Figure 2.8). A rounded macro-surface limits surface area oriented in any one direction, thereby smearing the reflectance over a greater range of emerging angles (Figure 2.8). The specular highlights on the flattened rami of the *Cicinurus* feathers (Figure A.1, inset G1–G3) appear wider as compared to *Xiphorhynchus*, due to *Cicinurus*' rougher, flatter dorsal surface.

2.5.2 Pigmentation

What we call *pigmentary color* is created “solely as a result of molecular absorbance and emission light” [Prum, 1999]. The hue of the pigmentary color is determined by the molecular structure. The density of its distribution in tissue determines the saturation or purity of the color. The most common pigments are melanins and carotenoids. Melanins produce black, brown, and tan colors (Figure A.1, insets A1–A3, B1–B3, D1–D3, E1–E3 and H1). Carotenoids produce mainly red (Figure A.1, insets F1–F3 and G1–G3) and yellow coloration; though sometimes green, violet, or blue [Durrer, 1986]. Greens may be either pigmentary or structural (Figure A.1, insets H2–H3, I1–I3, and K1–K3). Blue and UV-colored pigments are rare; most blue and UV colorations are structural (Figure A.1, insets C1–C3 and L1–L5). For a table of pigments refer to Heinz Durrer [Durrer, 1986]. Some

pigments that affect the appearance of feather color come not from the bird itself, but from environmental sources. For example, iron-oxide rich soil may infiltrate feathers or adhere as a powder on the plumage; about 120 bird species display a rusty color as a result of “bathing” in red colored soil [Berthold and Rau, 1968].

The range of pigmentation in barbs is diverse, while that in barbules is more limited. The dense and spectrally-uniform absorbing pigment, melanin, is especially important and prevalent in both structures. In barbs, melanin may behave simply as the sole source of color, may combine with other pigments with a darkening effect, or it may also, as we shall see later, serve as an important, albeit invisible, role in structural coloration [Prum, 2006]. In the finer-scale, more fragile barbule structures, melanin appears frequently in greater density, strengthening the feather against damage and thereby also dominating the coloration. Again, unstructured melanin can behave simply as a pigment or, when organized into scattering arrays, melanin can create brilliant iridescent colors.

2.5.3 Incoherent Scattering

Some feathers appear white due to incoherent structural scattering in unpigmented feather media, e.g. the generic white feather of *Gallus gallus* (Domestic Hen) and the brilliant white feathers of *Lagopus mutus* (Rock Ptarmigan). The unpigmented barb ramus and barbule are composed of a nearly transparent keratin compound. Multiple scattering events occur at the surface, within the keratin tissue, and at the surface boundary of hollow vacuoles commonly found at the center of barbs and barbules. These multiple events randomly redirect the light rays causing a portion of the light gathered over the environment to be redirected to the eye. The greater the number of scattering events, the more rays are redirected to the eye,

and the brighter the feather appears (up to a limit). The brilliant white feathers of *Lagopus mutus*, Rock Ptarmigan, additionally scatter from large, irregularly shaped, randomly organized air cavities in the barbules [Dyck, 1979].

2.5.4 Coherent Scattering

Much of the structural coloration of barbs and barbules of feathers may be attributed to photonic crystals. A photonic crystal is composed of a periodic nano-scale optical structure organized in a spatial arrangement that affects the propagation of photons of light [Kinoshita, 2008]. The nano-scale structure consists of high and low index of refraction dielectrics that regularly alternate in a frequency pattern that interferes with the wavelength of light passing through the material. Photonic crystals may be constructed with periodicity in one-, two-, and three- dimensions. The “photonic crystal” is a convenient catch all, but crystalline structures of various dimensions are frequently called by alternate names, e.g. “thin-film” or “stratified layers” instead of “1D photonic crystal”, “ordered photonic matrix” in place of “2D and 3D photonic crystals”.

Finally, not all structural coloration is strictly crystalline. The “quasi-ordered photonic matrix” has independently evolved in numerous species of bird. Below is a quick review of the different organizations of photonic structure that leads to coherent scattering in feathers.

2.5.4.1 Coherent Scatterers

Complex photonic nano-scale structures are embedded in barb rami and barbules. The structures are comprised of melanin, keratin, and air with the respective re-

fractive indices ~ 2.0 , ~ 1.56 , and 1.0 . Mechanisms of structural coloration have evolved in multiple orders and families independently. The structures—composed of only 3 primary constituents—manifest remarkable variation in their composition, size, shape, and arrangement. Durrer has proposed classifications of melanin granules and classifications of stratified, iridescent producing structures involving melanin (See Type 3.3 in Figure 2.4) [Durrer, 1977, 1986]. In certain species, air pockets form at the center of each melanin granule. Since his nearly exhaustive classification system was published, research in coherent scattering from air formations in keratin has extended our understanding of ordered (Section 2.5.4.3) and quasi-ordered photonic nano-structures (Section 2.5.4.4) in two and three dimensions.

2.5.4.2 Thin-films

Structural color in feathers is most frequently attributed to coherent scattering from stratified layers or one-dimensional photonic crystals. Models based in thin-film theory are the most commonly employed to describe the stratified mechanisms.

Single Layer Thin-film The cortex of a barb ramus or barbule may approximate a thin film of keratin defined by an air interface on the outside, and on the inside, a dark melanin medullary interface (Type 1 in [Durrer, 1986]). Barbs and barbules that display strong iridescence from single layer thin-film interference maintain a cortex of relatively uniform thickness, e.g. *C. Livia* [Nakamura et al., 2008] . In some feathers, the cortex–medullary boundary is defined—in cross-section—by a single row of melanin rods (Type 2.1.1 in [Durrer, 1986]). Others define the boundary with two or more closely packed rows of melanin (Type 2.2.1,

3.2.1 in [Durrer, 1986]). Underneath the row(s), the medulla may contain a sparse random distribution of keratin and melanin, but the critical thin film boundary is well ordered to maintain proper thickness.

Scattering theory predicts multiple beam interference in single layer thin films. Each internal reflection increases the optical path difference. The difference in optical path is a function of the incident angle, refractive index, and the number of internal reflections [Hecht, 1998]. Multiple peaks in the visible spectrum may be predicted when the thin film is thicker and the first-order reflection peak is located in the infrared spectrum—this mechanism is called a “thick” film [Land, 1972]. The colors from thick films often appear less vibrant since the purity of color is diminished by the combination of multiple peaks in the UV-visible spectrum, while the maximum energy was reflected in the infrared spectrum which our human eyes do not perceive.

Multi-Layer Thin-film The single layer thin film cortex of a barb ramus or barbule has evolved in some species into a matrix comprised of multiple layers. The common manifestation consists of layers of melanin deposited in keratin. The melanin layers are individually comprised of densely packed granules approximating a 1D system (Type 2.3, 3.3, 3.4, 4.3, 5.3, 6.3 in [Durrer, 1986]). Since the typical system contains a matching number of adjacent melanin and keratin layers, the repeating system has been described as composed of multiple keratin–melanin layer pairs.

An increase in the depth of the number of layer-pairs proportionally increases the saturation and intensity of the reflected color [Dyck, 1987]. Dyck concludes maximum reflectance from the green feathers of the *Ptilinopus spp.* (Fruit Doves)

and the *Ducula concinna* (Imperial Pigeon) is roughly a linear function of the number of melanin layers (up to 20 layers). In contrast, reflectance from an ideal system (with no light absorption) begins to taper off with only 5 layers. Besides increased reflectance, an increase in the number of layer-pairs also narrows the spectral bandwidth producing more saturated color reflectance. Yet irregularities in the formation of the layers can produce a non-ideal multilayer system where $n_a d_a \neq n_b d_b$ [Land, 1972, Kinoshita and Yoshioka, 2005, Kinoshita et al., 2008, Kinoshita, 2008]. The first order reflection peak of the non-ideal system exists at the same wavelength as the ideal system, but the shape of the peak exhibits diminished height and increased width, and second order maximums appear on either side of the central peak [Land, 1972].

An example of the delicate balance between regularity and irregularity in the nano-scale structure of an iridescent feather barbule is demonstrated in the micrograph of the traverse cross-section of *Chrysococcyx cupreus* (African Emerald Cuckoo) in Figure 2.12. We present directional scattering measurements of *C. cupreus* in Chapter 4 of this thesis. Although we do not present spectral reflectance values for *C. cupreus*, a review of Durrer and Villiger, 1970b [Durrer and Villiger, 1970], provides insight into the relationship between the photonic nano-scale structure and reflectance spectra.

2.5.4.3 Ordered Photonic Matrix

In the previous section I highlighted examples of 1D photonic crystal mechanisms in bird plumage and discussed their optical behaviour as a function of thin-film theory.

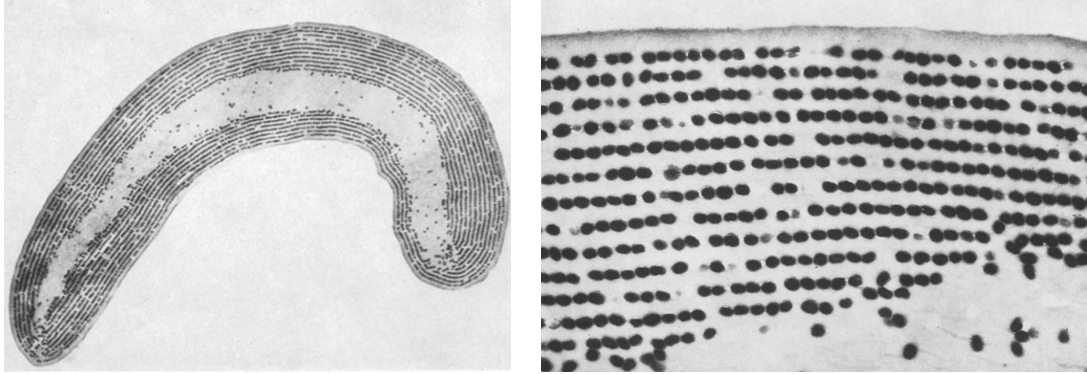


Figure 2.12: The multi-layer-pair iridescent producing structure of the barbule of *Chrysococcyx cupreus* contains up to 12 layer-pairs. The melanin sticks (1 micron long; 0.1 micron diameter) and keratin divisions form a periodic structure with naturally occurring irregularities or deviations in layer thickness. Cross-sections at 4,200 \times and 34,000 \times magnification [Durrer and Villiger, 1970]. Type StS in [Durrer, 1977]. Type 3.3 in [Durrer, 1986]. ©1970, Springer Berlin/Heidelberg. Reprinted with kind permission from Springer Science and Business Media.

Less recognized are examples of coherent scattering from 2D and 3D photonic crystal mechanisms.

A high level description of coherent scattering from a matrix follows: if nano-scale scatterers are regularly arranged in a crystal-like matrix, then light scattered at each nano-scale structure interferes constructively in directions dictated by the shape, size and orientation of the scatterers and by the frequency and angle of the incident light [Joannopoulos et al., 2008]. Descriptive language for the mechanism varies according to discipline, but the physical phenomenon based on diffraction is identical. Bragg's Law adapted to photonic crystals predicts the diffracted wavelengths. The diffracted spectrum consists of multiple spectral peaks based on integer multiples of the lattice constant.

An example of a two-dimensional keratin-air photonic crystal is found in the cortex of the *Pica hudsonia* (Black-billed Magpie) barbule [Vigneron and Lousse, 2006]. The *P. hudsonia* consists of contrasting black and white plumage. Much of

the incident light striking the black feathers is absorbed, but within a specific range of incident and viewing directions, iridescence can be perceived on the bluish wings and yellowish-green tail. A traverse cross-section of the feather barbules shows a flat ribbon-like shape and a clean separation between the cortex and medulla. The cortex bears the photonic nano-structure: visible holes in the traverse cross-section are arranged in a very coherent two-dimensional regular hexagonal lattice. A view of a disaggregated barbule reveals the longitudinal structure of the cortex—fused microtubes at least $1.5\mu\text{m}$ in length. The two-dimensional photonic crystal is actually an homogeneous block which contains an hexagonal lattice of parallel air channels.

2.5.4.4 Quasi-ordered Photonic Matrix

Many more species have been discovered employing quasi-ordered 3D photonic matrices as compared to regularly ordered 3D photonic matrices. Ever increasing research in recent years has been devoted to coherent scattering from quasi-ordered photonic nano-scale structure in bird plumage and avian skin [Dyck, 1971b,a, Prum et al., 1998, 1999b,a, Prum, 2003, Shawkey et al., 2006, Shawkey and Hill, 2006, Shawkey et al., 2009b]. A common class of quasi-ordered structural coloration, referred to as “spongy-keratin,” has been isolated in the barbs of multiple orders and families, including the *Cyanocitta stelleri* (Steller’s Jay), a closely related species to the *Cyanocitta cristata* (Blue Jay) that I study in Chapter 5 of this thesis. Spongy keratin is a 3D photonic nano-scale structure that possesses characteristics similar to a random diffraction grating², producing a diffracted spectrum consisting primarily of only one spectral peak [Hecht, 1998].

²A random diffraction grating consists of regularly shaped holes randomly scattered in space [Hecht, 1998].

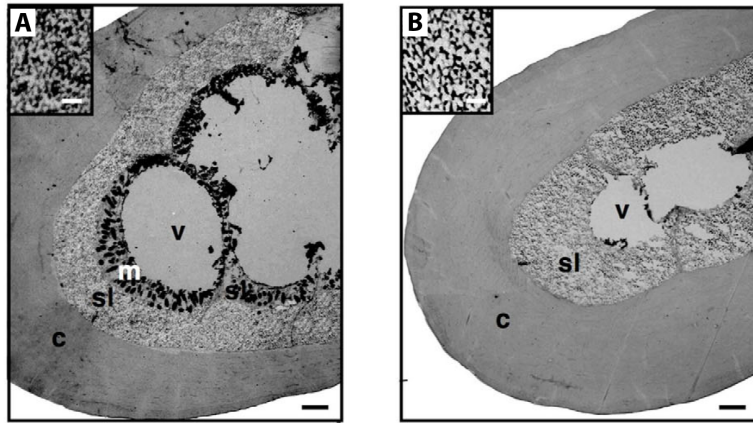


Figure 2.13: Barb nano-scale structure of a blue *C. stelleri* feather (A) and an amelanotic (albino) *C. stelleri* feather (B). TEM micrographs of barbs (scale bars, $1\mu\text{m}$) with insets in A and B showing close-ups of spongy layer (scale bars, $500\mu\text{m}$). c, cortex; sl, spongy layer; m, melanin granules; v, vacuoles [Shawkey and Hill, 2006]. Reprinted with permission.

A curious set of findings was discovered in connection to the brilliant white feathers of the albino *C. stelleri* [Shawkey and Hill, 2006]. Unlike the *Lagopus muta* (Rock Ptarmigan), which as we have seen obtains its brilliant white from incoherent scattering (Section 2.5.3), the albino jay lacks the ability to lay down light absorbing melanin pigmentation (Figure 2.13, Inset B) but preserves its spongy keratin layer. The reflectance of the albino specimen is characterized by blue-colored coherent scattering from the spongy keratin layer, and augmented by incoherent scattering which the melanin-pigmented under-layer typically absorbs in normal specimens. The measured reflectance spectra of the albino *Cyanocitta stelleri* displays approximately flat reflectance over the visible spectrum. The blue light contribution due to coherent scattering is much stronger than any effect from Rayleigh scattering. The increase in blue light reflectance from coherent scattering causes a “whitening” effect, making the material look less yellow and more brilliant white—not dissimilar to the perceived effect of optical brightening agents frequently used in detergents.

2.6 Summary

A thorough study of the directional reflectance from plumage must investigate the relationship between directional reflectance and the structure of the feather itself. Research methods should include investigations of (1) morphology, and (2) the direction and (3) color of the light scattering, at multiple scales of resolution. To capture the variation in directional reflectance across the feather, instrumentation must be able to sample each component of the reflectance—wavelength, incident direction, exitant direction—at multiple locations across the surface of the feather. Since light interacts with the surface of the feather and its subsurface structure, the morphology of the feather structure at each sample location on the feather needs to be measured in order to correlate the directional reflectance measurements to morphology. The overall shape and surface of the feather vane (the macro-scale) and of its component members (the milli-scale) scatter light according to principles of geometric optics. Subsurface nano-scale structure in many feathers generate so-called “structural coloration,” which is a purely physical optics phenomenon and can differ drastically from ordinary coloration mechanisms such as pigmentation. Iridescence, from which many feathers derive their vivid, eye-catching changeable color, is one type of structural color that varies as a function of viewing angle. Most materials of the natural world exhibit anisotropy. A predictive feather reflectance model must therefore consider how to fit the anisotropy of measured reflectance data. Prior work with hair, wood and cloth provides some insight.

APPENDIX A
FEATHER VANE APPEARANCE DIVERSITY

Photographs and micrographs show the diverse appearance of the feather vane. The milli structure produces a wide range of color, texture, and directional reflectance. Specimens belong to the study collection at the Museum of Vertebrates, Cornell University.

A1–A3 Hawk: Broad light–dark brown stripes traverse the rectrix feather vanes.

B1–B3 Guineafowl: Dark brown rings surround light brown spots on a medium brown ground. The color value of the background is achieved via a dithered pattern consisting of the same light and dark brown colors. Consistent color integration between the barb components is managed in order to grow a coherent pattern.

C1–C3 *Goura victoria*: The dusty appearance caused by small “lubricating” particles scattered over the surface of the barbs and constituent parts.

D1–D3 Owl : Long distal barbules with long cilia extend beyond the adjacent rami. The up-pointing pennulum and cilia of the distal barbule create a soft velvety nap which covers the rami. The unzipped dorsal surface of the feather in image *D2* displays the short and ordered proximal barbules as compared to the long distal barbules. Broad light–dark brown stripes traverse the feather vanes. The light stripe consists of light barbules and light cilia. The dark stripe consists of dark barbules with light and dark cilia.

E1–E3 Vulture: The distal barbules of this flight feather create a woven appearance.

F1–F3 *Xiphorhynchus*: The pigmented translucent rami appear glass-like. The rami reflect sharp white highlights and transmit red. Red caustic patterns

are prominently featured on the fiber at the keratin-air interface opposite the specular highlight.

G1–G3 *Cicinnurus*: The appearance of *Cicinnurus* is similar to *Xiphorhynchus* (F1-F3). The cross-sectional shape of the barb ramus is flatter than *Xiphorhynchus*. The flatter surface reflects a broader highlight. Surface roughness is visible in highlight discontinuities.

H1–H3 *Cicinnurus*: This decorative tail feather has only one vane which allows it to curl on itself to form a rosette. The rosette is iridescent on the obverse side and matte brown on the reverse. The vane of this feather—the iridescent rosette—is less than $\frac{1}{2}$ -inch in diameter and located at the end of a 5-inch long wiry rachis. The wiry attachment isolates the iridescent spot from the main body. The spot flutters independently of the body as the bird moves.

I1–I3 Unknown: Black velvet of a wing feather

J1–J3 *Quiscalus*: Oily-colored iridescence of the contour feathers of the back.

K1–K3 *Chrysococcyx cupreus*: Glossy iridescent reflection from the distal and proximal barbules of the contour feathers of the back.

L1–L5 *Tangara*: Diffuse blue reflectance of the contour feathers of the breast.

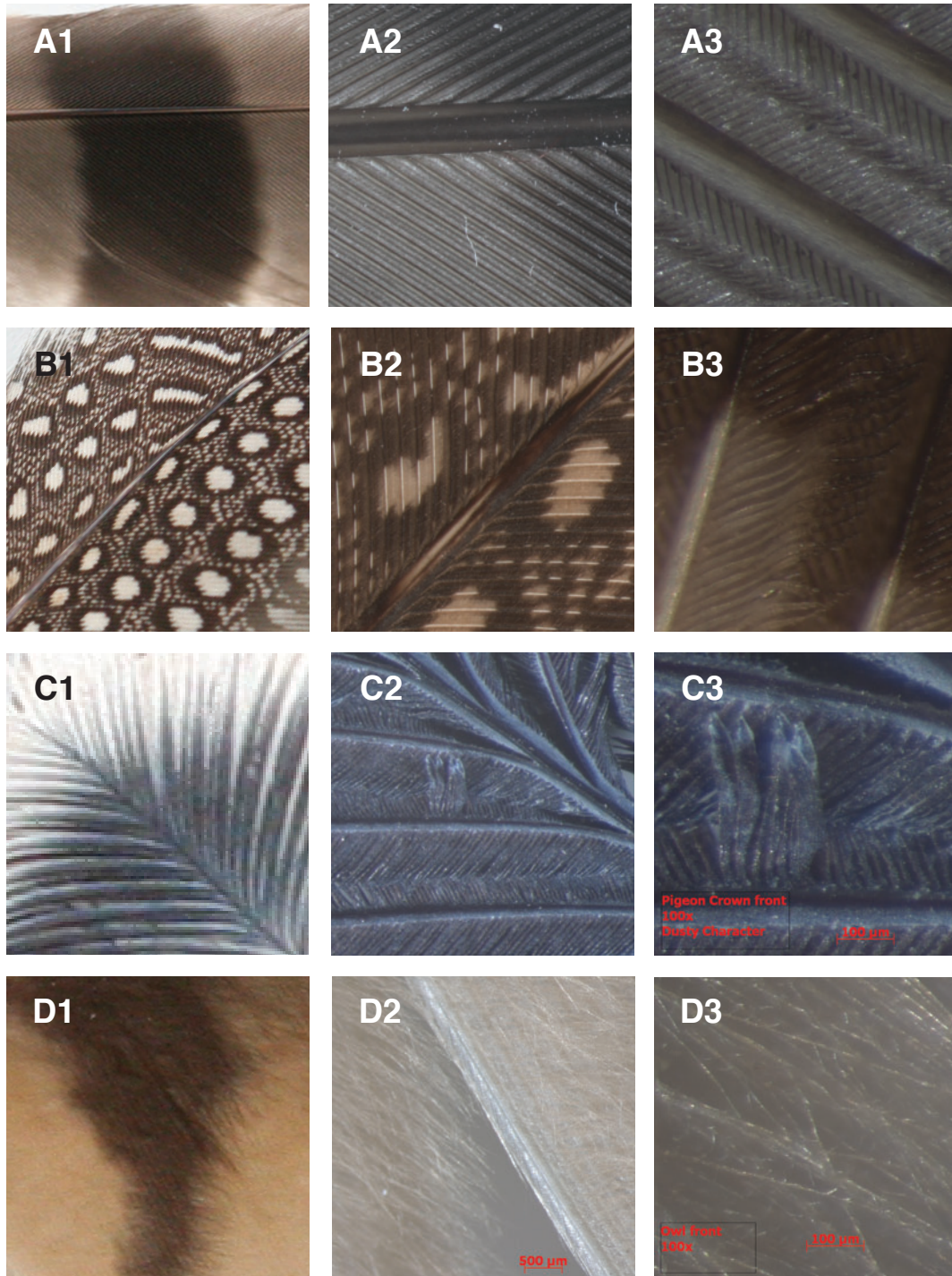


Figure A.1: Feather Vane Appearance Diversity

Figure A.1 (Continued)

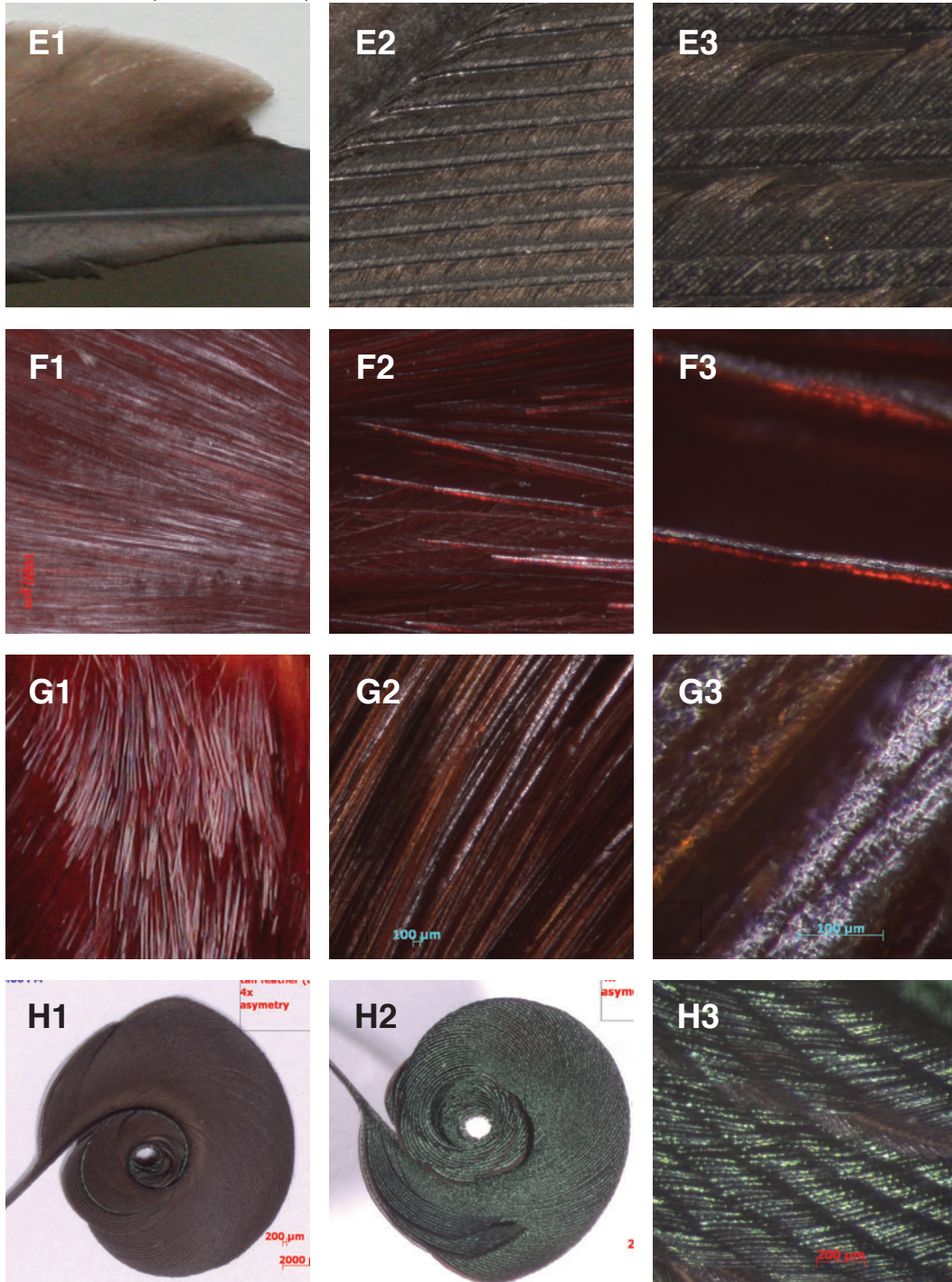
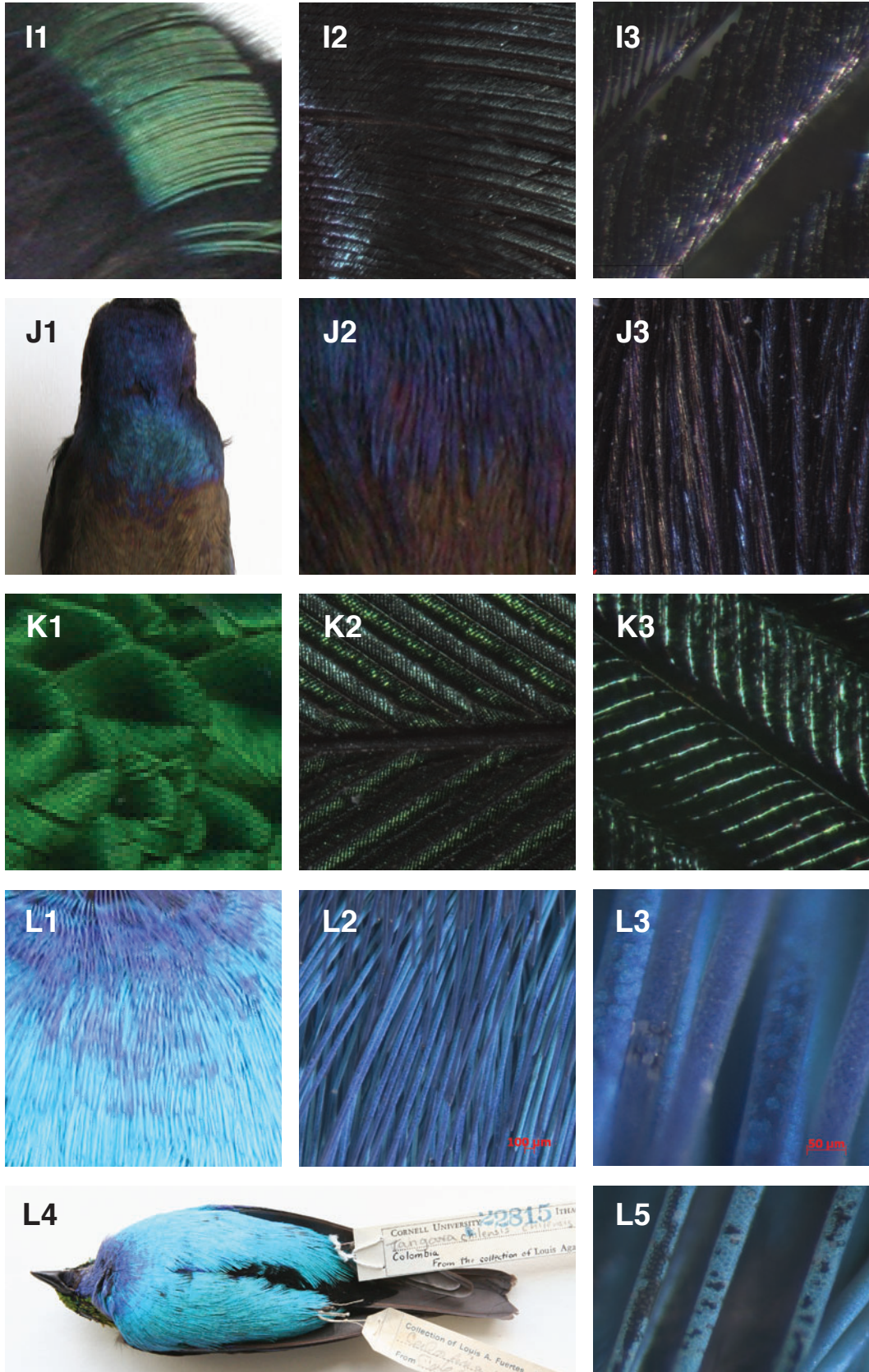


Figure A.1 (Continued)



CHAPTER 3
METHODS FOR MEASURING SPATIALLY- AND
DIRECTIONALLY-VARYING LIGHT SCATTERING FROM
BIOLOGICAL MATERIAL

Todd Alan Harvey¹, Kimberly S. Bostwick²³, Steve Marschner⁴

3.1 Abstract (Short)

In contrast to the limited sampling areas and directions of previous methods, we sampled light scattering from hundreds of incident directions uniformly distributed over a sphere and at millions of positions on the surface of our subjects. We visualized the directional light scattering at user-defined, biologically-relevant spatial positions and scales.

3.2 Abstract (Long)

The color and pattern of an organism's integument play ecologically and socially critical functions in most animal taxa. These phenotypic properties are determined by the interaction of light with the structure of the integument, which can exhibit optical scattering that varies both spatially (across the surface of the integument) and directionally (with change in lighting and viewing direction). From nano- to

¹Department of Biomedical Sciences,

²Department of Ecology and Evolutionary Biology,

³Museum of Vertebrates,

⁴Department of Computer Science, Cornell University, Ithaca, NY 14853, USA

macro-scales, the structure of the integument has evolved functionally to increase the signaling capability of the organism. In order to assess the influence of the morphology of different scales upon the overall appearance, tools to measure and analyze the color of biological structures need flexibility to isolate directional light scattering at various scales of magnification.

Previous research into the reflectance from integuments has too frequently discounted the contribution of directionality—e.g. diffuse vs. specular or isotropic vs. anisotropic reflection—to color expression. Most color measurements have fixed the geometry to carefully avoid angular affects (e.g. to eliminate specular reflection from color measurements, it is common to place the light normal to the surface and record the reflectance at 45° from the normal). Furthermore, studies that do link morphology to directionally-varying reflectance have focused on the nano-scale periodic mechanisms underlying iridescence [Durrer, 1986, Kinoshita, 2008, Land, 1972, Brink and van der Berg, 2004], ignoring the micro-, milli-, and macro-scale geometries and their contributions to the far-field optical signature [Westin et al., 1992, Nakamura et al., 2008]. We studied how the performance of a feather’s complex and varied milli-scale morphology (barb rami, distal barbules, and proximal barbules) expands the range of expression possible from nano-scale structures alone. By characterizing the functional consequences of the directional expression of milli-scale structures, we have enabled inquiry into their adaptive consequences.

In a single image recorded by the camera, we observed that light reflected differently at different locations on the surface of the integument, that is, light reflectance was spatially-varying. We methodically moved the light and camera around the subject using a spherical gantry [Marschner et al., 2003, 2005], with

which we captured 2 dimensions of *surface position* (X and Y), 2 dimensions of *light direction* (latitude and longitude), and 2 dimensions of *camera direction* (latitude and longitude) (Figure 3.2). We thereby explored the emerging light as both spatially-varying and as a function of the illumination direction and view direction.

In most previous experiments the light detector aggregates reflectance from a relatively large sample region [Vukusic and Stavenga, 2009, Dyck, 1987, Nakamura et al., 2008, Stavenga et al., 2010], requiring specimen dissection in order to isolate individual milli-scale structures [Nakamura et al., 2008, Yoshioka and Kinoshita, 2002, Stavenga et al., 2009]. Our non-destructive protocol preserved the morphology of an intact feather vane. By eliminating dissection and measuring the entire feather with a high resolution camera, our approach offers tremendous flexibility in studying light scattering from arbitrary regions of the vane.

Our three complementary methods— sampling reflectance using the gantry, browsing data in software, and visualizing the data graphically—provided greater ability to study color and pattern of the natural world (Figure 3.1).

3.3 Protocol

1. Measure Scattered Light in the Canonical Camera Direction:

Measure scattered light over the sphere of incident directions from the canonical camera direction, i.e. the camera is in the direction of the surface normal. This most fundamental or primary routine sparsely samples the whole sphere (Primary routine in Figure 3.1), after which a number of secondary routines may be devised to target specific features of the reflectance at higher sampling density.

1.1. Prepare and Mount the Object to be Measured

- 1.1.1. Prepare a thin ferrous metal mounting plate with a $\frac{1}{2}$ -inch aperture surrounded by a ring of targets (as seen in figures 3.2 and 3.9).
- 1.1.2. Prepare the material to be measured. If measuring a feather, groom the barbs to correct for any unzipped or misaligned sections of the pennaceous vane.
- 1.1.3. Lay the surface of the object (obverse face of the feather) against the back side (opposite the target ring) of the plate.
- 1.1.4. Center the region of interest over the $\frac{1}{2}$ -inch aperture in the plate.
- 1.1.5. Lay a sheet of magnetic film with a $\frac{5}{8}$ -inch aperture against the back side of the object (reverse face of the feather), thereby pressing the object flat against the plate.
- 1.1.6. Align the aperture of the film to the aperture of the plate without shearing the surface. The flattened surface, pinned around the circumference of the circular aperture, yields a planar macro-surface approximately coincident with the plate's surface.

1.2. Configure the Gantry

- 1.2.1. Locate the center of the circular aperture at the origin of the gantry coordinate system.
- 1.2.2. Place a light source on the gantry outer arm. Aim and narrowly focus the light at the object, ensuring that the aperture is uniformly illuminated for all light source angles.
- 1.2.3. Place a camera on the gantry inner arm. Adjust the camera distance and the focal length of the macro lens until the ring of targets fills the width of the sensor.

1.2.4. Calibrate the rotational movements (θ, ϕ) of the camera and lamp arms. Calibrate the inclination (θ) with respect to the object's surface normal so that the camera and the lamp are aligned with the surface normal when $\theta = 0$. Calibrate the azimuth (ϕ) of the camera to the azimuth of the lamp. The absolute azimuthal orientation is not critical since the captured images may be rotated later in the protocol.

1.3. Configure the Camera Focus and Exposure

1.3.1. Rotate the camera until the object is viewed at a grazing angle. Decrease the f-number to minimize the depth of field (DOF), then set the focus plane at the center of the aperture. Increase the f-number to increase the DOF until the ring of targets surrounding the aperture is in focus. A compromise between diffraction and DOF induced blur may be required.

1.3.2. Clip a color standard flat against the mounting plate. For RGB images use a Macbeth Color Checker. For UV-visible-NIR measurements use Spectralon.

1.3.3. Photograph the color standard in RAW format. Calculate the color channel multipliers to white balance the image.

1.3.4. Find the exposure bracket that spans the dynamic range of the scene under the most extreme viewing and lighting directions.

1.3.5. For each exposure time in the bracket, acquire a dark noise image by exposing the sensor with the lens cap on.

1.4. Acquire Measurements from a Sparsely Sampled Sphere of Incident Directions

1.4.1. Position the camera axis normal to the surface plane $\{\theta, \phi\}=\{0,0\}$.

- 1.4.2. Step the light through of a series of uniformly distributed positions on the sphere, using a coarse sampling (e.g. less than 500 points).
- 1.4.3. For each incident light direction in the sampling:
 - 1.4.3.1. Capture a raw image for each exposure time in the exposure bracket.
 - 1.4.3.2. Capture a single image illuminated by the camera mounted flash synchronized to a relatively short exposure time to suppress the gantry lamp illumination.
 - 1.4.3.3. Advance to the next incident light direction and repeat.
- 1.5. Process Measurements from Sparsely Sampled Sphere
 - 1.5.1. Using the debug mode of ddraw⁵ to disable its demosaicing function, convert from RAW format to greyscale, 16-bit, linear, PPM format:
 - 1.5.1.1. Each dark noise exposure.
 - 1.5.1.2. Each exposure of the object at each incident light direction.
 - 1.5.2. Integrate all low dynamic range (LDR) greyscale exposures under gantry lamp illumination into a single high dynamic range (HDR) color image for each incident light direction.
 - 1.5.2.1. Subtract the corresponding dark noise image from each LDR exposure.
 - 1.5.2.2. Demosaic each LDR exposure to yield a one-quarter scale image.
 - 1.5.2.3. White balance each LDR exposure using the color channel multipliers computed in step 1.3.3..

⁵Ddraw is an open-source computer program developed by David Coffin. It converts a camera's proprietary RAW-formatted image (i.e. unprocessed CCD data) to a standard image format. See <http://www.cybercom.net/~dcoffin/ddraw/>.

- 1.5.2.4. Merge dark-noise-subtracted LDR exposures into a single HDR image by summing all the values at each pixel position and dividing by the sum of the exposure times, omitting overexposed pixels from both sums.
- 1.5.2.5. Store HDR image in EXR format encoded in half-float precision and lossless wavelet (PIZ) compression.
- 1.5.3. If the camera direction is not the canonical direction or the measurement run is part of a multiple camera direction set (See secondary routines in Section 2. and Figure 3.1):
 - 1.5.3.1. Convert the single LDR greyscale exposure of the flash-illuminated tracking targets for each incident light direction to a demosaiced, one-quarter scale, LDR color image in EXR format.
 - 1.5.3.2. Follow the protocol in Projective Subroutine 3.3. to use the flash-illuminated image to project each HDR lamp-illuminated image into the canonical view.
- 1.5.4. Rotate the HDR images into the desired orientation—e.g. in our case a 90 degree rotation orients the rachis vertically and the feather tip up.
- 1.5.5. Crop the HDR images tightly around the circular aperture. Masking the targets and metal plate outside the aperture reduces file size by up to 25%.
- 1.5.6. Permute the data in the entire set of HDR images to create a set of files, one for each of several blocks in the image, that contain all the directional reflectance values organized by pixel. These directional reflectance cache files are organized to enable quick access to all the

directional color measurements at a single pixel position of the 2D projection of the 3D object.

1.6. Browse and Visualize Measurements

- 1.6.1. Launch the SimpleBrowser application with the processed measurements of the sparsely sampled sphere. A window opens containing the image of the object illuminated by the first incident lighting direction.
- 1.6.2. Only a fraction of the dynamic range of the HDR image may be displayed on a computer display. Decrease or increase exposure of the image to reveal over- and under-exposed regions.
- 1.6.3. Select either a single pixel, linear, or rectangular region of the feather vane shown in figure 3.3.
- 1.6.4. Plot the average directional light scattering from the selected region of the vane tabulated at incident directions on the unit sphere. A plot window displaying reflectance as a function of direction cosines opens adjacent to the image window (See R1 in figure 3.4). A change in the pixel selection in the image window automatically updates the directional scattering plot.
- 1.6.5. By default, the direction of maximum luminance (a transmittance direction in a typical feather measurement) is assigned an exposure of 1. Decrease or increase the exposure in one-half stop ($\sqrt{2}\times$) increments to expose the reflectance hemisphere of the spherical data set.
- 1.6.6. Cycle the reflectance color map on the unit sphere between RGB, chromaticity and luminance (See R1, R2, and R3 in figure 3.4).

- 1.6.7. Click the sphere to enable the trackball interface. Drag the interface to orbit the sphere. To see the reflectance hemisphere, return the sphere to its default position; to see the transmittance hemisphere rotate the sphere 180° from the default position (See T1, T2, T3 in figure 3.4).
- 1.6.8. Select the polar plot mode to see the radii of each incident direction on the unit sphere scaled by the respective luminance values of the irradiance recorded by the camera. Overlay the luminance scaled sphere with a chromaticity color map (See P3 in figure 3.4).
- 1.6.9. The direction of illumination of the displayed image is circled in red in the directional scattering plot. Click any other incident lighting direction to show the image of the feather illuminated from that direction.

2. Measure Scattered Light in Multiple Camera Directions:

Measure scattered light in one- and two-dimensions on the sphere of incident directions from the multiple camera directions, i.e. the camera is not always in the direction of the surface normal (Secondary routines in Figure 3.1)

- 2.1. Follow the protocol in Projective Subroutine 3.1. to calibrate the camera projection and position.
- 2.2. Follow the protocol in Projective Subroutine 3.2. to calibrate the target positions and projection offsets.
- 2.3. Measure Seven Non-uniformly Sampled Reflectance Hemispheres (Routine 2.1 in Figure 3.1)
 - 2.3.1. Examine the directional distribution of the reflected light measured from the camera view normal to the surface, i.e. $\{\theta, \phi\}=\{0,0\}$. Re-

sample the reflectance hemisphere to record camera radiance from non-specular directions more sparsely and specular directions more densely.

2.3.2. Apply the same criteria to sample the reflectance in 6 additional camera directions uniformly distributed over half a hemisphere, i.e. $\{\theta, \phi\} = \{30, 0\}, \{30, 90\}, \{60, 0\}, \{60, 45\}, \{60, 90\}, \{60, 135\}$. Predict the specular regions of the 6 additional runs from the viewing direction of each coupled with the reflection angle of the initial run.

2.3.3. For each of the 7 non-uniformly sampled hemispheres, acquire and process measurements following the description in section 1.4. and 1.5. above.

2.3.4. Visually browse the directional reflectance from the same region of the feather in each of the 7 non-uniformly sampled hemispheres, following the description in section 1.6. above. Arrange the directional reflectance plots for each of the 7 camera directions on a polar coordinate system, where the placement of each plot is based on its camera direction (See the visual results of routine 2.1 in Figure 3.1; also Figure 3.5).

2.4. Measure finely sampled semicircular paths to acquire detailed information about color change with angle (Routine 2.3 in Figure 3.1)

2.4.1. Launch the SimpleBrowser application and input the processed measurements of the non-uniformly sampled reflectance hemisphere with camera direction $\{\theta, \phi\} = \{0, 0\}$. Select one pixel in the image, then fit a plane to the 90th percentile of the luminance of the hemispherical reflectance at the selected pixel position.

- 2.4.2. Construct a 1D acquisition run which finely samples specular reflectance in the specular plane. Generate gantry arm angles in $\frac{1}{2}$ -degree half-angle increments in the plane defined in the previous step. Start with the half-angle equal to 0° and increase the half-angle to 90° . For each measurement in the acquisition run, keep the half-vector constant and equal to the surface normal so that each camera direction is located in the specular direction.
- 2.4.3. Acquire and process measurements following the description in section 1.4. and 1.5. above.
- 2.4.4. Visually browse the 1D directional reflectance following the description in section 1.6., while sampling a very small region (e.g. 3×3 pixels) centered on the same pixel used to fit the specular plane in step 2.4.1.. Find the direction of peak reflectance, i.e. shading normal. Construct 3 additional acquisition runs in the same manner as step 2.4.2., but set the half-vector to the shading normal rather than the surface normal. For the 3 additional runs, generate gantry arm angles that lie in planes containing the shading normal but which are rotated 45, 90, and 135 degrees with respect to the specular plane defined in step 2.4.1..
- 2.4.5. Acquire and process measurements following the description in section 1.4. and 1.5. above.
- 2.4.6. Visually browse the 1D directional reflectance following the description in section 1.6., while sampling a very small region (e.g. 3×3 pixels) centered on the pixel used to fit the specular plane in step 2.4.1.. Export from SimpleBrowser the average reflected radiance of this very small region.

- 2.4.7. In MATLAB, plot its chromaticity as a function of half-angle on a chromaticity diagram (Figure 3.6). Plot its hue, chroma, and luminance as a function of the half-angle (Figure 3.7).
- 2.4.8. Construct four more 1D acquisition runs in the same four planes as above, but this time configure the light and camera directions to measure the width and decay of the specular reflectance. Set the half-angle between the light and camera to a constant 10-degrees. Generate gantry arm angles in 1-degree half-vector increments around the axis orthogonal to the plane. Start with a half-vector equal to -80 degrees and increase the half-vector to +80 degrees, where 0 degrees equals the shading normal. Note that not all camera directions are located in the specular direction.
- 2.4.9. Acquire, process and export measurements following the descriptions in sections 1.4. and 1.5., and 2.4.6. respectively.
- 2.4.10. In MATLAB, plot its chromaticity on a chromaticity diagram as a function of the angle between the half-vector and the shading normal. Plot its hue, chroma, and luminance as a function of the angle between the half-vector and the shading normal.

3. Projective Subroutines:

The following three subroutines are accessed when a measurement run is part of a multiple camera direction set (Routines 2.1 and 2.3 in Figure 3.1). In such cases, the camera direction is not the canonical direction (normal to the surface), meaning that the object is photographed from a direction inclined from its surface normal (Figure 3.9). As such, each photograph needs to be rectified to match the canonical orientation by referencing the ring of targets on the mounting plate.

3.1. Calibrate Camera Projection and Position:

The purpose of this subroutine is to calculate the camera projection and position that will be used in the following part of the protocol.

- 3.1.1. Clip a checker-patterned calibration target flat against the mounting plate.
- 3.1.2. Capture one image at the canonical camera view (i.e. $\{\theta, \phi\}=\{0,0\}$) and several images at various other camera views spread over a 120-degree cone centered on the canonical view.
- 3.1.3. Load the images into the Bouguet Toolbox⁶, a MATLAB camera calibration toolkit. Extract the grid corners in each of the images to reconstruct the camera matrices. Export the intrinsic camera *projection* matrix (P) and the extrinsic camera *position* matrix (M). The intrinsic camera projection is composed of the focal length and the principal point. The extrinsic camera position is composed primarily of a translation; it translates the origin of the world to the camera position.
- 3.1.4. Solve for the matrix that transforms calibration-target coordinates to gantry turntable coordinates (X), i.e. Bouguet space to gantry space.
- 3.1.5. Unclip the checker pattern from the metal plate.
- 3.1.6. Return to the main protocol.

3.2. Calibrate Target Positions and Projection Offsets:

The purpose of this subroutine is to calculate the offsets between the calibration plane, the target plane, and the sample, and to locate the targets that will be used in the following part of the protocol.

⁶Bouguet Toolbox is a camera calibration toolbox for MATLAB developed by Jean-Yves Bouguet. See http://www.vision.caltech.edu/bouguetj/calib_doc.

- 3.2.1. Rotate the camera in gantry coordinates so that the optical axis is perpendicular to the surface plane, i.e. the canonical frame.
- 3.2.2. Capture an image of the ring of targets surrounding the aperture with flash illumination. This is the canonical image for image alignment.
- 3.2.3. Process the raw camera output (Protocol outlined in section 1.5.3.1. and 1.5.4.).
- 3.2.4. Mask the region inside and outside the ring target zone, eliminating stray specular highlights that may confuse target recognition, then find the targets in the image.
- 3.2.5. Rotate the camera to a grazing angle and capture an image.
- 3.2.6. Calculate the canonical camera pose ($M_c = M * R_c$) and the grazing angle camera pose ($M_g = M * R_g$) based on the extrinsic camera matrix M in step 3.1.3. which includes a translation based on the position of the Bouguet checker pattern.
- 3.2.7. Redefine M by offsetting its translation by the thickness of the paper target-ring. Iterate by trial and error (recalculating M using a different offset for the calibration plane) until the offset in gantry space between the plane of the Bouguet checkerboard and the plane of the ring of targets, i.e. thickness of the paper target-ring, has been solved. Verify the offset in each iteration by re-projecting the targets in the grazing angle image onto the targets of the canonical image.
- 3.2.8. Redefine M following the procedure of the previous step to re-project the apertured object in the grazing angle image onto the apertured object in the canonical image by trial and error until the

offset in gantry space between the plane of the ring of targets and the plane of the apertured object, i.e. thickness of the metal plate, has been solved.

3.2.9. Return to the main protocol.

3.3. Projective transform each HDR image into the canonical view or the view direction orthogonal to the surface plane.

3.3.1. Read a canonical image illuminated from a non-specular direction. (At grazing specular directions the diminished contrast between the white surface of the paper and the black ink can lead to target detection failure (Compare the clarity of image A and B in figure 3.9).

3.3.2. Locate the coordinates of the center of each target in the canonical image.

3.3.3. Load the target image illuminated by camera mounted flash for a given lamp-camera directional pair (B in figure 3.9).

3.3.4. Roughly transform the target image into the canonical camera frame using the gantry camera matrix M computed in step 3.2.7..

3.3.5. Locate the coordinates of the center of each target in the transformed target image (C in figure 3.9).

3.3.6. Match each target in the transformed target image to its reference target in the canonical image by finding the minimum distance between image and reference targets.

3.3.7. Discard any blurred targets caused by DOF at grazing angles (C in figure 3.9).

3.3.8. Solve the 2D projective transform that maps image targets in the canonical frame to canonical-image targets in the same frame.

- 3.3.9. Untransform the warped-to-fit targets from the canonical image frame back to the original image frame through the plane of the apertured object (M in step 3.2.8.) rather than the plane of the targets (M in step 3.2.7.).
- 3.3.10. Save the target coordinate pairs that map the apertured object in the target image to the apertured object in the canonical target image.
- 3.3.11. Load the HDR image illuminated by the lamp (A in figure 3.9).
- 3.3.12. Infer a spatial projective transform from saved target coordinate pairs to transform the HDR image into the canonical frame (E in figure 3.9).
- 3.3.13. Return to the main protocol.

3.4 Representative Results

The primary measurement of our protocol (Routine 1 of Figure 3.1) fixed the camera direction and only moved the light. Ideally, we could measure reflectance from many camera directions, even as many as the number of incident light directions, to yield a symmetrical data set. In practice, this would require far too many exposures. We can obtain sufficient information about different viewing positions by moving the camera a few times assuming 180° rotational symmetry about the surface normal. During the secondary measurement phase (Routine 2.1 of Figure 3.1), we acquired measurements from 7 viewing directions distributed over the hemisphere and within 60° of the zenith [Irawan, 2008, Irawan and Marschner, 2012].

In the figures of this paper, we show representative data measured from a feather of *Lamprolornis purpureus* (Purple Glossy Starling), the reflectance of which is iridescent, glossy, and anisotropic (Figure 3.5). In each of the 7 viewing directions, reflected light is gathered from hundreds of incident lighting directions on the hemisphere. The directions form a narrow band orthogonally oriented to the central axis of the feather (See feather image in figure 3.4). The iridescence color shift is subtle (blue-green at normal incidence and cyan at grazing incidence) when the feather is viewed normal to its surface as seen in the $(0^\circ, 0^\circ)$ RGB plot of figure 3.5). As the viewing angle approaches grazing, the angle between the viewing direction and the incident directions is maximized, leading to a more striking color shift (blue-green at 0° and magenta at 240° between incident and viewing directions) as seen in $(60^\circ, 0^\circ)$ RGB plot in 3.5.

We can afford to step the light and camera at much finer angular resolution when we restrict the movements to 1 dimension. Figure 3.6 shows the chromaticity of the reflectance of *L. purpureus* plumage as a function of the angle between the incident and viewing directions, where the incident and viewing directions are in the plane containing the specular band. As the iridescent color arcs through chromaticity space, the hue shifts from blue-green to purple.

Spatial variation in the directional reflectance is visible where different (x,y) coordinates of the integument correspond to different milli-scale structures. In the case of *L. purpureus* only one structure—the distal barbule—is visible over most of the area. By contrast, in *C. cupreus*, three milli-scale structures—the rami, distal barbules, and proximal barbules—are clearly distinguished in the data; we can observe that reflectance from the feather is oriented with respect to the longitudinal axis of each structure (Figure 3.8).

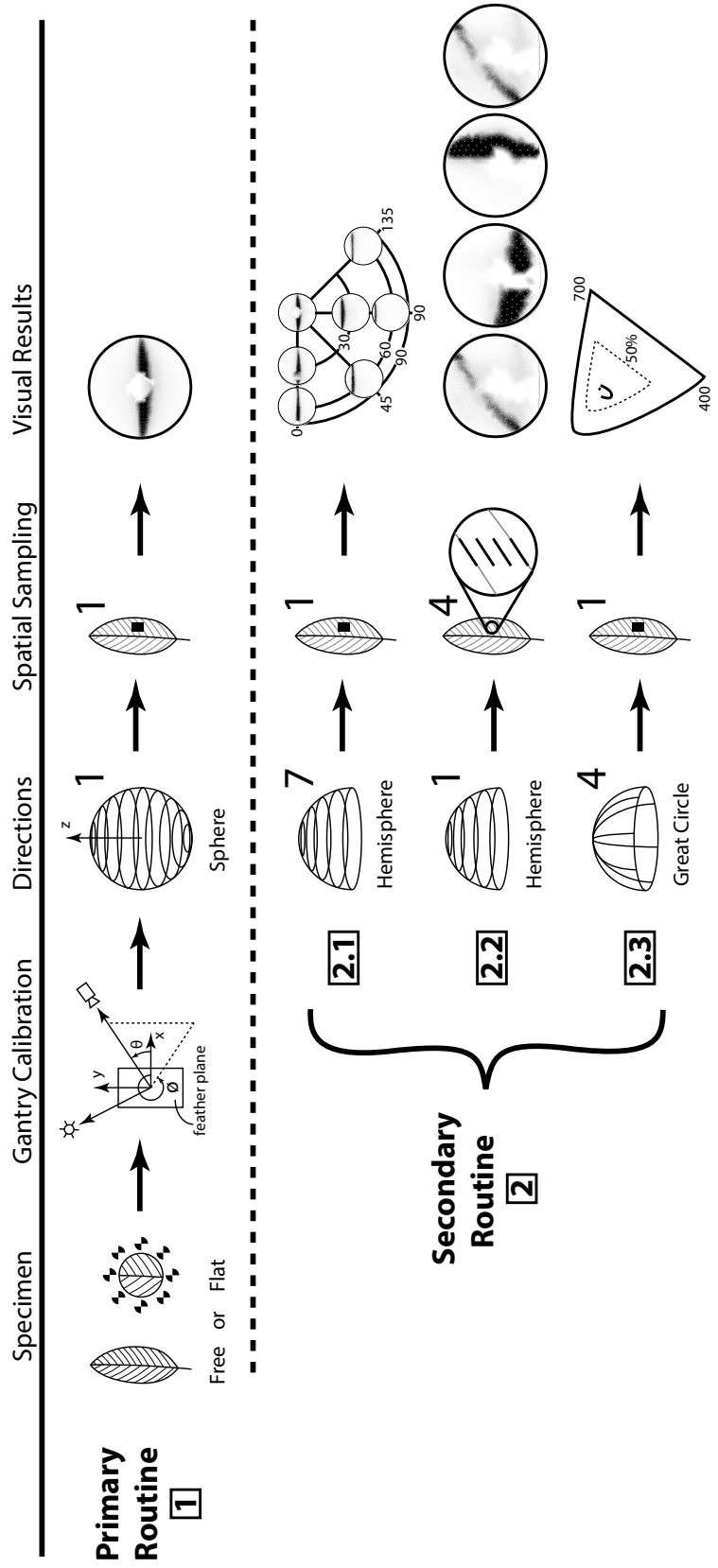


Figure 3.1: This schematic overview depicts two mounting methods, the spherical gantry coordinate system, types of acquisition sampling and their respective results.

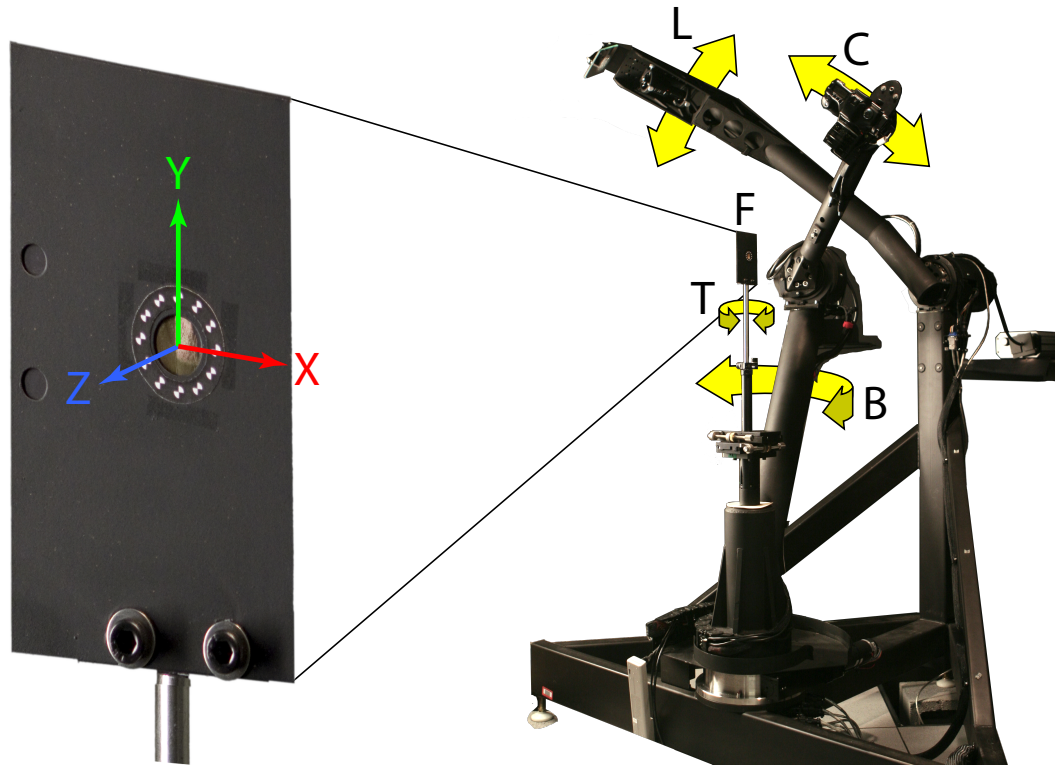


Figure 3.2: The flattened feather is visible through an aperture in a metal plate surrounded by a ring of targets. A spherical gantry can be posed to measure light scattering from a feather at multiple incident lighting and viewing directions. L=Light arm (latitude). C= Camera arm (latitude). B=Camera Base (longitude). T=Turntable (longitude). F=Feather.

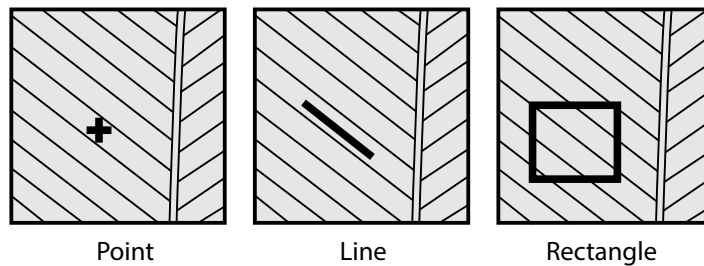


Figure 3.3: Average directional scattering may be computed from a point, line or rectangular region of feather vane.

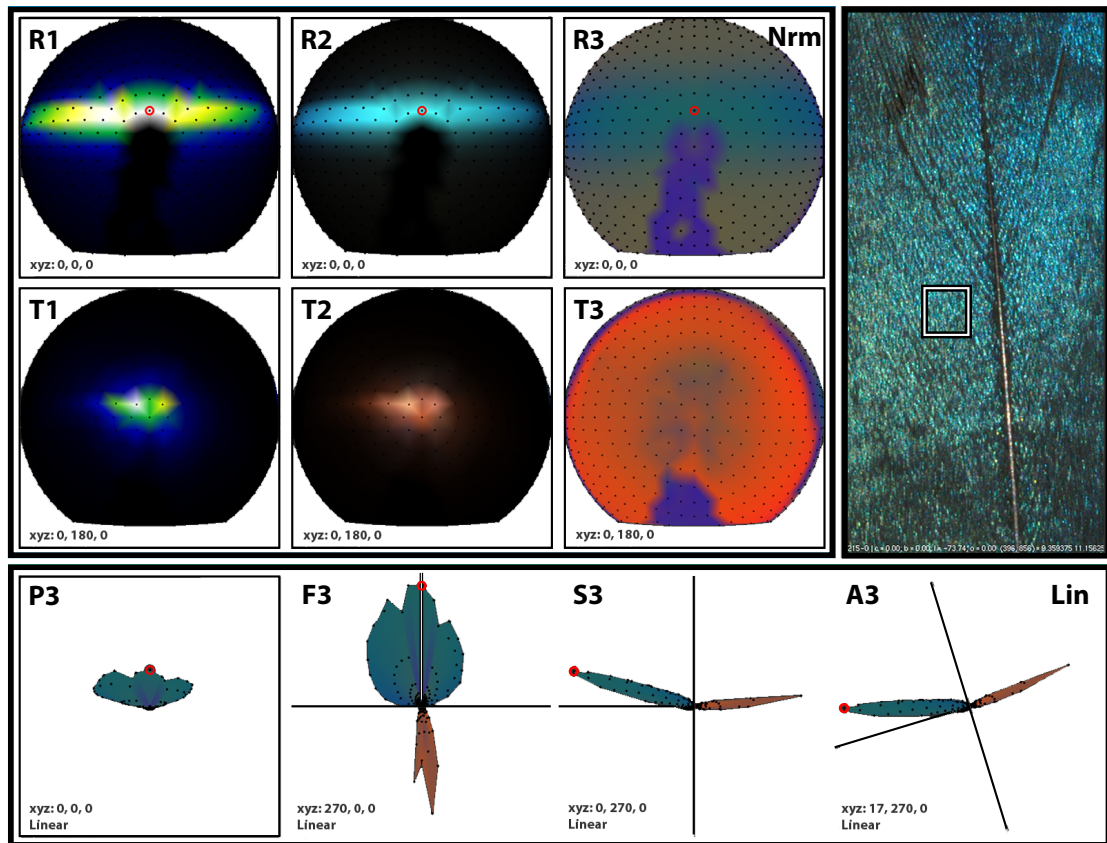


Figure 3.4: Example of directional scattering plotting functions (R^* =Reflectance, T^* =Transmittance, P^* =Top, F^* =Front, S^* =Side, A^* =Arbitrary) and color schemes (*1=Luminance, *2=RGB, *3=Chromaticity).

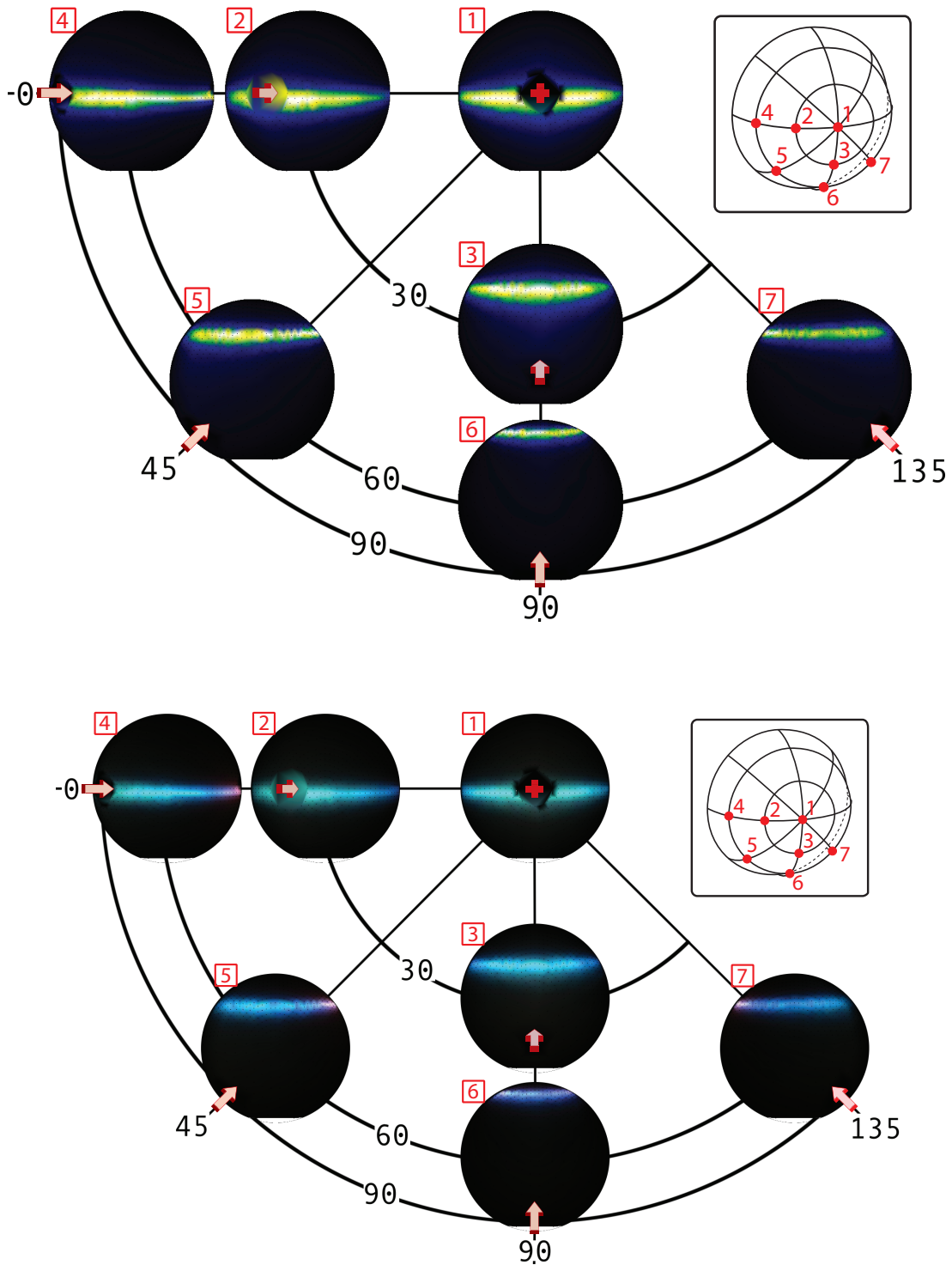


Figure 3.5: The luminance (top) and RGB color (bottom) of the hemispherical reflectance in direction cosine space as viewed from the (elevation angle, azimuth angle) coordinate pairs: $(0^\circ, 0^\circ)$, $(30^\circ, 0^\circ)$, $(30^\circ, 90^\circ)$, $(60^\circ, 0^\circ)$, $(60^\circ, 45^\circ)$, $(60^\circ, 90^\circ)$, and $(60^\circ, 135^\circ)$. The reflectance is averaged from a 25×25 pixel rectangular region of the lateral vane of a tertial *L. purpureus* (Purple Glossy Starling) feather. The red arrows represent camera directions.

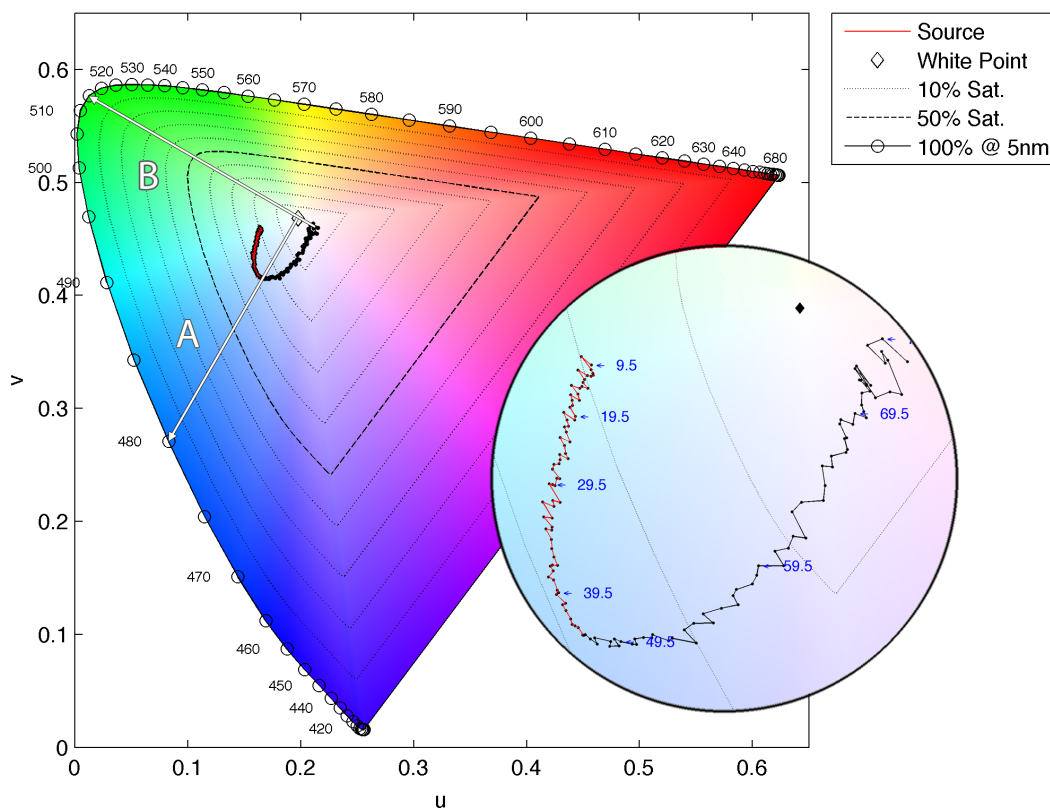


Figure 3.6: Chromaticity of the reflectance as a function of the half-angle between the incident lighting and viewing directions: CIE 1976 Uniform Chromaticity Scales (USC) with inset.

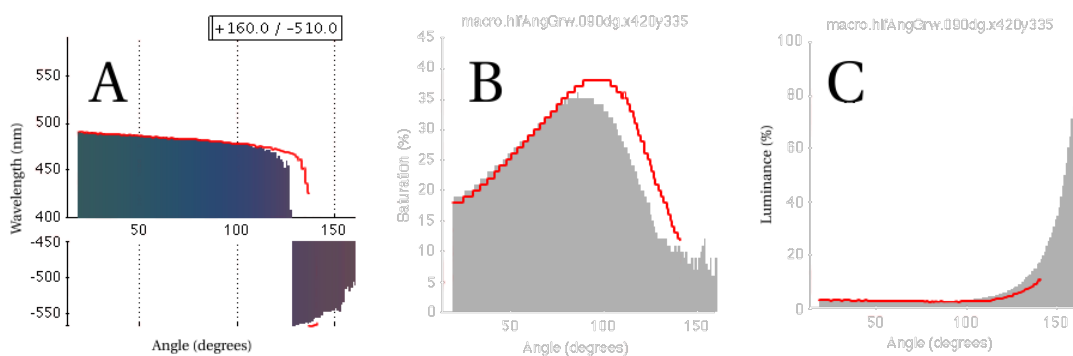


Figure 3.7: Color reflectance as a function of the angle between the incident lighting and viewing directions, in-plane with the fiber tangent (red) and perpendicular to the tangent (shaded): (A) Hue, (B) Percent chroma, (C) Percent luminance. The color shading in plot A is the RGB color of the reflectance. Negative wavelength values represent colors in the non-spectral purple triangle.

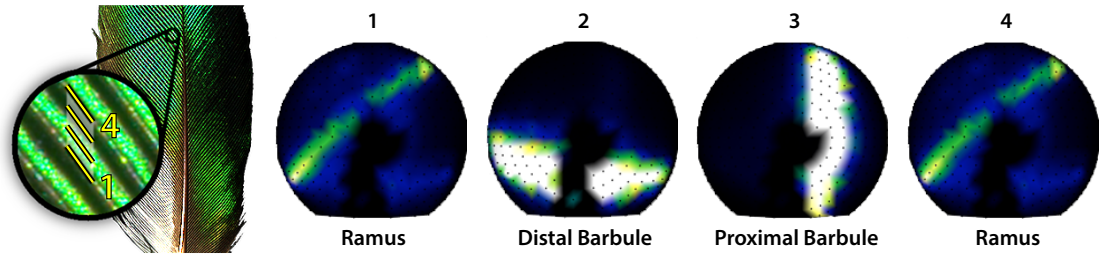


Figure 3.8: Average directional reflectance of distal barbules and proximal barbules between two adjacent rami of the *C. cupreus* (African Emerald Cuckoo).

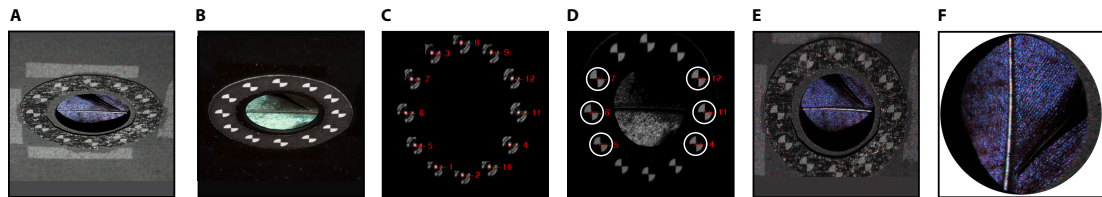


Figure 3.9: (A) Non-rectified image illuminated by gantry lamp, (B) Non-rectified image illuminated by flash on camera, (C) Filtered target candidates on affine transformed flash-illuminated image, (D) Acceptably sharp targets within depth of field, (E) Rectified lamp-illuminated image, (F) Rotated feather tip up, cropped and masked.

3.5 Disclosures

None.

3.6 Discussion

Though the performance and function of many pigimentary and structural colorations are well recognized, the morphology of many integuments is so complex that their structural detail and function are poorly understood [Vukusic, 2011]. Integuments have developed specializations that vary spatially over the surface of

the organism to differentially reflect light directionally toward the viewer. Directionality has received attention primarily in the study of iridescence due to its color shift with change of incident and viewing angle, and research into iridescence of biological integument has garnered primarily 1D and some 2D measurements [Nakamura et al., 2008, Stavenga et al., 2010, Dyck, 1987]. But generalized 6D measurements have not been routine in the study of integuments, iridescent or otherwise [Dana et al., 1999, Chen et al., 2002, Levoy et al., 2009] and the literature on organismal color phenotypes is constrained by the lack of directional color data of the type our method provides.

The feather is an especially rich integumentary material comprising arrangements of milli-scale structure of the barb: rami, distal barbules, and proximal barbules. The small scale of the elements and their complex arrangements make it difficult to discern the light scattering performance of the individual elements. Our protocol successfully isolated milli-scale structure from the influence of macro-scale geometry. By characterizing the functional consequences of the directional expression of milli-scale structures to the far-field signature of the feather, we enabled inquiry into their adaptive consequences.

We faced practical tradeoffs between spectral, spatial and angular resolution. We chose high spatial, medium angular and low spectral for our studies. Other combinations could be used, but some (e.g., all high) lead to unworkably long measurement times. Attention must be focused where it is important for the particular phenomena being studied. In choosing to employ an RGB camera with a Bayer filter mosaic, we designed our protocol to match the human visual system. The RGB camera could be replaced and our protocol adapted to measure the relative color stimulus of any organism, e.g. sensitivity in the UV spectrum is

needed to measure avian tetra-chromatic color [Stevens et al., 2007]. A spectral imaging camera would provide the most general solution.

We demonstrated our protocol with tertial wing feathers since they are colorful and easily flattened against a reference plate. Unfortunately, the aperture of the metal plate revealed only a fraction of the feather surface. If we could simultaneously measure the 3D shape of the feather surface while measuring its reflectance, we could avoid mechanically flattening the feather and instead measure the entire feather in its natural, unflattened state.

Interactive, specialized, integrated tools for visualizing data provide substantial benefit to scientists exploring and interpreting large data volumes. The greater the integration and interactivity, the easier connections in the data are observed. In our software, a user can interactively plot average directional scattering as a function of surface position (Figure 3.4). Further development of our software could integrate other plotting functions (Figures 3.6, 3.7) to extend the interactive experience.

3.7 Acknowledgements

This research was supported by funding from the National Science Foundation (NSF CAREER award CCF-0347303 and NSF grant CCF-0541105). The authors would like to thank Jaroslav Křivánek, Jon Moon, Edgar Velázquez-Armendáriz, Wenzel Jakob, and James Harvey for their intellectual contributions.

CHAPTER 4

**DIRECTIONAL REFLECTANCE AND MILLI-SCALE FEATHER
MORPHOLOGY OF THE AFRICAN EMERALD CUCKOO,
*CHRYSOCOCCYX CUPREUS***

Todd Alan Harvey¹, Kimberly S. Bostwick^{2,3}, Steve Marschner⁴

Birds have evolved diverse plumage through complex morphological modifications. We investigate how the interplay of light with surface and subsurface feather morphology determines the *direction* of light propagation, an understudied aspect of avian visual signalling. We hypothesize that milli-scale structural modifications of feathers produce anisotropic reflectance, the direction of which may be predicted by the orientation of the milli-scale structure. The subject of this study is the visually stunning African Emerald Cuckoo, *Chrysococcyx cupreus*, noted for its shimmering green iridescent appearance. Using a spherical gantry, we measured the change in the directional reflectance across the feather surface and over a hemisphere of incident lighting directions. Using a microCT scanner, we also studied the morphology of the structural branches of the barb. We tracked the changes in the directional reflectance to the orientation of the structural branches as observed in the CT data. We conclude that (1) the far-field signal of the feather consists of multiple specular components, each associated with a different structural branch, and (2) the direction of each specular component is correlated to the orientation of the corresponding structure.

¹Department of Biomedical Sciences,

²Department of Ecology and Evolutionary Biology,

³Museum of Vertebrates,

⁴Department of Computer Science, Cornell University, Ithaca, NY 14853, USA

Keywords: feather; morphology; reflectance; directional reflectance; anisotropy; appearance

4.1 Introduction

Birds have evolved diverse plumage through complex morphological modifications producing what Durrer has called the “most luxurious costumes in the animal kingdom” [Durrer, 1986]. These costumes have sparked inquiry among scientists, engineers, artists, and designers who seek to dissect, measure, and model the novel appearance of birds. Many female birds preferentially select a mate based in part on this ornamentation. Pioneering work has recently affirmed the importance of direction to acoustical signalling in the context of avian mating [Patricelli et al., 2007, 2008]; as with acoustical signalling, direction is an essential aspect of visual signalling [Lythgoe, 1979]. Whether feathers are displaying courtship signals or camouflaging a silhouette, the direction of light propagation is integral to what the potential partner or predator sees.

Plumage appearance—in all its variation—is explained by the complex interactions of light with feather structure at and under the surface cortex of the feather. Appearance can be discussed in terms of colour (chroma, saturation, and intensity), direction (incident and viewing), and location on the integument. Too frequently researchers focus entirely on the first, treating reflectance as directionally non-dimensional and limiting investigation of variation across the surface of the organism to gross-scale colour patches of the integument.

Iridescence is one particularly striking feature in many species. Through diffraction and interference, nanoscale light-reflecting structures produce colours and patterns that shift and change as the bird, viewer, or light moves, creating a dynamic appearance that draws the human—and presumably the avian—eye. Most previous research on plumage colour has carefully fixed the directions of viewing and illumination to ensure repeatable measurements of this ephemeral reflection, but in this paper our focus is directly on this dynamic aspect of plumage appearance.

Describing the whole appearance of an organism, for any viewer under any kind of illumination, boils down to describing the light reflected from the integument as a function of the direction from which it arrives (the incident direction) and the direction from which it is observed (the reflected direction). This paper is devoted to studying this dependence of reflectance on direction.

Because morphology varies with position on the body, light interacts differently at each position on the integument of the organism, even when incident and viewing directions remain constant. For example, during the courtship display of the male *Stellula calliope* hummingbird, whiskered gorget feathers of the throat extend to form a localized planar region of purple iridescence [Tamm et al., 1989]. In contrast, reflective crystals in the scales of silvery fish are arranged to compensate for its body's curved cross-section so that the whole flank reflects under water as if it were a flat vertical mirror, camouflaging the fish against the overhead water [Denton and Nicol, 1966]. When considering directional reflectance for an organism, position on an animal's body at both the whole-organism scale and the milli-scale is as critical as incident light direction and view direction for determining appearance and thereby the efficacy of visual signals.

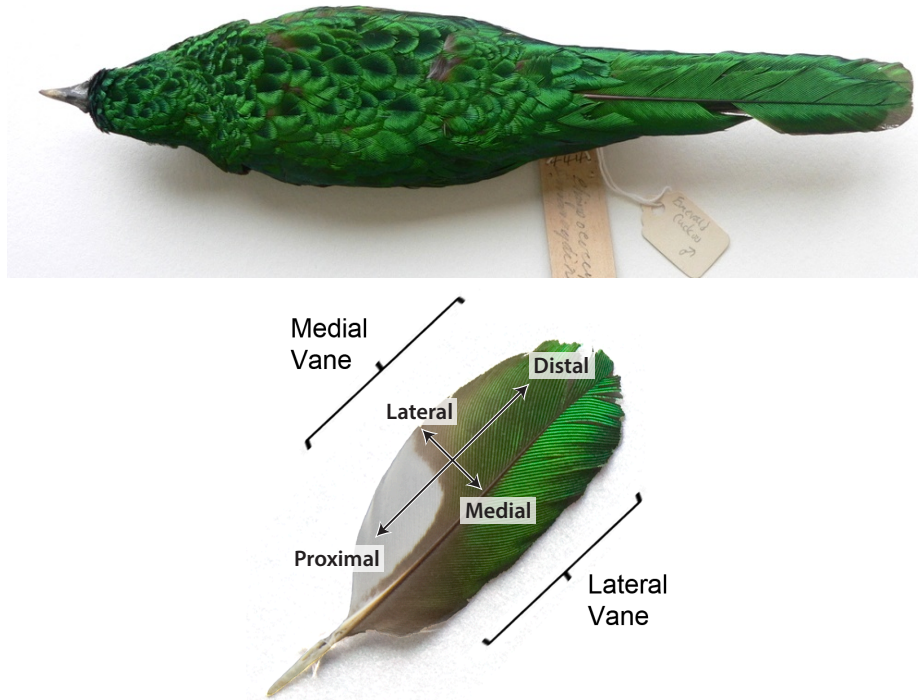


Figure 4.1: (Upper) *Chrysococcyx cupreus* male specimen in the Cornell Museum of Vertebrates. (Lower) The obverse face of a plucked tertial feather of the left wing.

Given the many morphometric studies and the significant interest in bird colouration, surprisingly little investment has been placed in relating plumage morphometrics to variation in directional reflectance as a function of position on the plumage. Important questions need to be addressed. How does morphological variation in feathers bring about change in directional reflectance? How does the change in the direction of incident light affect plumage appearance? These objective queries should assist in answering other, more behavioural inquiries, such as, how critical is the female viewpoint to the success of a male courtship display?

Structural modifications of feathers produce diverse and complex forms of directional reflectance. We hypothesize that milli-scale structural modifications of feathers produce anisotropic reflectance, the direction of which may be predicted by

the orientation of the milli-scale structure. In our investigation, the high-contrast shimmering plumage of *C. cupreus* (Figure 4.1), coupled with its specialized barb morphology [Durrer and Villiger, 1970], offers an ideal study specimen to examine the correlation between spatial variation in milli-scale structure of the vane and directional variation in optical scattering.

4.2 Background

While the typical feather superficially appears flat, in fact the surface topography is three-dimensional and complex. The vaned feather is constructed of two opposing vanes flanking the main shaft, or rachis (Left, Figure 4.2). Along the length of the rachis, barbs branch off at regular intervals. Each barb consists of a long thin shaft, or ramus, from which branch two rows of barbules, one set proximally, and the other distally. Each barbule consists of two main parts, a basal shaft and pennulum (Right, Figure 4.2). Hooklets interlock the distal barbule of one ramus to the proximal barbule of the adjacent ramus. While not shown in the illustration, the modified pennulum of an iridescent barbule may include a broad flattened surface for reflecting light [Durrer, 1986]. The regularly branched network of specialized fibrous structure, as described, creates a periodic milli-scale surface topography interleaving four types of structure: ramus, base of the proximal barbule, base of the distal barbule, and pennulum of the distal barbule.

Nano-scale structures under the cortex, or surface, of the barb create 1D, 2D, and 3D spatial variation in the refractive index of the volume [Land, 1972, Durrer, 1986, Joannopoulos et al., 2008]. Light of UV, visible, and near-IR wavelengths interacts with these structures to produce a class of reflectance called structural

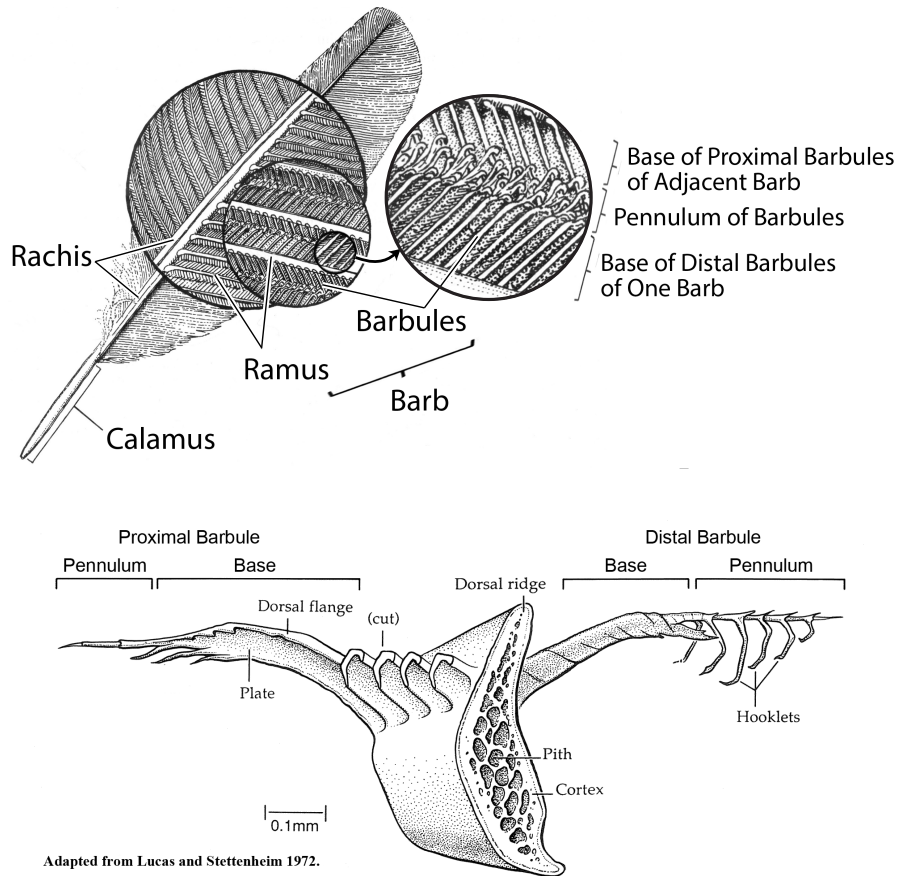


Figure 4.2: (Upper) The relationship between milli-scale barb structures and the macro-scale pennaceous feather vane. Adapted from [Clark Jr., 2004]. (Lower) A cross-section of barb ramus with its attached distal and proximal barbules. Adapted from [Lucas and Stettenheim, 1972].

colour [Prum, 2006]. Iridescence (i.e. colour change with angle between illumination and viewing [Newton, 1704]) is a dramatic structural colour effect of some feathers, including those of *C. cupreus*. In the case of *C. cupreus*, iridescence is produced by periodic layers of melanin sticks in the β -keratin of its barbs and barbules [Durrer, 1977]; the principle of interference between waves reflected from a pairwise stack of keratin–melanin layers explains the green iridescent colour of the vane [Durrer and Villiger, 1970].

Durrer observed that the iridescence of *C. cupreus* is visible from an unusually large range of angles, not dissipating, as typical, from certain viewpoints [Durrer and Villiger, 1970]. He used electron microscopy to visualize the nano- and milli-scale structure of its feather and attributed its unusual iridescent behaviour to its modified feather morphology. His micrographs provided us the means to see its periodic layers of nano-scale melanin sticks, responsible for iridescent reflectance, closely contouring the milli-scale surface cortex of its barb. Additional modifications include the distal and proximal barbules—inclined up to 90 degrees with respect to each other—capped by the cupped distal pennulae. Durrer described the impact of the distal barbule’s pennulum geometry on colour production: its exposed convex shape reflected light in many directions while at the same time supporting the inclined distal and proximal barbules.

When a bird is viewed in the field, the probability that incident light reflects in the direction of the observer is in part dependent on the geometric roughness of structural interfaces at and under the surface of the plumage. Like all real world materials, the light reflected from plumage should spread in a range of directions commensurate to the degree of the roughness, whether random or regular [Hecht, 1998]. A glossy material, having little roughness, concentrates reflected light in a small angular region near the direction of mirror reflection, also called the ideal specular direction (Figure 4.3). Anisotropic glossy materials (e.g. brushed metal, hair, finished wood, fabric, and even feathers) have directionally dependent micro- or milli-scale roughness and change appearance when rotated about the geometric normal [Ward, 1992].

Directional reflectance is measured using a gonireflectometer, which rotates the position of a light source and a detector around a study subject, enabling



Figure 4.3: The variation in the direction of reflected light is commensurate to the variation in micro-scale surface roughness.

it to be illuminated and viewed from any direction. The incident and reflected angles are measured from the pole of the reflectance hemisphere, which coincides with the feather’s surface normal. Measurements tabulated from directions on the hemisphere define the subject’s bi-directional reflectance distribution function (BRDF) [Nicodemus et al., 1977]. Light scattering adheres to the principle of reciprocity: the result of a directional reflectance measurement is the same whether we hold the camera constant while moving the light over the hemisphere or vice versa.

A gonireflectometer can employ different detectors with varying capabilities. A photometer integrates all detected wavelengths in a single brightness measurement balanced to the human visual system. A spectrometer measures light across many spectral bands. Although classical photometers and spectrometers aggregate all detected light within their field of view, imaging detectors subdivide the field into individual cells on a grid, where each cell measures the reflectance of a substantially smaller area of surface than that of the full field of view [Vukusic and Stavenga, 2009]. A standard RGB colour camera can be employed as a cost effective, high spatial resolution, low spectral resolution imager [Stevens et al., 2007].

As far as we know, the first directional reflectance measurement of plumage employed a goniophotometer to detect luminous flux [Dyck, 1987]. Since then, the

availability of low cost fibre optic spectrometers increased the use of goniospectrometers to detect radiant flux [Osorio and Ham, 2002, Yoshioka and Kinoshita, 2002, Nakamura et al., 2008, Stavenga et al., 2010].

One of the earlier directional reflectance studies of feathers surveyed the spectral and directional reflectance of structurally-coloured feather vanes [Osorio and Ham, 2002]. The researchers limited their measurements to one directional dimension and did not investigate morphological relationships. Yet, a few studies have associated directional reflectance from structurally coloured feathers to millimetre scale modifications of the feather vane. The presence of hemispherical reflectors, one per cell, along the length of the iridescent barbules of the *Ptilinopus rivoli* (White-bibbed Fruit Dove) increases the angular distribution of the directional reflectance and uniformity of the colour reflectance as compared with species without the above modification [Dyck, 1987]. In a study of the iridescent neck plumage of *Columba livia* (Rock Dove), the direction of reflected light from a single dissected barbule was compared to that of (1) an array of adjacent barbules attached to one side of the ramus, and (2) arrays of proximal and distal barbules attached to both sides of the ramus [Nakamura et al., 2008]. Their results showed that (1) barbules reflect light approximately perpendicular to their longitudinal axis, and (2) reflected light from distal and proximal barbules produce a cross-shaped pattern consistent with the angle between the barbules in two dimensions. Finally, a recent two-dimensional reflectance study of the open pennaceous breast feather of *Parotia lawesii* (Lawes's Parotia), demonstrates how the unique boomerang-shaped barbule cross-section is partially responsible for a larger and more abrupt colour change than otherwise possible [Stavenga et al., 2010].

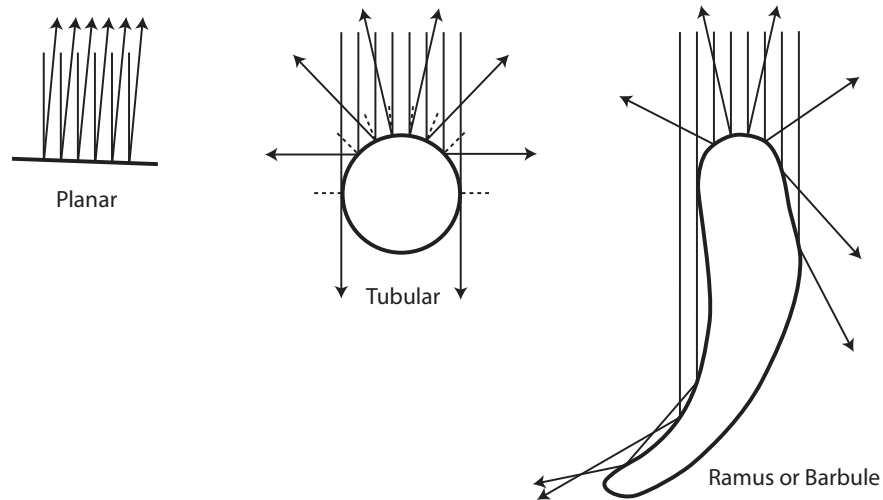


Figure 4.4: Collimated incident light reflects from a planar mirror in only one direction, but the mirrored rod reflects light in a circle of directions around its axis; likewise with the canonical ramus or barbule.

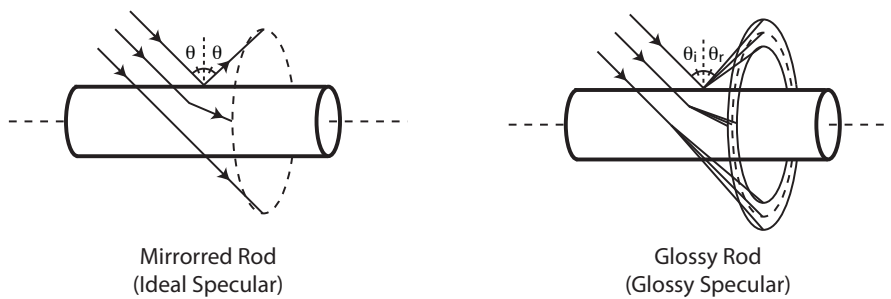


Figure 4.5: Incident light from a single direction reflects into a cone of directions around the axis of an elliptical fibre. Surface roughness at the micro-scale thickens and blurs the reflection cone.

4.3 Geometric Framework

Spherical geometry is a useful tool for mapping reflected light as a function of direction. In this paper we measure light reflected at a given position on the feather as a function of direction. The best way to think about directionality is as the unit vector pointing away from the feather, towards the light (if we are discussing reflectance as a function of illumination direction) or towards the camera (if we are discussing reflectance as a function of view direction). Since the set of all possible unit vectors is the unit sphere, we think of functions of direction as functions defined on the sphere. Light that reflects from a surface only covers half the sphere—the directions on the same side of the surface as the illumination—so we speak of reflected light as a function over the hemisphere.

The field of computer graphics has developed various mathematical models for reflectance as a function of position and direction, for the purpose of synthesizing realistic images of real or imaginary objects. Many models for isotropic [Cook and Torrance, 1982] and anisotropic [Ward, 1992, Poulin and Fournier, 1990, Ashikmin et al., 2000, Kajiyama, 1985] surfaces have been developed. Efficiently and accurately capturing spatial and directional variation together is an active research area [Gardner et al., 2003, Wang et al., 2008]. Considerable research has gone into explaining and predicting reflectance as a result of light interaction with surface geometry at various scales [Westin et al., 1992, Han et al., 2007]. For a range of materials formed from fibres, including hair [Kajiyama and Kay, 1989, Marschner et al., 2003], wood [Marschner et al., 2005], and fabric [Zhao et al., 2011, Irawan and Marschner, 2012], models based on the geometry of specular reflection from cylinders or rods have proved effective; we apply similar models in this paper to feathers.

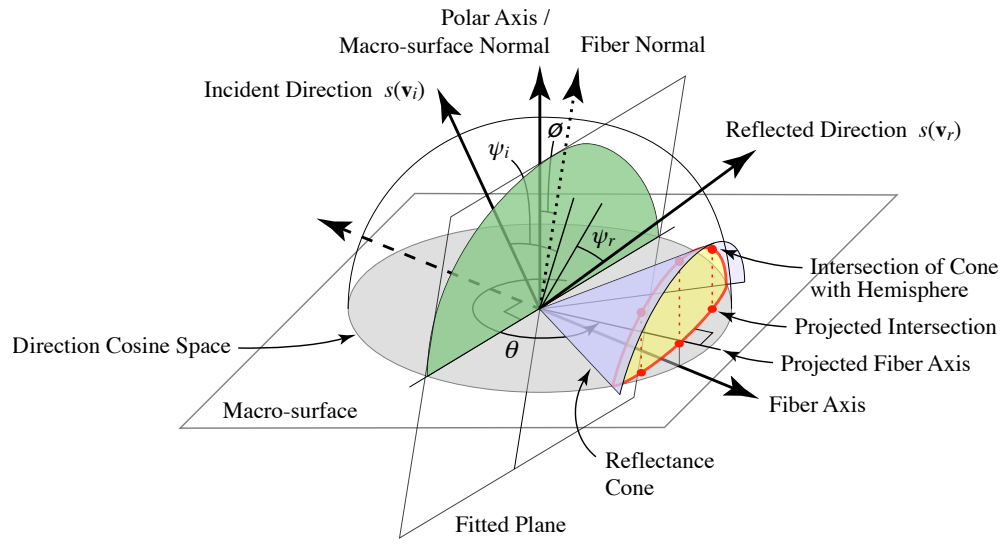


Figure 4.6: Geometry of the fibre reflection: Specular reflection from a fibre may be described as a cone-like distribution. The reflectance cone intersects the reflectance hemisphere in a circle lying in a plane orthogonal to the fibre’s longitudinal axis. When this partial circle is orthographically projected along the polar axis of the hemisphere, it appears as a curved band of high reflectance in direction cosine space and perpendicular to the projection of the fibre axis [Adapted from Marschner et al., 2005].

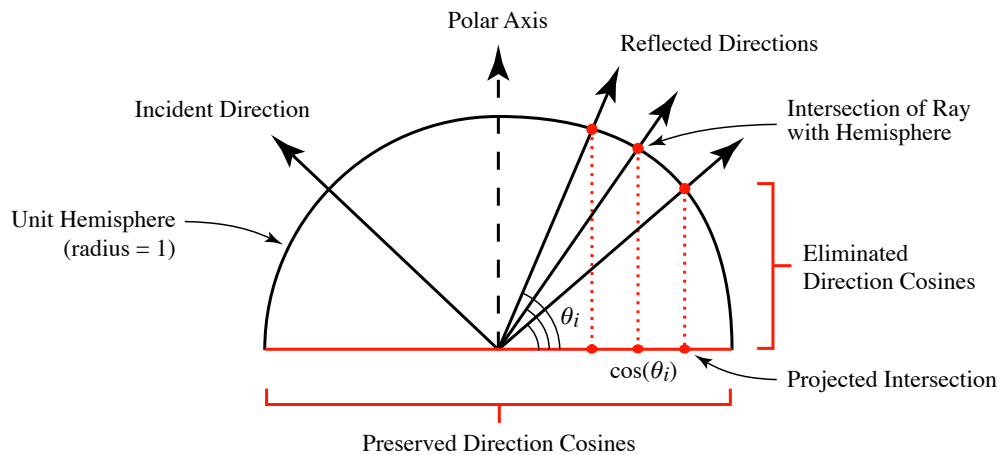


Figure 4.7: The projection of a reflection vector onto each coordinate axis yields a direction cosine for each axis. An azimuthal orthographic projection of the reflectance vectors’ intersection with the reflectance hemisphere eliminates the direction cosines parallel with the polar axis and preserves those in the macro-surface plane.

A few of these previous studies have observed that, unlike the planar mirror, many surfaces comprised of fibres (e.g. hair or fabric) reflect light anisotropically, i.e. reflectance varies with rotation about the surface normal. Incident light from a single direction, striking the fibres, whose surfaces present a full circle of surface normals, reflects into a multitude of directions around the axis of the fibre (Figure 4.4). Furthermore, each reflected direction forms an angle with the fibre axis equal and opposite to the incident direction (Left, Figure 4.5). The set of all vectors at the same angle with a particular axis forms a cone centred on the axis. Following the characteristic phenomenon observed with fibres, we postulate that a feather’s ramus or barbule can be understood as an axis around which light reflects in a cone. Since the surface of the ramus or barbule is rough at the micro-scale (Figure 4.3), in practice, the reflected light forms a thickened, blurry cone (Right, Figure 4.5): the reflectance is “bright” when the outgoing direction is in the cone and decreases smoothly as the outgoing direction moves off the cone. The thickness of the cone depends on the surface roughness of the fibre; smooth fibres produce narrow, well-defined cones whereas rough fibres produce broader ones.

When presenting our results, we consider directions as points on the sphere. Accordingly, the intersection of the idealized zero-thickness reflectance cone with the reflectance hemisphere forms a partial circle on the direction hemisphere lying in a plane orthogonal to the fibre direction (Figure 4.6). Each reflection vector comprising the partial circle on the direction hemisphere may be divided into three direction cosines, formed by projecting the vector on each of the three coordinate axes (Figure 4.7). When this partial circle is orthographically projected along the polar axis of the hemisphere (aligned to the macro-surface normal of the flat material in our study), the cosine in the direction of the surface normal is eliminated. A direction cosine map is formed by the two remaining cosines (Figure 4.8), sufficient

to uniquely identify directions on the hemisphere [Harvey and Krywonos, 2006]. This orthographic azimuthal projection of the hemisphere onto a plane collapses the three-dimensional vectors into two-dimensions. (This is the same projection that occurs when the north pole of the earth is viewed from outer space.) The projected partial circle appears as a curved band of high reflectance (luminous or bright) in direction cosine space (in the plane of the macro-surface in our study), and predicted to lie perpendicular to the direction cosines of the fibre's longitudinal axis. In this paper, our reflectance measurements will be represented using direction cosine space.

4.4 Methods

We non-destructively measured a left tertial feather of *C. cupreus* (CU03338, Cornell University Museum of Vertebrates). One of a group of feathers proximal to the innermost secondaries, or inner wing-feathers, the tertial feather is, like flight feathers, relatively large and planar and, like contour feathers, has the added attraction of intense colour. With a spherical gantry, we measured the reflectance of individual milli-scale structures of the vane; a microCT scanner enabled us to measure morphology.

4.4.1 Directional Reflectance Measurements

The feather was attached vertically by only its calamus (base of the rachis or quill) to a post mounted atop a rail on the central platform of the spherical gantry (Figure 4.9). So that the viewpoint of the camera with respect to the feather remained

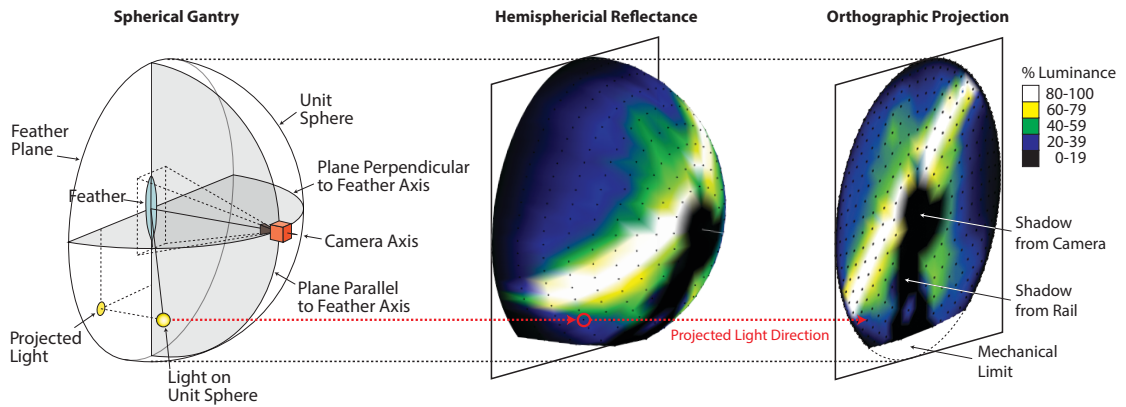


Figure 4.8: (Left) Schematic of the spherical gantry configuration. (Middle) Luminance of the reflectance sampled at 400 lighting directions over the hemisphere. (Right) An orthographic projection of the reflectance hemisphere, or direction cosine plot.

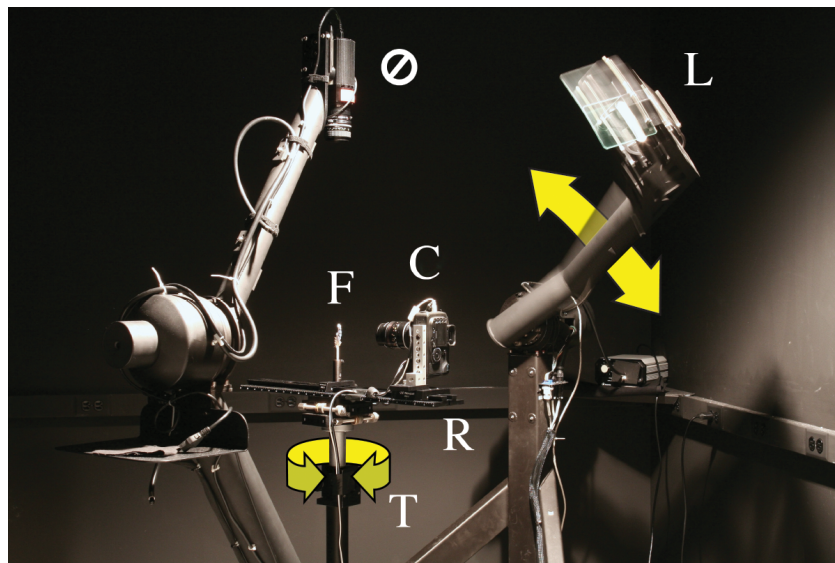


Figure 4.9: The camera (C) and feather (F) are affixed to a horizontal rail (R) atop a turntable (T). The feather may be illuminated from nearly any direction by light source (L). The second camera (\otimes) was not used. Yellow arrows represent axes of rotation.

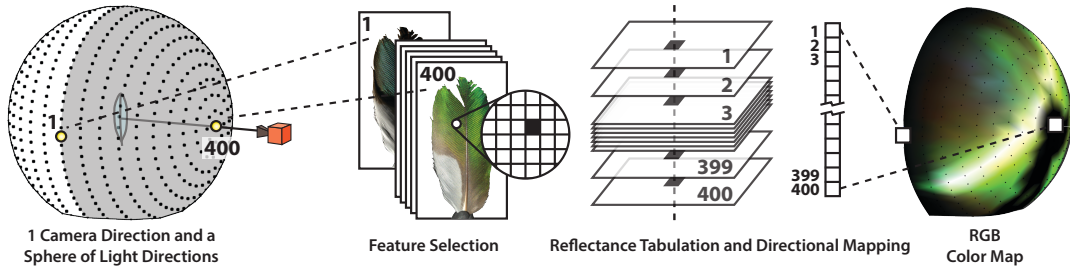


Figure 4.10: Each image of the feather was illuminated from a single direction on the uniformly sampled sphere. Since the camera direction was fixed, there exists a one-to-one correspondence between the pixels of the images and the features of the feather. The directional reflectance from any feature on the feather can be tabulated pixel-by-pixel from the registered images. The colours of tabulated reflectance were mapped to their corresponding directions on the reflectance hemisphere.

stationary throughout the measurement process, we directly attached the camera to one end of the rail. Since the feather was not absolutely planar, its surface was only approximately oriented perpendicular to the camera’s optical axis. The feather was imaged on the camera sensor with a 55mm macro lens at a distance of approximately 27cm yielding a magnification factor of 1:2. The feather was 40.6mm high and its image was 19.6mm ($0.5\times$ or half-life-size). A lamp on the outer gantry arm, which rotates about a horizontal axis, illuminated the feather, and the feather/camera platform was mounted to a turntable that rotates around a vertical axis.

We measured the directional reflectance across the entire feather at high spatial and angular resolution. High spatial resolution resolved the milli-scale structure of the vane. High angular resolution resolved the glossy specular reflectance of the vane. We sampled the spatially-varying light scattering over the entire surface of the feather by photographing it at 2 mega-pixel resolution ($78\frac{\text{pixels}}{\text{mm}}$) from a viewpoint normal to the obverse face of the feather, once for each of 737 illumination directions distributed uniformly over the sphere (Figure 4.10). Approximately half

(400) of the directions comprised the reflectance hemisphere. The remaining half (400), including the shared equator, comprised the transmittance hemisphere and will not be discussed further here.

The images of the feather acquired under different incident lighting directions were registered such that the same pixel in each image corresponded to the same location on the feather (Figure 4.10). The light reflected from a single location on the feather was thus measured as a function of the direction from which it arrived by looking at the same pixel coordinate in each image. Directional reflectance was thereby tabulated pixel by pixel from the stack of registered images (For a complete review see Chapter 3). We used our data browsing software to select lines and rectangles on the feather surface and to compute average directional reflectance over the corresponding pixels. In this way, we visualized the directionally-varying light scattering at any number of user defined, biologically relevant spatial positions and scales.

4.4.2 Reflectance Metrics

Given these browsing tools, we assessed how the different biological structures contributed to the aggregate directional reflectance of the feather vane by measuring pixels pertaining to the four biologically relevant, visible and resolved branches of the barb: ramus, base of the proximal barbule, base of the distal barbule, and penulum of the distal barbule (Chapter 3). Because these structures repeat regularly along the vane of the feather, one interval is representative of the vane. We selected a line of pixels located on the ramus of one barb, then we moved our selection in a step-wise fashion at one-pixel intervals across the surface of the feather vane to reach the ramus of the adjacent barb (Figure 4.11). We were able to identify

incremental changes in directional scattering corresponding to the four structural elements of the barb. Next we selected a large rectangular region of feather vane encompassing the entire progression and plotted the average directional reflectance to illustrate the relative contribution of each class of milli-scale structure to the far-field optical signature.

The first stage of analysis calculated the contribution of each of the four structures to the overall reflectance of the feather. Table 4.1 tabulates for each structure: (1) the *Fractional Image Area* it occupies, (2) the average reflectance of a cross-sectional unit area, integrated over the hemisphere (*Directionally-integrated Reflectance*), (3) the total reflectance of the entire structure, integrated over the hemisphere (*Directionally- and Spatially-integrated Reflectance = Fractional Image Area \times Directionally-integrated Reflectance*), and (4) its *Relative Peak Reflectance* in a single direction.

Since the camera and rail cast a shadow on the feather when illuminated from certain directions (Figure 4.8), we had to fill in the missing reflectance measurements by interpolation. The interpolation was conducted by computing the convex hull of the directional reflectance. The volume of the convex hull is the integration of the reflectance over the hemisphere. In this manner, we computed the directionally-integrated reflectance at each of 44 divisions between adjacent rami (Figure 4.11). Finally, we proportionally assigned the directionally-integrated reflectance at each division to the 4 structural branches of the barb in order to aggregate the reflectance per structural branch. We were not able to account for the reflectance outside the mechanical limit of the spherical gantry—fortunately it does not figure prominently into the reflectance calculations of the medial vane.

The second stage of analysis addressed the orientation of the bands of high reflectance. As discussed in Section 4.3 and Figure 4.6, reflections from fibres of the vane were postulated to produce cones, or sets of direction vectors at a fixed angle to the fibre axis. Since the intersection of such a cone with the direction hemisphere lies on a plane perpendicular to the fibre axis, we used plane fitting [Marschner et al., 2005] to find the fibre axes consistent with the observed reflection cones. The inclination (ϕ) and azimuth (θ) of the reflectance of each structural branch is defined by the orientation of the normal vector of the plane (green plane in Figure 4.6) fit to the reflectance distribution of each structure. This plane normal is expected to be the fibre direction. For each of the 44 divisions between adjacent rami in Figure 4.11, we measured the inclination angle of the plane normal (similar to latitude) from the zenith of the reflectance hemisphere and the azimuth angle (similar to longitude) around the zenith in a direction counter-clockwise from the rachis. We assigned the measurements to their respective structural branches, and calculated the *Average Inclination*, *Average Azimuth*, and the angular variance (*Inclination Variance* and *Azimuth Variance*) of each structure (Table 4.1). These averages should predict the orientations of the respective structures. The weaker anisotropy of the reflectance of the distal pennulae proved more difficult to fit than other structures; 2 of the 9 positions along its length required a manual estimation.

Lastly, in order to characterize which structural branches produce more or less sharply defined reflection cones, we measured the angular distribution of the anisotropic reflectance of each structural branch in a direction orthogonal to the fitted plane at *Full Width Half Maximum* (*FWHM*).

4.4.3 MicroCT Measurements and Morphometrics

We used a microCT scanner (Xradia Versa XRM-500) to measure the longitudinal axis of the cortex of the barb, in order to approximate the longitudinal axes of the nano-scale melanin sticks underneath. . We non-destructively measured a small region of the medial vane roughly equivalent in position to the region measured in Figure 4.11. The scanner settings were 70 kilovolts, 6 watts, 85 microampere, $2.5 \frac{\mu m}{voxel}$ resolution, 8 second exposure time, 4000 projections.

Using the volume analysis software Osirix, first, we obliquely cross-sectioned the vane volume in planes parallel to the longitudinal axes of the bases of the proximal and distal barbules (Figure 4.12a). From these oblique cross-sections of the vane, we measured the *Average Inclination* angle of the longitudinal axes of the bases of the barbules with respect to the macro-scale surface of the feather (Table 4.1). Second, we viewed the vane in a direction normal to its macro-surface plane, and measured the *Average Azimuth* angle of the rami and bases of the barbules in a counter clockwise direction with respect to the rachis.

4.5 Results

From the tabulated directional reflectance measurements of *C. cupreus*, we observed that different positions on the feather reflected light in different directions and with varying degrees of anisotropy. In order to demonstrate how milli-scale morphology of the vane has impacted its optical signature, we correlated the orientation of each structural branch of the barb to the orientation of its directional reflectance. Figure 4.13 shows four representative signatures belonging to four

milli-scale structures: ramus, base of the proximal barbule, base of the distal barbule, and pennulum of the distal barbule. The morphology of these structures, their directional and integrated reflectance, and their relative contribution to the reflectance of vane as a whole are organized below by subsection.

4.5.1 Barb Axes Predict the Orientation of the Reflectance Cones

From microCT measurements, we observed the profile of the vane zigzagging in a plane orthogonal to the rami; the peaks of the profile repeated with a frequency equal to the interval of the rami branching from the rachis (a2–a3 of Figure 4.12a). When we considered the construction in three dimensions, we found that the barbules, tilted up and away from the macro-surface of the vane, did not occupy the path of shortest distance (a perpendicular) from the rami to the peaked ridgeline. Instead the barbules joined the rami to the ridgelines at acute complementary angles in the plane of the macro-surface (a1 of Figure 4.12a and b1 of Figure 4.12b). Therefore, we cross-sectioned the vane in planes normal to the macro-surface that contained the longitudinal axes of the base of the distal and proximal barbules (a4 and a5 reconstructed from the red and green planes in b3 of Figure 4.12). From these two views, we measured the average angles at which the bases of the barbules, distal and proximal to the ramus, were tilted up and away from the macro-surface of the vane (ϕ_d and ϕ_p in Figure 4.12). The topography of the vane is perhaps best described as forming a three-dimensional herringbone pattern where alternating rows of barbules are lifted up in opposite directions to form valleys with ridgelines capped by the distal pennulae (b2 of Figure 4.12b).

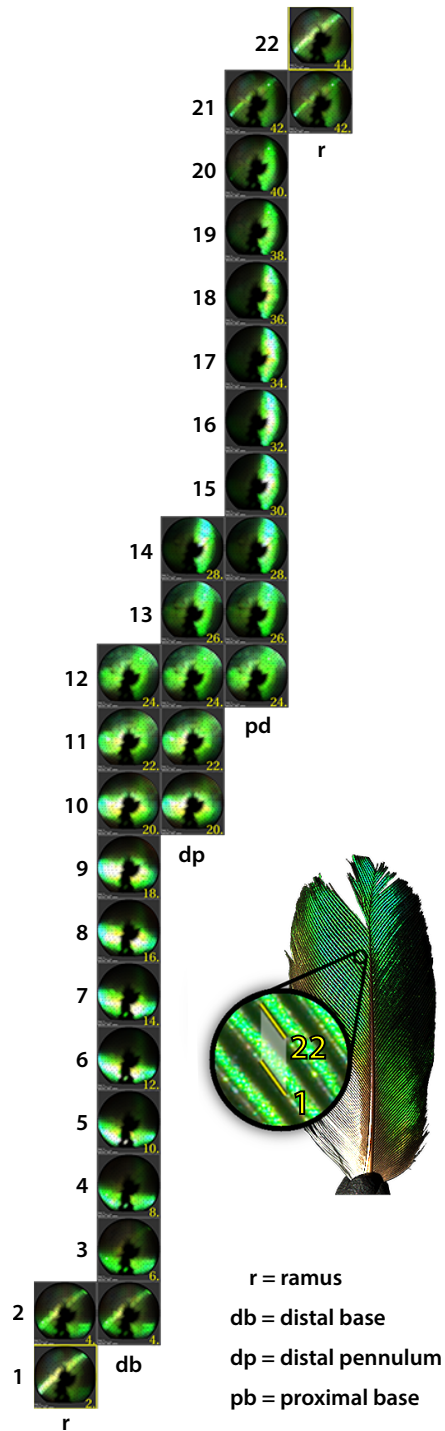
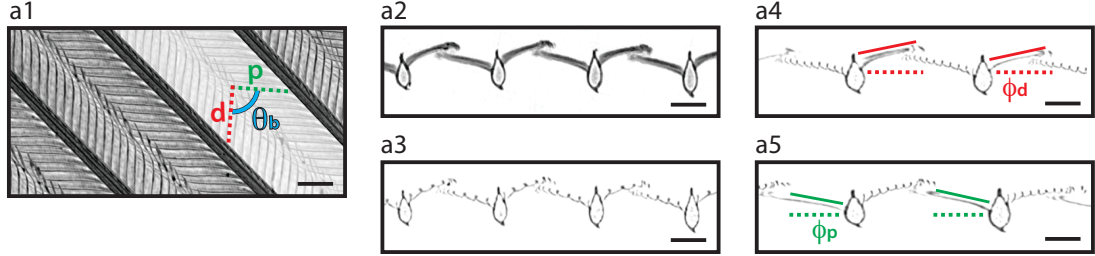
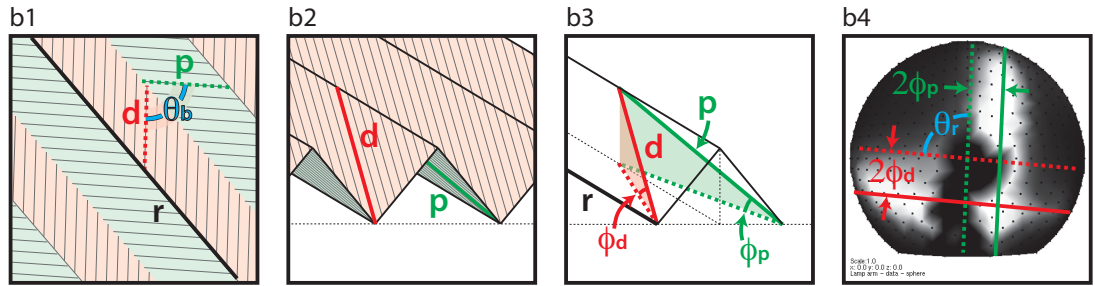


Figure 4.11: RGB directional reflectance of a region between 2 barbs of the medial vane was subdivided into 44 linear divisions. The Average reflectance of 22 subsampled divisions is shown: (1) of line 1 along a length of ramus; (2–21) along sequential lines following step-wise movements; (22) of line 22 along a length of the adjacent ramus.



(a) MicroCT reconstructions: (a1) Obverse view oriented with rachis up and macro-surface in the plane of the page matches the gantry experimental setup. (a2–a3) Transverse cross sections of the rami. (a4) Longitudinal cross-sections of the base of the distal barbule in plane with the macro-surface normal. (a5) Longitudinal cross-sections of the base of the proximal barbule in plane with the macro-surface normal. A slab consists of multiple slices. Scale bar = $100\mu\text{m}$.



(b) Schematic diagrams: (b1) Obverse view. (b2) Oblique transverse cross-section. (b3) Inclination of the bases of the distal and proximal barbules. (b3) Average directional reflectance of a rectangle region containing distal and proximal barbules.

Figure 4.12: MicroCT images (a) and schematic diagrams (b) of the barb structure of the medial vane. (r) Ramus. (d) Distal barbule. (p) Proximal barbule. (ϕ_d) Inclination angle of the base of the distal barbule. (ϕ_p) Inclination angle of the base of the proximal barbule. (θ_b) Azimuth angle between bases of the distal and proximal barbules projected in the plane of the macro-surface. (θ_r) Angle between the two planes fitted to the reflectance of the bases of the distal and proximal barbules.

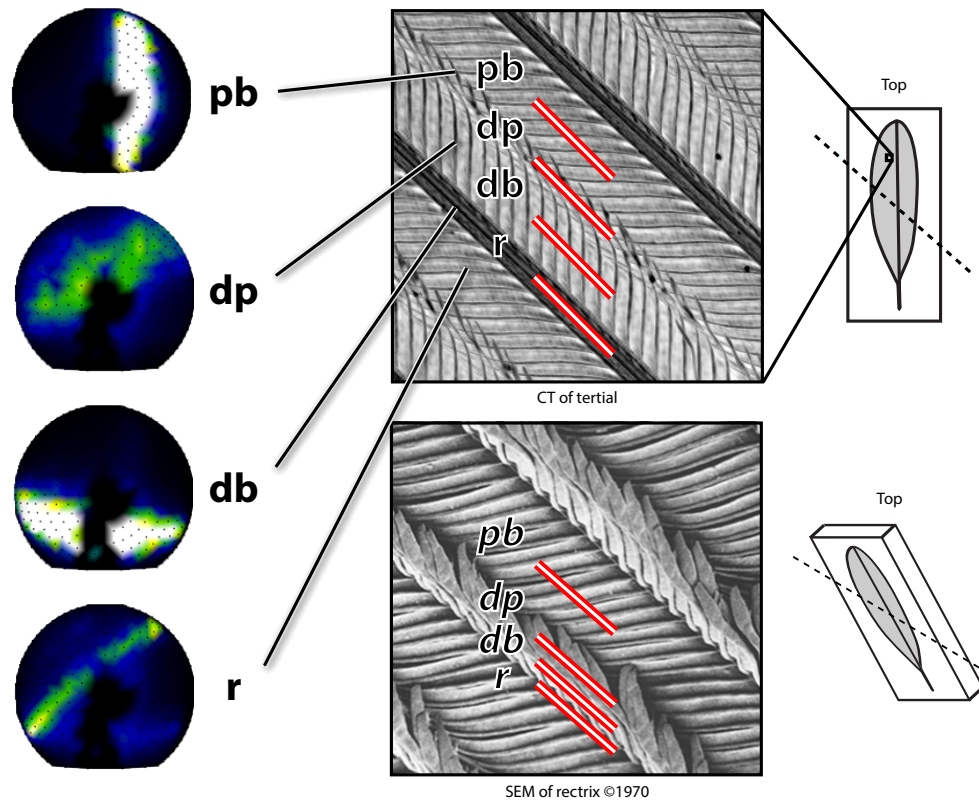


Figure 4.13: The luminance of the directional reflectance of different components of the barb—ramus (*r*), base of the distal barbule (*db*), pennulum of the distal barbule (*dp*), base of the proximal barbule (*pb*)—was measured from a position normal to the surface of the medial vane of a tertial feather and plotted in direction cosine space. The view of the tertial feather, reconstructed from microCT, is perpendicular to its macro-surface, and therefore the more three-dimensional aspects are less apparent. By comparison, Durrer’s SEM of a rectrix feather helps visualize the structure of the vane. Viewed at an angle rotated around the axis of rami, the bases of the proximal barbules and pennulae of the distal barbules lie in planes in proximity to that of the image, while the bases of the distal barbules rise up out of the plane of the image and are foreshortened. SEM adapted from Durrer and Villiger [Durrer and Villiger, 1970], ©1970, Springer Berlin/Heidelberg. Reprinted with kind permission from Springer Science and Business Media.

We measured the whole hemisphere of directional reflectance at 44 discrete linear divisions across a one-barb interval between two adjacent rami of the medial vane. Following the description in Section 4.4.2, we generated 44 hemispherical maps shown as 44 circular plots in Figure 4.11, one for each of the 44 linear divisions. Each of the structural branches of the barb was represented; we identified the location of the following structures from their reflectance signatures: ramus (Plots 1–2), base of the distal barbule (Plots 2–12), pennulum of the distal barbule (Plots 10–14), base of the proximal barbule (Plots 12–21), and adjacent ramus (Plots 21–22). Boundaries between structures produced sudden changes in directional distribution (Plots 2 and 21), except where the distal pennulum bridged the orthogonally-oriented reflectance of the bases of the distal and proximal barbules (Plots 10–14).

The anisotropic reflectance of each structural branch (as identified in the 44 divisions) formed discrete bands on the hemisphere; however, the bands differed in width, position and sharpness. The base of the proximal barbule reflected incident light in a band roughly parallel to the proximodistal axis of the vane, but medially shifted from the surface normal. The base of the distal barbule reflected light in a band parallel to the mediolateral axis of the vane, but proximally shifted. Reflectance from the ramus crossed the axes of the vane in a proximal-lateral to distal-medial direction. We discovered that the ramus reflected light with the greatest degree of anisotropy, yielding the narrowest reflectance band on the hemisphere. The anisotropy of the reflectance from the bases of the proximal and distal barbules was weaker as compared to the ramus, so their reflectance bands are wider. The fourth structure we measured, the distal pennulum, manifested the weakest anisotropy. As a result of its structural function of bridging the two bases, the pennulum’s directional reflectance changed dramatically over its length.

Its inconsistent signal did not produce a signature readily recognized and fit to a singular cone.

The most important example of milli-scale structural orientation upon the directional reflectance of *C. cupreus* was manifested by the bases of the barbules and their respective bands of high reflectance inclined from the pole of the hemisphere by a factor of $2\times$ that of their structural inclination (b3 and b4 of Figure 4.12b). In fact, the orientation of the bases of the barbules measured from the microCT reconstruction exactly predicted the orientation of the axes of the cones of reflectance fit from the directional reflectance measurements (Table 4.1). The inclination equalled 10° or 11° and the relative azimuth between opposing bases equalled 89° ($\theta_r = 265^\circ - 176^\circ$ and $\theta_b = 266^\circ - 177^\circ$; see θ_r and θ_b in Figure 4.12). We made no attempt to measure the average orientation of the axis of the distal pennulum from the CT data, but we calculated its orientation from reflectance data. Notably, the inclination and azimuth of the axis of the distal pennulum varied along its length, 21° and 88° respectively, as required to span the directional differences of the opposing bases.

Although the width of the reflectance per cross-sectional unit area of the bases of the distal and proximal barbules was similar, the width of the total reflectance of the entire base of the distal barbule is greater than that of the proximal barbule. The difference in the width can be traced to the $3\times$ greater variance in the inclination of the reflectance along the length of the base of the distal barbule (Table 4.1). The greater variance effectively spread the reflectance across a $2\times$ greater width of the hemisphere (21° as compared to 11° at FWHM) as seen in Figure 4.14. We expect the increased variance is due the apparent increased curvature

Reflectance	Ramus	Distal Base	Distal Pennulum	Proximal Base
Fractional Image Area (†)	0.09	0.35	0.14	0.42
Directionally-Integrated Reflectance (†)	0.01	0.46	0.04	0.49
Directionally- and Spatially-Integrated Reflectance (†)	0.00	0.44	0.02	0.54
Peak Reflectance (‡)	0.15	0.73	0.32	1.00
Average Inclination (deg)	8	11	10	10
Inclination Variance (deg)	1	15	21	5
Average Azimuth (deg)	40	176	35	265
Azimuth Variance (deg)	1	11	88	12
Full Width Half Maximum (deg)	–	21	–	11
Morphology				
Average Inclination (deg)	0	11	–	11
Average Azimuth (deg)	41	177	–	266

Table 4.1: Reflectance and morphology statistics of four structural branches of the barb. Reflectance is calculated from a view direction roughly normal to the obverse face of the feather. Morphology is reconstructed from microCT where the rami define the local macro-surface plane. † Relative to the sum total. ‡ Relative to maximum component.

along the length of the distal barbules, as seen in microCT reconstructions of the vane. Since no measurements were made, no predictions can be presented.

4.5.2 Directionally and Spatially-integrated Reflectance of Discrete Structures

Measurements of directionally- and spatially-integrated reflectance as a function of the barb's branching milli-scale structure makes it possible to compare the relative contributions of each branch to the reflectance of the vane (Table 4.1).

Base of the Proximal and Distal Barbules Arrays of parallel barbule bases adjoined to form two contiguous, reflective, milli-scale surfaces proximal and distal to the ramus. In aggregate, the surface of the bases of the barbules comprised 77% of the projected surface area of the obverse face of the vane. In addition to their surface area advantage, their average hemispherical reflectance was $19\times$ greater than that of the rami and distal pennulae combined. The spatially-integrated hemispherical reflectance of the bases of the distal and proximal barbules, 44% and 54% respectively, are proportionally equivalent to their individual projected surface areas. In sum, they produce 98% of the reflectance of the vane. No other branch of the barb produces comparable reflectance.

Pennulum of the Distal Barbule The convex curvature of the pennulum distributed reflectance over the greatest portion of the hemisphere; as such, the pennulum produced the weakest anisotropy of the four structural branches of the barb, effectively minimizing the reflectance in any given direction. But anisotropy

is not the only factor working to minimize the intensity of the reflectance of the pennulum. The average directionally-integrated reflectance of the pennulum was only 9% of that of either barbule bases. The relatively low average directionally-integrated reflectance is further compounded by the relatively small percentage of the vane surface (14%) covered by projected distal pennulae, yielding an exceptionally low (2%) hemispherical reflectance integrated across the surface as compared with that of the bases of the barbules (98%).

Ramus Of all the structural branches, the ramus reflects most anisotropically, concentrating reflectance within the narrowest cone. Since high anisotropy concentrates reflected energy in the narrowest range of directions, the potential for exceptionally high reflectance exists. Yet the ramus measured relatively low reflectivity; its peak reflectance was least of all branches of the barb (15% of the base of the proximal barbule). The narrow width of its reflectance band compounded by its low reflectivity yielded a diminutive average hemispherical reflectance of 1%. Finally, its exceptionally low projected surface area (9%) further reduced its spatially-integrated hemispherical reflectance to a negligible quantity, virtually eliminating its contribution to the overall feather appearance in the far-field.

4.5.3 Emerging Properties of the Vane in the Far-field

The previous subsection presented results of directionally- and spatially-integrated reflectance as a function of the barb's branching structure. In this subsection we combine the reflectance of the individual structural branches of the barb to investigate the emerging properties of the feather. First, we present the far-field optical signature of the feather, i.e. the directional reflectance of a small region

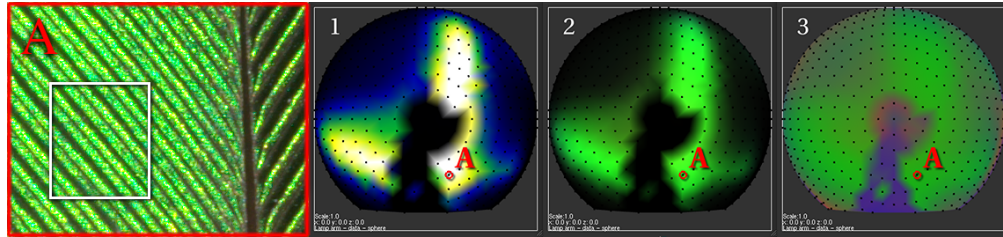


Figure 4.14: Average directional reflectance plotted in direction cosine space of a rectangular region of image (A), including rami, base and pennulum of the distal barbule, and base of the proximal barbule of the medial vane of *Chrysococcyx cupreus*. (1) Luminance. (2) RGB. (3) Chromaticity.

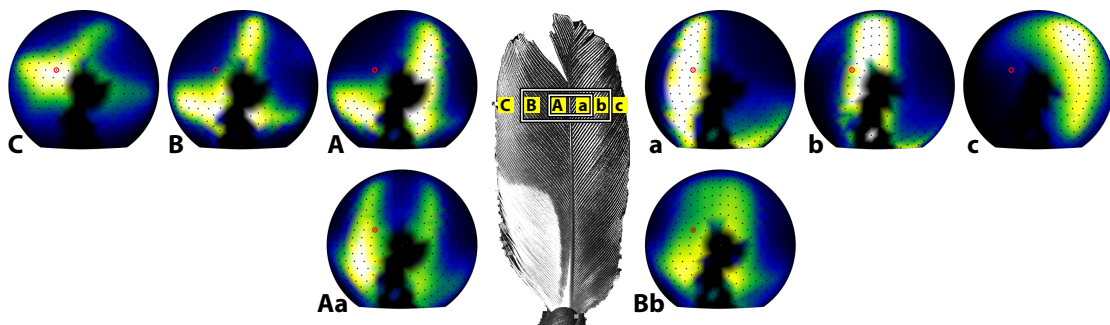


Figure 4.15: Average directional reflectance of rectangular regions of *Chrysococcyx cupreus*: (A–C) 3 regions of the medial vane, (a–c) 3 regions of the lateral vane, and (Aa & Bb) 2 regions spanning both vanes. Luminance plotted in direction cosine space.

of the feather approximating the resolution limit of the human eye at a distance where the individual milli-scale structures of the feather cannot be resolved. Then, we address the shift and symmetry in the reflectance induced by the macro-scale distortions of the two feather vanes.

We selected a rectangular region of the medial vane containing several barbs (A of Figure 4.14) and plotted the average directional reflectance of this region (1–3 of Figure 4.14). The 2 bands of high reflectance from the barbule bases dominated the far-field optical signature. The low reflectance of the distal pennulae, the influence of which is seen in the chromaticity plot, hardly registered in the luminance and RGB plots. Reflectance from the rami is not detectable in any of the plots. From this measurement we see that the far-field optical signature of a small rectangular region of the feather vane is explained by a subset of the milli-scale geometry of that region, which the eye cannot resolve, the bases of the barbule; the remaining milli-scale structures are irrelevant.

Yet, the influence of another and larger structural scale—the macro-scale—becomes apparent in the far-field when the feather is viewed as a whole. To ascertain the influence of the macro-scale structure (e.g. curl and twist of the vane) upon the crossed reflectance bands produced by the milli-scale structure, we subdivided the feather and measured the far-field optical signature at each subdivision (Figure 4.15). At six samples sites (A–C and a–c) we measured a significant mediolateral shift in the reflectance of the base of the proximal barbule. For regions near the central shaft, such as sites (A, a), the vane opposite the light source reflected in the polar direction. For regions near the marginal edge, such as sites (C, c), the vane in the direction of the light source reflected in the polar direction. Whether

measured in proximity to its central shaft or its marginal edge, the reflectance exhibited symmetry between the two vanes.

Due to the symmetry of the milli-scale structure of the opposing vanes, the reflectance from a region comprised of equal portions of both vanes (Aa of Figure 4.15) contained two opposing bands in the proximodistal axis of the vane and double the reflectance in the mediolateral axis. In the broader region (Bb), the two opposing bands shifted medially, merging as a single blurry band straddling the polar direction.

In summary, iridescence was viewed in more directions than otherwise possible due to the symmetry of the inclined bases of the barbules of the two feather vanes. A feather that reflects light from just one structure can cover only one band on the hemisphere. The *C. cupreus* feather expands its coverage over the hemisphere through its four bands originating from four structures belonging to two vanes. The two bands of a single vane are complemented by the two bands of the opposing vane to cover a greater portion of the reflectance hemisphere as compared to one vane alone. At near distance, the symmetry of the multiple bands produce rings and eyelets. At far distance, they increase the blur, directional distribution, and isotropy of its signal.

4.5.4 Grazing Angle Reflectance of the Rami

On the whole, the directionally- and spatially-integrated reflectance of the ramus was negligible (Section 4.5.2). Yet some components of its reflectance actually augmented the dominant far-field optical signature of the feather. Unlike the bases of the barbules, the reflected light around the axis of the ramus was largely

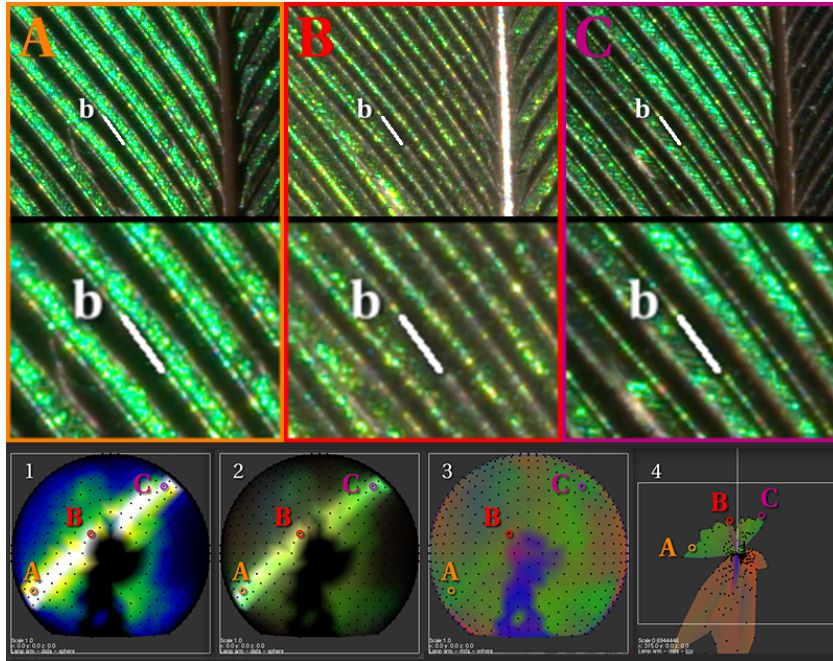


Figure 4.16: (A–C) *Chrysococcyx cupreus* illuminated from different directions and imaged at 2 magnification scales: (A) illuminated from a proximal–lateral direction with respect to the feather vane. (B) illuminated near normal incidence. (C) illuminated from a distal–medial direction with respect to the feather vane. (1–4) Average directional light scattering of the linear region of barb ramus *b* plotted in 4 formats: (1) luminance, (2) RGB, (3) chromaticity, and (4) chromaticity coloured, log-scale luminance displaced.

biased in directions approaching the plane of the macro-surface (Figure 4.16). In directions A and C of Plot 1, we observed that grazing incident illumination produced increased reflectance (at least $2.5\times$ greater) in the direction of the macro-surface normal. In Plots 2 and 3, we observed that the reflectance of the rami, like that of the bases of the barbule, was both brilliant and saturated green. Since the ramus was oriented 45° from that of the barbule bases, it had the potential to produce a signature distinguished from that of the bases. On the contrary, we found that the same grazing incident illumination that produced a brilliant green ramus, also produced brilliant green barbule bases. At high magnification, we resolved the ramus independently of the adjoining fields of green of either barbule base. But without magnification, the undifferentiated signal of the ramus was subsumed by that of the barbule bases. The ramus effectively contributed an additional 9% fractional surface area to the signal of the barbule bases (35% and 42%) when illuminated from certain grazing angles.

4.6 Discussion

The feather vane is constructed upon a hierarchy of morphological scale (including nano-, milli-, and macro-scales), for which we found corresponding optical consequences. Our results supported our hypothesis that the direction of reflectance from a feather can be explained by the orientation of its milli-scale structure. We developed a geometrical model that exactly predicted the direction of a feather's reflectance from its component parts.

Previous research has explained how colour is produced from the interference of light waves with periodic nano-scale structure under the cortex of the barbs of *C*.

cupreus [Durrer and Villiger, 1970]. Rather than focus on the wavelength or colour of the reflectance, we sought to study the direction of the reflectance in relation to the direction of the nano-scale structure of the barbs of the vane. When measuring morphology and reflectance by traditional methods, rami and barbules must be dissected from the composite vane [Yoshioka and Kinoshita, 2002, Nakamura et al., 2008, Vukusic and Stavenga, 2009, Stavenga et al., 2010]. The required dissections and cross-sections make it practically impossible to reconstruct the direction of the longitudinal axes of the nano-scale sticks responsible for light reflectance from various branches of the barb. We achieved a breakthrough when we observed the layers of nano-scale sticks contouring the milli-scale barb cortex in Durrer's electron micrographs. Since the milli-scale barb cortex can be readily imaged by microCT, we developed a novel method using the cortex as a proxy for the sticks. Using a microCT scanner to measure morphology and an imaging scatterometer (spherical gantry) to measure reflectance, we correlated the direction of the proxy geometry to the direction of the reflectance from the nano-scale structures of the vane.

Our protocol was non-destructive and, equally important, preserved the morphological relationships within the fabric of the intact vane. By comprehensively measuring the entire feather and eliminating dissection, our approach provided tremendous flexibility during post-acquisition investigations, when we digitally isolated the component parts of the feather to study the morphology and reflectance of each part separately and in aggregate. In this manner, we investigated not only the individual reflectance signatures of the component parts at the milli-scale, but also the spatially-integrated reflectance of the component parts at the macro-scale as seen in the far-field. While measurements of the intact vane were critical to identifying the spatially-integrated signal seen by other organisms, only when milli-scale

structures were analysed in the context of the intact vane, could we identify the component parts most relevant to its integrated signal.

Our geometrical model correctly predicted the integrated signal of the structural innovations of *C. cupreus*: its three-dimensional herringbone zigzag of milli-scale structure, formed by the inclined bases of its barbules. Unlike the extended distal barbules of many glossy iridescent feathers, those belonging to the wing, tail and body of *C. cupreus* did not extend so far as to cover the proximal barbules and rami. The signal from these exposed bases of the proximal barbules proved as relevant as those of the distal barbules. The potentially competing signal of the exposed rami was obscured by the signals of both barbule bases.

Our predictive model explains the signalling potential of *C. cupreus* and enables us to discuss the link between function and morphology that allowed selective pressures to lead to adaptive innovations in the individual component parts of its feathers. The inclined orientation of the bases of the distal and proximal barbules of a single vane produced a two-part signal (comprised of two orthogonal bands of high reflectance which cross at a position on the hemisphere shifted from the macro-surface normal) with minimized overlap and maximized directional distribution over the hemisphere. The combined components of the two-vented signal maximized coverage in 3 of 4 quadrants of the reflectance hemisphere, with twice the reflectance in the proximal direction. Though we measured one feather, all the feathers of *C. cupreus* grow in the same direction (towards the tail) wrapped around the proximal–distal axis of the organism (Figure 4.1). So when one feather has twice the reflectance in a proximal (face-forward) direction, all the feathers have twice the reflectance in a face-forward direction. The courtship behaviour of *C. cupreus* is undocumented, and it is unknown if the ringing pattern, easily observed

when viewing the organism in a direction perpendicular to its proximal–distal axis (Figure 4.1), is sexually selected. Less obvious, but perhaps more critical, the structure that creates the ringing directs the greater portion of its reflectance in face-forward directions. Furthermore, the 2× wider face-forward signal produced by the curved base of the distal barbule (as compared to the proximal barbule; see Table 4.1) allows for a greater range of forward-facing directions from which the potential mate can admire the resulting rim lit contour of the organism’s body. Thus, we infer that a forward-facing view is likely important in communication between potential mates.

Although iridescence was viewed in more directions than otherwise possible due to the symmetry of the inclined bases of the barbules of the two feather vanes, for a given location on an individual feather, a large fraction of hemisphere remained untouched. Because we can relate the feather’s reflectance at the milli-scale to that at the macro-scale, we can explain how some iridescent green reflectance emerges from all the feathers over *C. cupreus*’ body (Figure 4.1), regardless of their orientation. Our measurements in Section 4.5.3 demonstrated how the smoothly contoured macro-scale shape of the feather shifted the directional distribution of reflected light to increase coverage over the hemisphere. At near distance (A, B, C, a, b, c of Figure 4.15), sharp specular rings outline individual feathers. At far distance (Bb of Figure 4.15), the integrated signal was blurred and iridescent green color was viewed over a greater range of directions with increased isotropy. Our results justify Durrer and Villiger’s observation that iridescence from *C. cupreus* can be viewed from many more directions than typical avian iridescent plumage [Durrer and Villiger, 1970].

We also confirmed Durrer and Villiger's claim that morphological adaptations extend iridescent colour production from the base to the pennulum of the barbule, but contrary to their writings we demonstrate that the increased angular reflectance is *not* due to colour production from the distal pennulae. Despite its iridescent colour, surface area and unobstructed position at the peak, the distal pennulae does *not* significantly contribute to the reflectance of the feather. We assert that the primary role of the distal pennulum is structural. The pennulum is a fascinating, anomalous structure that connects the bases of opposing barbules, forming the peak of the zigzag of the vane. The distal pennulum likely developed a broad cross-section primarily to capture the tip of the proximal barbule to support the colour production of the bases of the distal and proximal barbules, rather than function as reflectors themselves.

C. cupreus does not fit the classic conception of iridescence—a shifting rainbow of colour. Rather than displaying dramatic colour change, *C. cupreus* harnesses the directional constraints of its multi-part reflectance for a different dramatic effect, focusing light to create its idiosyncratic, shimmering patterns. While the tertial flight feather (Right, Figure 4.1) was the subject of our detailed analysis, general observation and preliminary study indicated that the same optical consequences are found in the rectrices of the tail and shingled contour feathers of body. The variation in the appearance over the surface of *C. cupreus* can be attributed almost exclusively to variation in the direction of the reflectance. With the exception of its yellow or white lower breast and belly, *C. cupreus* is covered in shimmering green. Where some birds employ colour and plumage patches to create discontinuities and contrast, *C. cupreus* made maximum use of the directional constraints of anisotropic specular reflectance to create its eye-catching patterns of high and low reflectance (Left, Figure 4.1).

Acknowledgements

This research was supported by funding from the National Science Foundation (NSF CAREER award CCF-0347303 and NSF grant CCF-0541105). I wish to thank Dr. Ellis Loew and Dr. Susan Suarez, Cornell University, for their guidance and review of this manuscript; Kalliope Stournaras, University Freiburg, for her translation of the Durrer and Villiger manuscript; Dr. James Harvey, CREOL, University of Central Florida, for his suggestions on optical scattering theory; and Josh VanHouten, Yale University, and Mark Riccio, Cornell University, for microCT measurements. Thanks to my many colleagues in Computer Graphics at Cornell University who contributed to this work over several years: Dr. Donald Greenberg introduced me to the topic of feathers and supported my early investigations; Dr. Jon Moon taught me how to configure and use the Cornell Spherical gantry; Wenzel Jakob contributed programming expertise in Java and OpenGL; Dr. Jaroslav Křivánek reworked the demosaicing pipeline and implemented a plane fitting function to our framework; Edgar Velázquez-Armendáriz offered his Java and Matlab implementations of OpenEXR for our use; Hurf Sheldon for IT support. Finally, special thanks to Dr. Richard Prum, Department of Ecology and Evolutionary Biology, Yale University, for his financial and intellectual support over the past year.

CHAPTER 5

THE BLUE JAY, *CYANOCITTA CRISTATA*: DIFFUSE SCATTERING CASE STUDY

We divide the scattered light into component categories based on its directional nature. When the incident light is scattered over a broad range of angles, we apply the term *diffuse*. Diffuse reflection is the complement of *specular* reflection. When a material exhibits ideal diffuse reflection—frequently called Lambertian reflection—the apparent brightness is the same regardless of the view point. In this ideal form the luminance is isotropic. When scattering is diffuse, i.e. exitant rays are distributed broadly over the hemisphere of outgoing angles, but not isotropic, we call the behaviour *directional diffuse* reflection.

We have observed diffuse reflectance in most of the feathers we measured. The diffuse reflectance of the raw camera radiance approximates a ball-shaped cosine function when the unit vector of each directional sample is scaled by the luminance of the reflectance in that direction (See definition of *linear-displaced radial distance* (*Lin*) in appendix B).

We have measured feathers with black, dark brown, blue, and white diffuse reflectance. Diffuse reflection also appears as a small but measurable component of brilliant specular iridescent feathers, such as the African Emerald cuckoo (*Chrysococcyx cupreus*), Hadedda ibis (*Bostrychia hagedash*), and Purple Glossy starling

(*Lamprotornis purpureus*). Of the feathers we studied, the Blue jay (*Cyanocitta cristata*) offers the most enlightening example of diffuse scattering.

5.1 Relationship Between Structure and Diffuse Reflection

The diffuse reflection observed in a single blue jay feather is largely a subsurface scattering phenomenon. The various regions of the feather exhibit distinctly different diffuse characteristics—the most immediately obvious being color—due to their individual subsurface structures. The unpigmented keratin composing the white tip readily scatters light in all directions. The melanin content of the black barbs and black barbules absorbs the greater portion of light scattered below their respective surfaces [Shawkey and Hill, 2006], yielding diminished reflectance over the UV-visible spectrum. Since the medullary melanin is deposited without periodicity, the reflected light rays are expected to be oriented in all directions without bias. The blue barbs are structurally colored by a medullary material called spongy keratin (Figure 5.1) not found in the black barbs [Hill and McGraw, 2006a]. The broad, rounded, cross-sectional surface of the blue barb matched with the embedded three dimensional photonic nano-structure delivers a saturated diffuse blue reflectance. The blue barbs are the signature feature of the Blue Jay and they dominate the feather reflectance both within the blue bands and across the feather overall.

5.2 Local Area Averages

A study of the Blue Jay tertial wing feather with its three colored domains—blue, black, and white—forms a case study of the relevance of diffuse scattering

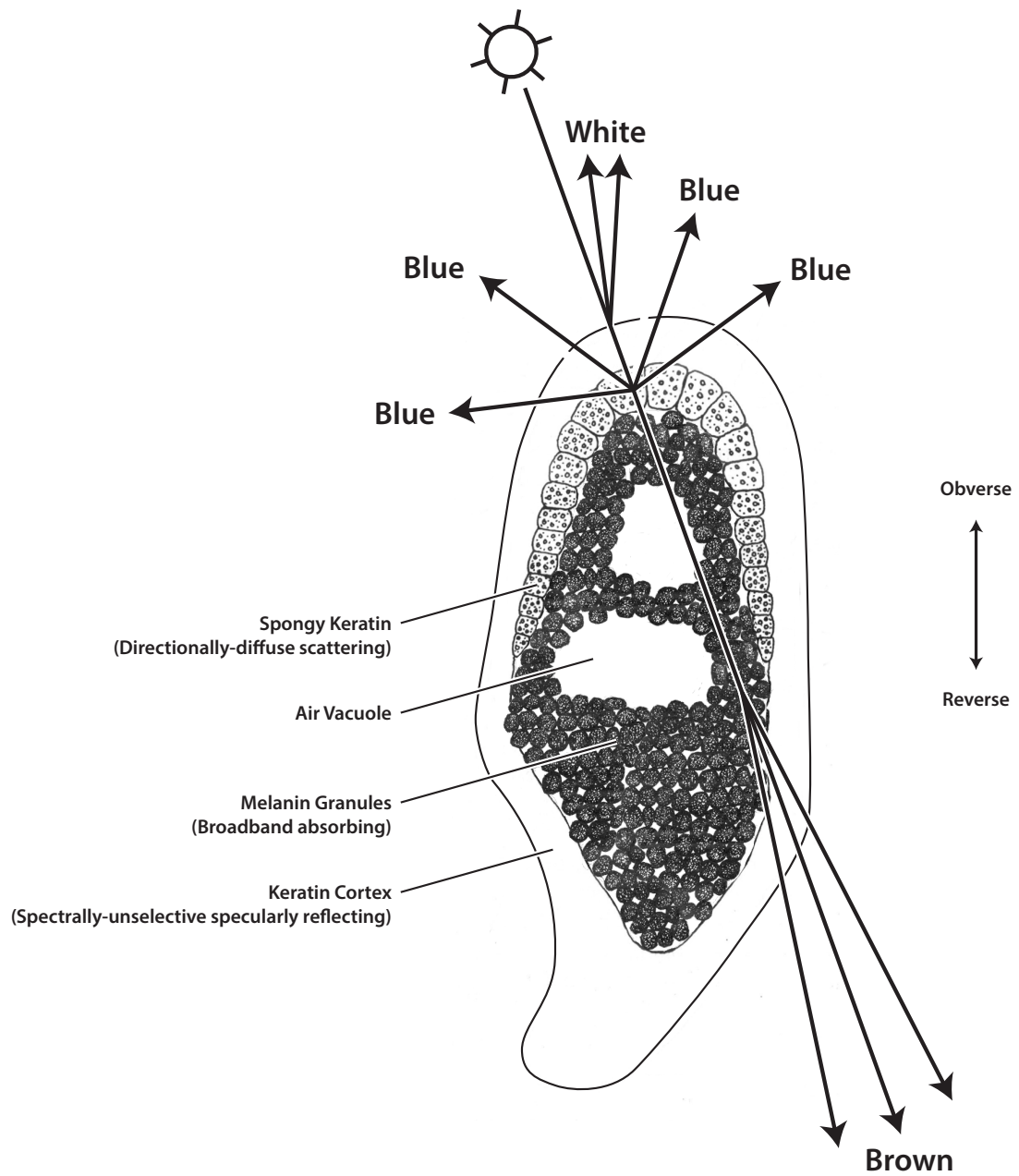


Figure 5.1: Cross-section of a blue-colored Blue Jay feather barb. Light is scattered by the air vacuoles of the blue-producing cells of the “spongy keratin”. Light is absorbed and scattered by the brown-black melanin granules. Adapted from [Clark Jr., 2004].

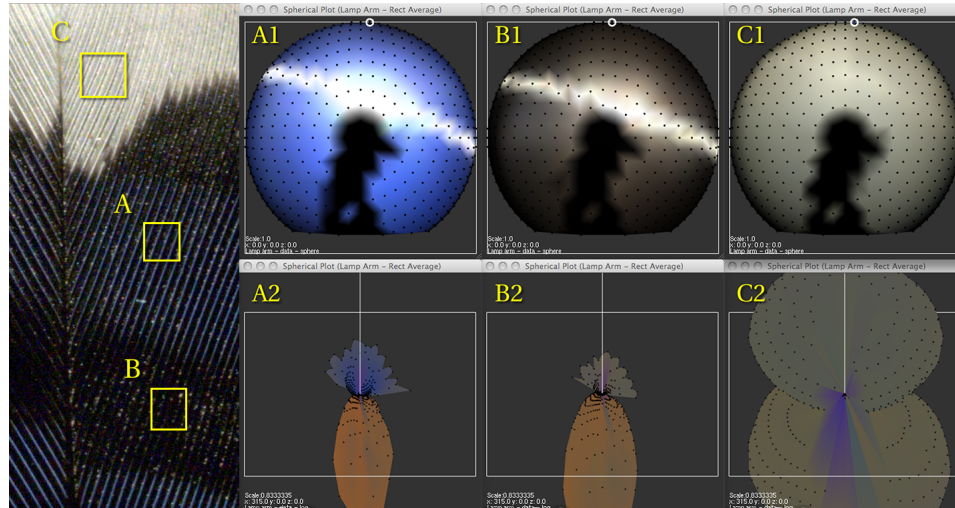


Figure 5.2: 2D directional light scattering averaged over three *rectangular* regions of the Blue Jay feather: blue stripe (A), black stripe (B), and white tip (C). Rfl-Nrm-RGB (A1–C1) and Arb-Log-Chr (A2–C2) plot the reflectance of the respective rectangle regions.

to feather appearance. Diffuse scattering dominates the reflectance of the white tip of the obverse face of the Blue Jay vane. The reflectance averaged over a large rectangular region displays a directionally diffuse character—not perfectly isotropic—without a clear specular highlight (Figure 5.2, Region C). In contrast to the white tip, a similarly-sized rectangular region of a black band produces significantly less diffuse reflection, so much so that a white specular highlight is clearly visible in contrast with the dark diffuse base (Figure 5.2, Region B). While the luminance is significantly diminished, the directional shape of the diffuse reflection is largely unchanged (*ibid*). The luminance of the diffuse reflection of the blue-colored bands falls between the two extremes outlined by the behaviour of the black stripe and white tip (Figure 5.2, Region A). The directional shape of the diffuse blue reflection is similar to that of the white and black regions (*ibid*).

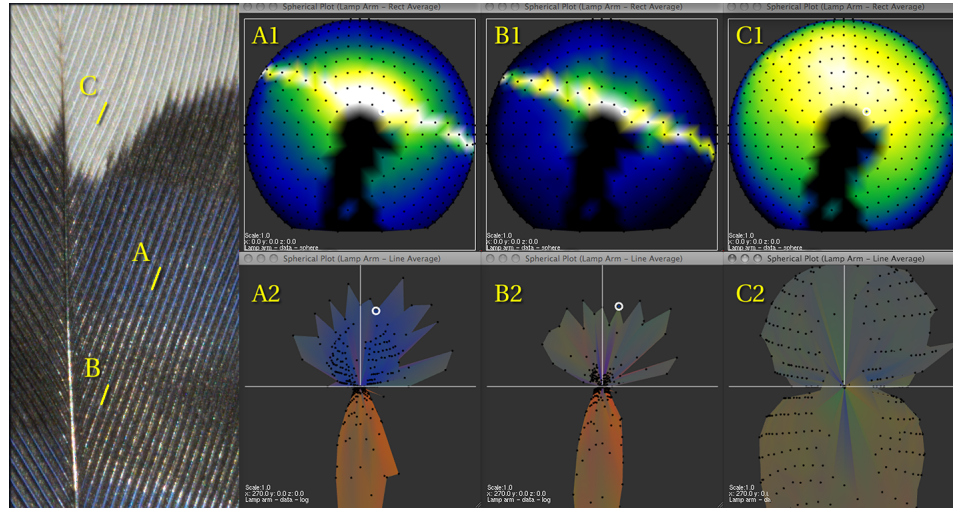


Figure 5.3: 2D directional light scattering averaged over *linear* sections of three rami of the Blue Jay feather: blue ramus (A), black ramus (B), and white ramus (C). Rfl-Nrm-Lum (A1–C1) and Frt-Log-Chr (A2–C2) plot the reflectance of the respective linear regions.

5.3 Variation in the Diffuse and Specular Reflectance of Barbs

A single image of the obverse face immediately reveals that the major difference between the blue and black striped regions is due to the barbs, not the barbules. To explore the average diffuse scattering characteristics of the barbs exclusive of the barbules, a one-pixel wide linear arrangement of pixels aligned with the axis of a barb is averaged. The average radial maxima (brightness) of the diffuse lobes—white, blue, and black—are approximately 1, $\frac{1}{2}$, and $\frac{1}{6}$ respectively (Region C, Region A, and Region B of figure 5.3). The average radial maxima of the specular lobes of the blue and black barbs are approximately $\frac{2}{3}$ as measured on the same scale (ibid). The blue barbs produce slightly brighter and narrower specular highlights (best confirmed from a larger rectangle average). The narrower lobe

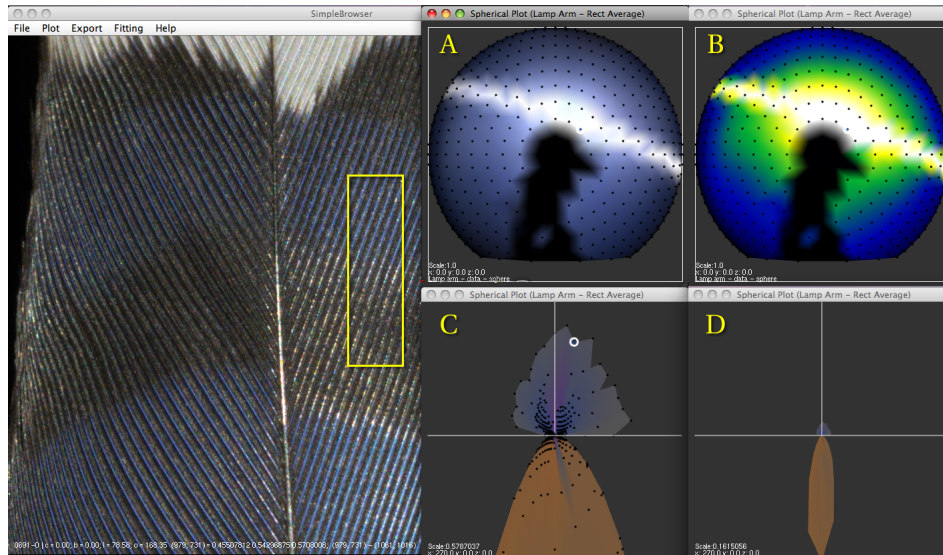


Figure 5.4: 2D directional light scattering averaged over a rectangular region containing a portion of a blue and black stripe of the Blue Jay feather. Rfl-Nrm-RGB (A) and Rfl-Nrm-Lum (B) plot the reflectance. The Front-Log-Chr plots are scaled to fit the reflectance (C) and transmittance (D).

may explain the rougher appearing surface highlights observed in the video with the light source orbiting the Blue Jay feather (not published here). Extensive discussion on specular reflection in feathers is found in chapter 4.

5.4 Global Area Average

C. cristata has developed a splendid mechanism to broadcast its signature color at varying distances. The global reflection averaged over blue and black stripes is the same as the blue striped region but diminished somewhat in luminance (Figure 5.4). Thus, the coarsely resolved Blue Jay is the same “color”, just a little darker. On the other hand, up close the Blue Jay plumage dazzles with its striped patterns of alternating black, blue, and white.

5.5 Integration of Non-Diffuse Components

Excluding the white tip and the blue barbs, the remaining feather structure is composed of black barbs and black barbules—broad spectrum absorbers—which suppress diffuse reflection. The alignment of the specular reflection of the black barbs serves to augment that of the blue barbs. The impact of the specular component of the black barbules is minimized two-fold: first, the chaotic surface structure of the zipped barbules spreads the reflection over a broad region, and second, the reflection is oriented in directions similar to the dominant—brighter and sharper—specular highlight of the barbs and the directionally diffuse reflectance of the barb (Figure 5.5). Whether used functionally or not, the barbules belonging to the lateral vane (right vane in image) do not appear to visually dilute or compete with the striking blue barbs.

5.6 Summary

The Blue Jay feather is a vivid diffuse reflector. It is comprised of two main components: diffuse blue and diffuse white. The blue barbs dominate the feather reflectance across the blue and black banded region of feather despite the disproportionately small fraction of vane they represent (as seen in the image of the feather). The white tips are visible at great distances where even the blue appearance is not so easily discerned.

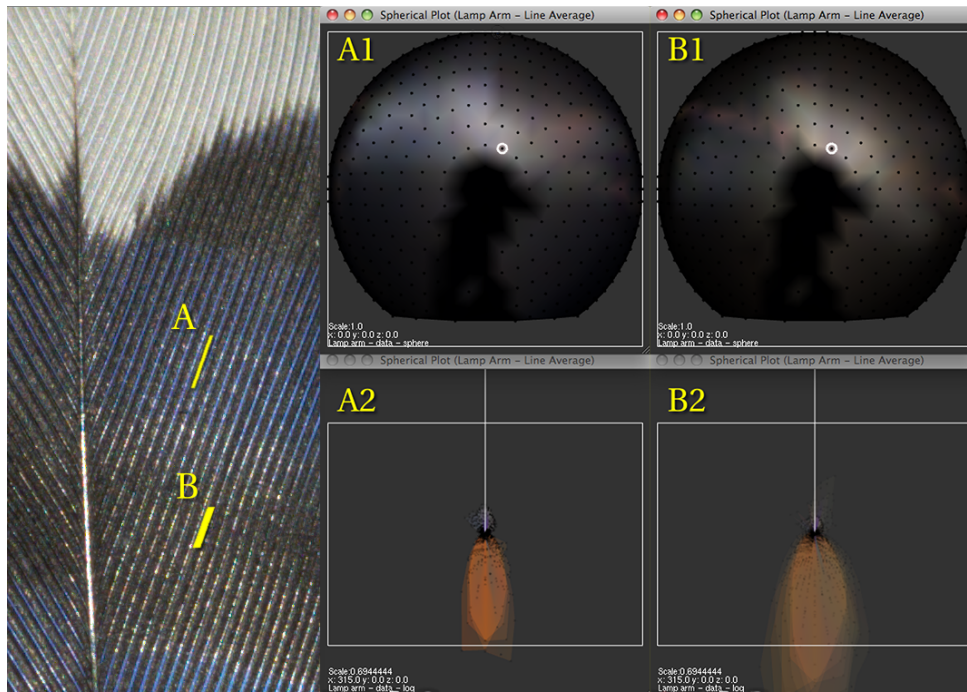


Figure 5.5: 2D directional light scattering averaged over a four-pixel-wide linear section of barbules (A) located within a blue stripe of the Blue Jay feather and averaged over an eight-pixel-wide linear section of barbules (B) located within a black stripe of the Blue Jay feather. Rfl-Nrm-RGB (A1–B1) and Arb-Log-Chr (A2–B2) plots are rotated 45° about the medial–lateral feather axis.

APPENDIX B

DIRECTIONAL SCATTERING PLOTS

The directional scattering from a feather is sampled at discrete positions on the sphere of directions. Each directional scattering sample has an associated camera direction, light direction, and color component. For most of our measurements we hold the camera (i.e. outgoing direction) stationary and manipulate the light position (i.e. incoming direction). The directional scattering plots in this thesis are configured to represent the color component of the scattering as a function of light position. Our software graphically displays the directional scattering on a three-dimensional spherical coordinate system. Different plotting functions and color schemes are used to identify and measure features of interest within the directional light scattering of our feathers. The plotting functions are described below and referred to repeatedly throughout the remainder of the thesis.

B.1 Normalized Radius

The first plotting function, *normalized radial distance* (Nrm), maps the set of incoming directions onto a unit sphere. Each gantry position in the data set defines a vertex on the sphere. The sphere, surrounding the feather, is located at the center of world. Half the vertices of the sphere are located forward of the feather plane and are visible. The remaining vertices are located behind the feather plane and are obscured.

The plots in this thesis drawn with *normalized radial distance* display at most a hemisphere of the sphere of incoming directions. In the paper form of the thesis we often show the sphere of incoming directions as two separate hemispheres—a

reflectance hemisphere (Figure B.1, Plots R1–R3) and a transmittance hemisphere (Figure B.1, Plots T1–T3)—but within our interactive software, directional scattering is represented as a single sphere which may be tumbled using a trackball widget or key commands to view any arbitrary hemispherical section of the set of all positions on the sphere.

B.2 Displaced Radius

Rather than locate the vertices of the directional scattering on the unit sphere, we may displace each vertex along a line which extends from the origin to its position on the unit sphere, i.e. alter the radial distance for each vertex on the sphere of incoming directions. The magnitude of the radial distance for each vertex on the mesh is proportional to the luminance (CIE-Y) of the color at each vertex. Consider two example cases: 1) A low luminance measurement for an incoming direction will decrease the radial distance of the vertex on the unit sphere for that direction, i.e. displace the vertex toward the origin of the sphere. 2) A high luminance measurement for an incoming direction will increase the radial distance of the vertex on the unit sphere for that direction, i.e. displace the vertex away from the origin of the sphere. The radial distance representing reflected luminance may be plotted in either linear (Figure B.1) or logarithmic (Figure B.1, Plots *4) scales. We refer to the linear form as the *linear-displaced* radial distance directional scattering plot (*Lin*). The logarithmic form we call the *logarithmic-displaced* radial distance directional scattering plot (*Log*).

The radial distance of the displaced directional scattering plots may be proportionally scaled to fit inside the frame of the plot window of the interactive data

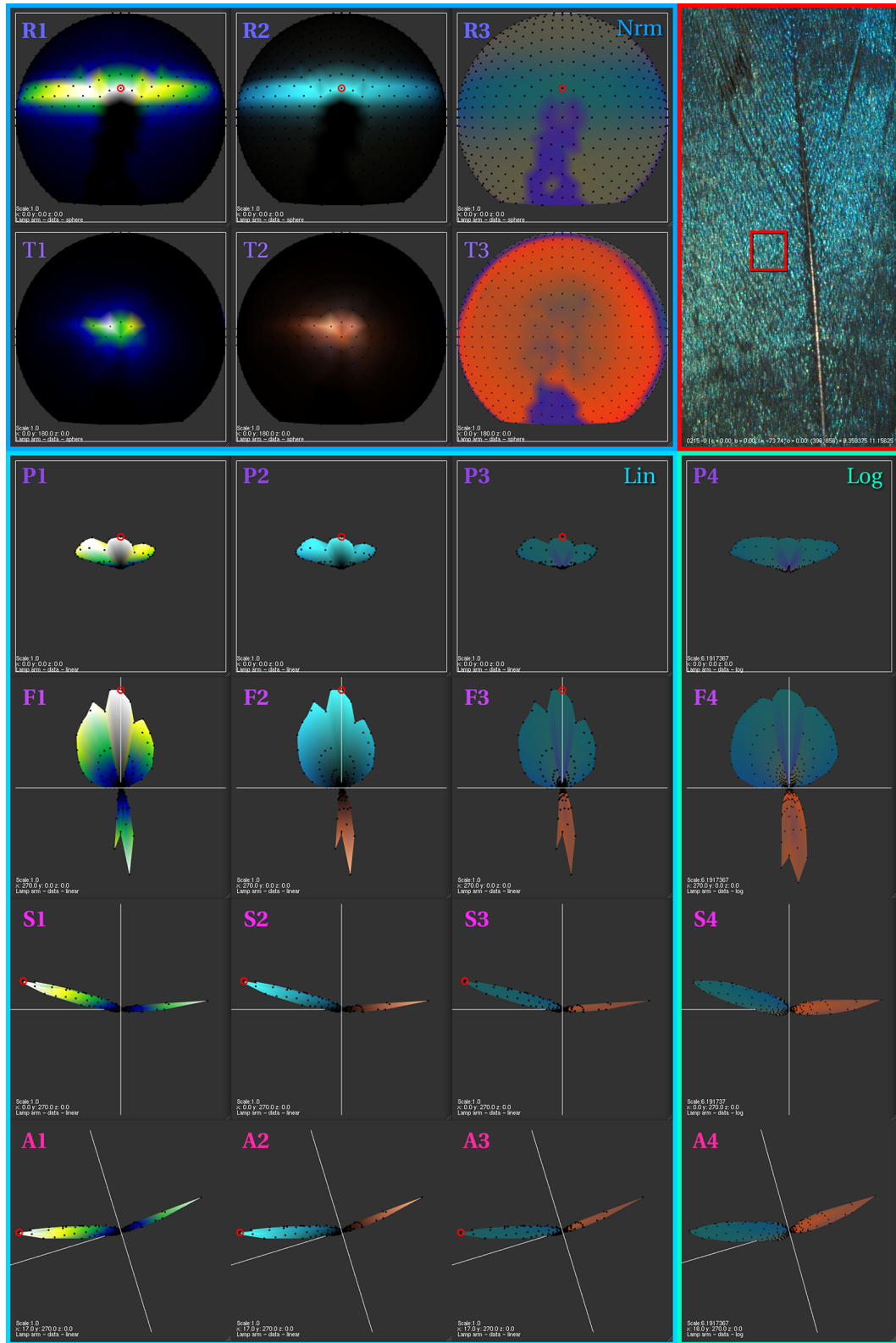


Figure B.1: Example of directional scattering plotting functions and color schemes.

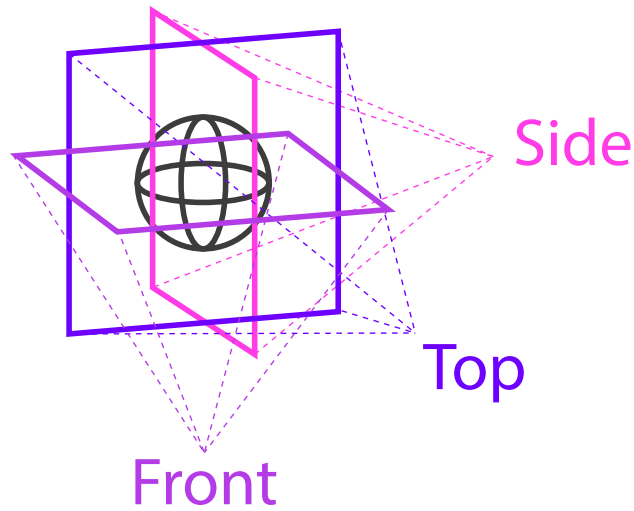


Figure B.2: Three plot views—top (T), front (F), and side (S)—of the directional scattering function.

visualization software. Like the normalized radial distance directional scattering plot, the view of the displaced radial distance directional scattering plot may be adjusted to suit. Three axes of rotation—X, Y, and Z—provide the necessary control. We often represent the 3D-volume of the directional scattering on paper through the use of three illustrations of the same lobe each drawn from 3 orthogonal viewpoints—*top* (Figure B.1, Plots P1–P3), *front* (Figure B.1, Plots F1–F4), and *side* (Figure B.1, Plots S1–S4). The Top, Front, and Side views are aligned with the +X, -Z, and +Y of the gantry coordinate system, and the +Z, -Y, and +X of the feather image coordinate system, respectively (Figure B.2).

The top view of the directional scattering plot is oriented in the direction opposing the macro-surface normal for each feather. Although the feather rachis points upwards in the gantry, the different orientations of different branches of the barbs complicate the alignment. Simply stated, idealized alignment is not possible for every feature on the feather (e.g. barb, distal barbule, proximal barbule) and therefore the top, front and side views may not provide the best view of a given

feature of interest. In such cases, we can rotate the scattering lobe an arbitrary amount to better view its profile or measure its angular shift (Figure B.1, Plots A1–A4).

B.3 Color Schemes

The mesh of the normalized or displaced directional scattering plots is shaded by various color schemes highlighting the intrinsic qualities of the directional reflectance and/or transmittance. We use three schemes: *luminance* (Figure B.1, Plots *1), *RGB* (Figure B.1, Plots *2), and *chromaticity* (Figure B.1, Plots *3–*4).

Luminance The luminance (*Lum*) or human perceptual brightness scheme calculates the luminance (CIE-Y) of the directional scattering from the RGB color measurements and shades the mesh of the directional plot with a 6 step color scheme—black, blue, cyan, green, yellow, and white—representing 0%, 20%, 40%, 60%, 80%, and 100% luminance respectively. The color of luminance values between any two steps is interpolated from the colors of those two steps. The saturation point (white) is set automatically to the 100-percentile of the scattering data. The color map may be proportionally scaled in software. The pseudocolor plots in this thesis are *not* necessarily rendered in the same scale, since the maximum scatter value of each feather differs; furthermore the author may have overridden the default and applied a proportional scale to any color map. Since the pseudocolor scale for a given plot is not labeled by default, except where otherwise noted, the comparison of the relative magnitude of the directional scattering between different plots should not be made.

RGB The RGB (*RGB*) scheme renders the directional scattering plot in human perceptual color space based on tri-chromatic vision. The exposure of the RGB plots may be scaled in software. The magnitude of the exposure is governed by the same factors as the pseudocolor scheme.

Chromaticity The chromaticity (*Chr*) scheme calculates the chromaticity of the directional reflectance from the RGB color measurements. The chromaticity is the specification of a color based on its hue and chroma regardless of its luminance. By its definition, the exposure of the chromaticity-colored plots may not be scaled.

We render directional scattering plots in the chromaticity scheme to view the hue and chroma over all incoming scatter direction without under- and/or over-exposure typical in the RGB plot. The luminance-normalized color of the chromaticity plots allow for subjective color comparisons without the intervention of luminance to override our perceptual response. We frequently render the displaced directional plots in the chromaticity color scheme, since the luminance is accounted for in the displacement.

B.4 Naming Conventions

Combinations of viewing directions, plotting functions and color schemes are used to identify and measure features of interest within the directional scattering from a region of feather vane. Listed below are abbreviated names of typical combinations of directional scattering plots. These abbreviated names are used to identify the plot types in the figure captions throughout the thesis.

Viewing Directions

Top Rfl	Top or Reflectance view (obverse surface normal)
Frnt	Front view (proximal–distal axis)
Sid	Side view (medial–lateral axis)
Bot Trs	Bottom or Transmittance view (reverse surface normal)
Arb	Arbitrary View

Plotting Function

Nrm	Normalized radial distance
Lin	Linear-displaced radial distance
Log	Logarithmic-displaced radial distance

Color Scheme

Lum	Luminance color map
RGB	RGB color map
Chr	Chromaticity color map

Example Combination

Top-Nrm-RGB Top view,
Normalized radial distance,
RGB color map.

Rfl-Nrm-RGB	Reflectance hemisphere ¹ , Normalized radial distance, RGB color map.
Bot-Nrm-Lum	Bottom view, Normalized radial distance, Luminance color map.
Trs-Nrm-Lum	Transmittance hemisphere ² , Normalized radial distance, Luminance color map.
Top-Lin-Chr	Top view, Linear-displaced radial distance, Chromaticity color map.
Sid-Log-Chr	Side view, Logarithmic-displaced radial distance, Chromaticity color map.

B.5 Coordinate Systems

Each plot contains some helpful information which denotes the coordinate system for the plot—especially useful for rotated coordinate systems. The plane of the macro-surface is represented by the white square centered on the origin in plots R*, T*, P* of figure B.1, the white horizontal line crossing the origin in plots F* of figure B.1, and the white vertical line crossing the origin in plots S* of figure B.1. The macro-surface normal is drawn as a white line emanating from the origin and

¹same as Top (Obverse) view

²same as Bottom (Reverse) view

oriented normal to the plane in each plot. When the macro-surface is in the plane of the paper, the surface normal is perpendicular to the paper and not readily visible in the plots.

The macro-surface of the feather is oriented to match the plane of the paper in the unrotated directional scattering plots (Figure B.1, Plots R*, T*, P*) Furthermore, the unrotated plots match the flattened feather image orientation. The proximal–distal feather axis is located in the vertical axis of the page. The medial-lateral feather axis is located in the horizontal axis of the page. The distal direction points to the top of the page.

CHAPTER 6

CONCLUSION

The feather is comprised of nano-, milli-, micro-, and macro-scale structures. When incident light interacts with the elements which form the feather structure, light may be scattered over a sphere of outgoing directions.

We developed non-destructive tools and methods to investigate the signaling potential of the milli-scale structure of feathers. We measured the directional reflectance of select samples of plumage using a spherical goniometer. We measured the milli-scale morphology of the same vanes using a micro-CT scanner. Our work shows that each component part of the barb of the feather (i.e. ramus, base of the distal barbule, pennulum of the distal barbule, and base of the proximal barbule) has its own optical signature by which it can be recognized. We have also shown how the signatures of some component parts feature more prominently in the far-field optical signature, i.e. the integrated signature seen at normal resolving power. We identified and measured the signal direction of each component, correlating it to the milli-scale morphology of the vane from the micro-CT measurements. We have shown that the orientation of the milli-scale structure of the vane (barb) agrees exactly with predictions made from the reflectance measurements. The exciting implication of our predictive model is that perhaps all the directional effects in feathers can be understood in the same way and, furthermore, that we have identified a previously unrecognized link between function and morphology that would allow various selective pressures to generate adaptive changes.

We have conducted a small, but important step in a potentially much larger project. Our studies suggest that directional reflectance is a component of the phenotype of an organism, an expression of the genes which is manifest by light

interaction with its morphology. Collecting a large library of directional reflectance measurements over a broad range of avian plumage would assist in describing the full gamut of avian directional signaling—useful for studying the evolution and development of plumage. Potential implications for behavioral studies are exciting. We consider feather signaling as active and directional. By characterizing the functional consequences of the directional expression of milli-scale structures, we have enabled inquiry into their adaptive consequences. Questions, such as how critical is the female viewpoint to the success of a male courtship display, become more focused. A larger collection of data (library) has further potential application for appearance modeling in the field of computer graphics, which in turn may serve scientific research through visualization.

BIBLIOGRAPHY

- M. Ashikmin, S. Premože, and P. Shirley. A microfacet-based BRDF generator. *SIGGRAPH '00: Proceedings of the 27th annual conference on Computer graphics and interactive techniques*, pages 65–74, July 2000.
- L. Auber. The structures producing "non-iridescent" blue colour in bird feathers. *Proceedings of the Zoological Society of London*, 129(4):455–486, Dec. 1957.
- P. P. Berthold and R. R. Rau. [Electron microscopical studies on the infiltration of iron oxide in the feathers of anatids]. *Zeitschrift fur Zellforschung und mikroskopische Anatomie (Vienna, Austria : 1948)*, 85(4):492–500, Jan. 1968.
- D. Brink and N. van der Berg. Structural colours from the feathers of the bird *Bostrychia hagedash*. *Journal of Physics D-Applied Physics*, 37(5):813–818, 2004.
- G. S. Butcher and S. Rohwer. The evolution of conspicuous and distinctive coloration for communication in birds. *Current ornithology*, 6, 1989.
- Y. Chen, Y. Xu, B. Guo, and H.-Y. Shum. Modeling and rendering of realistic feathers. *ACM Transactions on Graphics (TOG)*, 21(3):630–636, July 2002.
- G. A. Clark Jr. Form and Function: The External Bird. In S. Podulka, R. W. Rohrbaugh, and R. Bonney, editors, *Handbook of bird biology*. Princeton University Press, Nov. 2004.
- D. H. Clayton, S. E. Bush, B. M. Goates, and K. P. Johnson. Host defense reinforces host-parasite cospeciation. *Proceedings of the National Academy of Sciences of the United States of America*, 100(26):15694–15699, Dec. 2003.
- R. L. Cook and K. E. Torrance. A Reflectance Model for Computer Graphics. *ACM Transactions on Graphics (TOG)*, 1(1):7–24, Jan. 1982.

- K. Dana, B. Ginneken, S. Nayar, and J. Koenderink. Reflectance and texture of real-world surfaces. *ACM Transactions on Graphics (TOG)*, 18(1):1–34, 1999.
- E. J. Denton and J. A. C. Nicol. A survey of reflectivity in silvery teleosts. *Journal of the Marine Biological Association of the United Kingdom*, 46(03):685–722, Oct. 1966.
- S. M. Doucet and G. E. Hill. Do museum specimens accurately represent wild birds? A case study of carotenoid, melanin, and structural colours in long-tailed manakins *Chiroxiphia linearis*. *Journal of Avian Biology*, 40(2):146–156, Mar. 2009.
- L. A. Dugatkin and H. K. Reeve. *Game Theory and Animal Behavior*. Oxford University Press, USA, Mar. 2000.
- H. Durrer. Schillerfarben der Vogelfeder als Evolutionsproblem. *Denkschriften der Schweizerischen Naturforschenden Gesellschaft*, 1977.
- H. Durrer. Colouration. In J. Bereiter-Hahn, editor, *Biology of the Integument, Vol. 2, Vertebrates*, pages 239–247. Springer-Verlag, Berlin, Heidelberg, New York, Tokyo, 1986.
- H. Durrer and W. Villiger. Schillerradien des Goldkuckucks (*Chrysococcyx cupreus* (Shaw)) im Elektronenmikroskop. *Cell and Tissue Research*, 109(3):407–413, 1970.
- J. Dyck. Structure and Spectral Reflectance of Green and Blue Feathers of the Rose-faced Lovebird (*Agapornis roseicollis*) . *Biologische Skrifter*, 18(2):1–85, 1971a.

- J. Dyck. Structure and colour-production of the blue barbs of *Agapornis roseicollis* and *Cotinga maynana*. *Zeitschrift fur Zellforschung und mikroskopische Anatomie (Vienna, Austria : 1948)*, 115(1):17–29, 1971b.
- J. Dyck. Structural Colors. *Proc. Int. Ornithol. Congress*, 16:426–437, 1974.
- J. Dyck. Winter plumage of the Rock Ptarmigan: Structure of the air-filled barbules and function of the white colour. *Danskorn. Foren. Tidsskr.*, 73:41–58, 1979.
- J. Dyck. The evolution of feathers. *Zoologica Scripta*, 14(2):137–154, Apr. 1985.
- J. Dyck. Structure and light reflection of green feathers of fruit doves (*Ptilinopus* spp.) and an Imperial Pigeon (*Ducula concinna*). *Biologiske Skrifter (Denmark)*, 30:2–43, 1987.
- H. Gadow. On the Colour of Feathers as affected by their Structure. *Proceedings of the Zoological Society of London*, 50(3):409–422, Oct. 1882.
- A. Gardner, C. Tchou, T. Hawkins, and P. Debevec. Linear light source reflectometry. *ACM Transactions on Graphics (TOG)*, 22(3):749–758, 2003.
- F. B. Gill. *Ornithology*. W. H. Freeman, 2007.
- D. Gomez. Simultaneous crypsis and conspicuousness in color patterns: comparative analysis of a neotropical rainforest bird community. *American Naturalist*, 2007.
- C. Han, B. Sun, R. Ramamoorthi, E. Grinspun, C. Han, B. Sun, R. Ramamoorthi, and E. Grinspun. Frequency domain normal map filtering. *ACM Transactions on Graphics (TOG)*, 26(3):28, July 2007.

- J. E. Harvey and A. Krywonos. Radiance: the natural quantity for describing diffraction and propagation (Proceedings Paper). *Proc. of SPIE's International Symposium on Optics and Photonics*, 6285, Aug. 2006.
- E. Hecht. *Optics*. Addison Wesley, Boston, 1998.
- G. E. Hill and K. J. McGraw, editors. *Bird Coloration, Volume 1: Mechanisms and Measurements*. Harvard University Press, Cambridge, MA, Feb. 2006a.
- G. E. Hill and K. J. McGraw, editors. *Bird Coloration, Volume 2: Function and Evolution*. Harvard University Press, Cambridge, MA, Mar. 2006b.
- A. Huxley. A theoretical treatment of the reflexion of light by multilayer structures. *Journal of Experimental Biology*, 1968.
- P. Irawan. *Appearance of woven cloth*. PhD thesis, Cornell University, Ithaca, NY, 2008.
- P. Irawan and S. R. Marschner. Specular reflection from woven cloth. *ACM Transactions on Graphics (TOG)*, 31(1):11:1–11:20, Feb. 2012.
- J. D. Joannopoulos, S. G. Johnson, J. N. Winn, and R. D. Meade. *Photonic Crystals: Molding the Flow of Light (Second Edition)*. Princeton University Press, 2 edition, Feb. 2008.
- J. T. Kajiya. Anisotropic reflection models. *ACM SIGGRAPH Computer Graphics*, 19(3):15–21, July 1985.
- J. T. Kajiya and T. Kay. Rendering fur with three dimensional textures. *ACM SIGGRAPH Computer Graphics*, 23(3):271–280, 1989.
- S. Kinoshita. *Structural colors in the realm of nature*. World Scientific, 2008.

- S. Kinoshita and S. Yoshioka. Structural colors in nature: the role of regularity and irregularity in the structure. *ChemPhysChem*, 2005.
- S. Kinoshita, S. Yoshioka, and J. Miyazaki. Physics of structural colors. *Reports on Progress in Physics*, 71(7), 2008.
- M. Land. The physics and biology of animal reflectors. *Progress in biophysics and molecular biology*, pages 75–106, 1972.
- M. Levoy, Z. Zhang, and I. McDowall. Recording and controlling the 4D light field in a microscope using microlens arrays. *Journal of microscopy*, 235(2):144–162, Aug. 2009.
- A. Lucas and P. R. Stettenheim. Avian Anatomy Integument. *U.S. Government Printing Office*, 1:235–340, 1972.
- J. N. Lythgoe. *The Ecology of Vision*. Oxford University Press, USA, 1979.
- S. R. Marschner, H. W. Jensen, M. Cammarano, S. Worley, and P. Hanrahan. Light scattering from human hair fibers. *ACM Transactions on Graphics (TOG)*, 22(3):780–791, July 2003.
- S. R. Marschner, S. Westin, A. Arbre, and J. Moon. Measuring and modeling the appearance of finished wood. *ACM Transactions on Graphics (TOG)*, 24(3):727–734, July 2005.
- D. E. Mascha. The Structure of Wing-Feathers. *Smithsonian Miscellaneous Collections*, 48(1), 1905.
- C. Mason. Structural colors in feathers I. *Journal of Physical Chemistry*, 27(3): 201–251, 1923a.

- C. Mason. Structural colors in feathers II. *Journal of Physical Chemistry*, 27(5): 401–447, 1923b.
- E. Nakamura, S. Yoshioka, and S. Kinoshita. Structural Color of Rock Dove’s Neck Feather. *Journal of the Physical Society of Japan*, 77(12):124801, 2008.
- I. Newton. *Opticks*. Samuel Smith and Benjamin Walford, London, 1704.
- F. Nicodemus, J. Richmond, J. Hsia, and I. Ginsberg. Geometric considerations and nomenclature for reflectance. Monograph 161, National Bureau of Standards (US), 1977.
- D. Osorio and A. Ham. Spectral reflectance and directional properties of structural coloration in bird plumage. *Journal of Experimental Biology*, 205(14):2017–2027, 2002.
- G. L. Patricelli, M. S. Dantzker, and J. W. Bradbury. Differences in acoustic directionality among vocalizations of the male red-winged blackbird (*Agelaius phoeniceus*) are related to function in communication. *Behavioral Ecology and Sociobiology*, 61(7):1099–1110, Jan. 2007.
- G. L. Patricelli, M. S. Dantzker, and J. W. Bradbury. Acoustic directionality of red-winged blackbird (*Agelaius phoeniceus*) song relates to amplitude and singing behaviours. *Animal Behaviour*, 76(4):1389–1401, Oct. 2008.
- P. Poulin and A. Fournier. A model for anisotropic reflection. *ACM SIGGRAPH Computer Graphics*, 24(4):273–282, Sept. 1990.
- H. C. Proctor. Feather mites (Acari: Astigmata): ecology, behavior, and evolution. *Entomology*, 48:185–209, Jan. 2003.

- H. C. Proctor and I. Owens. Mites and birds: diversity, parasitism and coevolution. *Trends in ecology & evolution*, 15(9):358–364, Sept. 2000.
- R. O. Prum. The anatomy and physics of avian structural colours. *Proc. Int. Ornithol. Congr.*, 1999.
- R. O. Prum. Structural colouration of avian skin: convergent evolution of coherently scattering dermal collagen arrays. *Journal of Experimental Biology*, 2003.
- R. O. Prum. Evolution of the morphological innovations of feathers. *Journal of Experimental Zoology Part B: Molecular and Developmental Evolution*, 304B(6):570–579, Nov. 2005.
- R. O. Prum. Anatomy, Physics, and Evolution of Structural Colors. In G. E. Hill and K. J. McGraw, editors, *Bird Coloration, Volume 1: Mechanisms and Measurements*, pages 295–353. Harvard University Press, Cambridge, MA, Feb. 2006.
- R. O. Prum and A. Brush. The evolutionary origin and diversification of feathers. *The Quarterly review of biology*, 2002.
- R. O. Prum and J. Dyck. A hierarchical model of plumage: Morphology, development, and evolution. *Journal of Experimental Zoology Part B: Molecular and Developmental Evolution*, 298:73–90, 2003.
- R. O. Prum and S. Williamson. Theory of the growth and evolution of feather shape. *Journal of Experimental Zoology Part B: Molecular and Developmental Evolution*, 291(1):30–57, 2001.
- R. O. Prum, R. H. Torres, S. Williamson, and J. Dyck. Coherent light scattering by blue feather barbs. *Nature*, 396(6706):28, 1998.

- R. O. Prum, R. H. Torres, C. Kovach, S. Williamson, and S. Goodman. Coherent light scattering by nanostructured collagen arrays in the caruncles of the malagasy asities (Eurylaimidae: aves). *Journal of Experimental Biology*, 202 Pt 24: 3507–3522, 1999a.
- R. O. Prum, R. H. Torres, S. Williamson, and J. Dyck. Two-dimensional Fourier analysis of the spongy medullary keratin of structurally coloured feather barb. *Proceedings of the Royal Society of London Series B-Biological Sciences*, 266 (1414):13–22, 1999b.
- E. Rutschke. Gross Structure in Bird Feathers. *Proc. Int. Ornithol. Congress*, 16: 414–425, 1974.
- M. D. Shawkey and G. E. Hill. Feathers at a fine scale. *The Auk*, 2004.
- M. D. Shawkey and G. E. Hill. Significance of a basal melanin layer to production of non-iridescent structural plumage color: evidence from an amelanotic Steller’s jay (*Cyanocitta stelleri*). *The Journal of Experimental Biology*, 209(Pt 7):1245–1250, Apr. 2006.
- M. D. Shawkey, S. L. Balenger, G. E. Hill, L. S. Johnson, A. J. Keyser, and L. M. Siefferman. Mechanisms of evolutionary change in structural plumage coloration among bluebirds (*Sialia* spp.). *Journal of Royal Society Interface*, 3(9):527–532, Aug. 2006.
- M. D. Shawkey, S. R. Pillai, G. E. Hill, L. M. Siefferman, and S. R. Roberts. Bacteria as an agent for change in structural plumage color: correlational and experimental evidence. *American Naturalist*, 169 Suppl 1:S112–21, Jan. 2007.
- M. D. Shawkey, S. R. Pillai, and G. E. Hill. Do feather-degrading bacteria affect sexually selected plumage color? *Naturwissenschaften*, 2009a.

- M. D. Shawkey, V. Saranathan, H. Pálsdóttir, J. Crum, M. H. Ellisman, M. Auer, and R. O. Prum. Electron tomography, three-dimensional Fourier analysis and colour prediction of a three-dimensional amorphous biophotonic nanostructure. *Journal of Royal Society Interface*, pages S213–S220, 2009b.
- H. Sick. Morphologisch-funktionelle Untersuchungen über die Feinstruktur der Vogelfeder. *Journal für Ornithologie*, 85:206–373, 1937.
- D. G. Stavenga, H. L. Leertouwer, P. Pirih, and M. F. Wehling. Imaging scatterometry of butterfly wing scales. *Optics Express*, (1):193–202, Jan. 2009.
- D. G. Stavenga, H. Leertouwer, N. J. Marshall, and D. Osorio. Dramatic colour changes in a bird of paradise caused by uniquely structured breast feather barbules. *Proceedings of the Royal Society B: Biological Sciences*, 278(1715):2098–2104, 2010.
- P. R. Stettenheim. Structural Adaptations in Feathers. *Proc. Int. Ornithol. Congress*, 16:385–401, 1974.
- P. R. Stettenheim. The Integumentary Morphology of Modern Birds-An Overview 1. *Integrative and Comparative Biology*, 40(4):461–477, 2000.
- M. Stevens, C. A. Párraga, I. C. Cuthill, J. C. Partridge, and T. S. Troscianko. Using digital photography to study animal coloration. *Biological Journal of the Linnean Society*, 90(2):211–237, Jan. 2007.
- A. Surmacki and J. K. Nowakowski. Soil and preen waxes influence the expression of carotenoid-based plumage coloration. *Naturwissenschaften*, 94(10):829–835, Oct. 2007.

- S. Tamm, D. P. Armstrong, and Z. J. Tooze. Display Behavior of Male Calliope Hummingbirds during the Breeding Season. *The Condor*, 91(2):272–279, May 1989.
- J. J. Videler. *Avian Flight*. Oxford Univ Pr on Demand, Oct. 2006.
- J. P. Vigneron and V. Lousse. Colored reflections from the black-billed magpie feathers. In K. Creath, editor, *The Nature of Light: Light in Nature*, page 628508, San Diego, CA, USA, 2006. SPIE.
- P. Vukusic. Structural colour: elusive iridescence strategies brought to light. *Current biology : CB*, 21(5):R187–9, Mar. 2011.
- P. Vukusic and D. G. Stavenga. Physical methods for investigating structural colours in biological systems. *Journal of Royal Society Interface*, 6(Suppl_2): S133–S148, Apr. 2009.
- J. Wang, S. Zhao, X. Tong, J. Snyder, and B. Guo. Modeling anisotropic surface reflectance with example-based microfacet synthesis. *ACM Transactions on Graphics (TOG)*, 27(3), Aug. 2008.
- G. Ward. Measuring and modeling anisotropic reflection. *ACM SIGGRAPH Computer Graphics*, 26(2):265–272, July 1992.
- S. Westin, J. Arvo, and K. E. Torrance. Predicting reflectance functions from complex surfaces. *ACM SIGGRAPH Computer Graphics*, 26(2):255–264, July 1992.
- S. Yoshioka and S. Kinoshita. Effect of macroscopic structure in iridescent color of the peacock feathers. *Forma*, 17(2):169–181, 2002.

S. Zhao, W. Jakob, S. R. Marschner, and K. Bala. Building volumetric appearance models of fabric using micro CT imaging. *ACM Transactions on Graphics (TOG)*, 30(4), 2011.